Copyright Warning & Restrictions

The copyright law of the United States (Title 17, United States Code) governs the making of photocopies or other reproductions of copyrighted material.

Under certain conditions specified in the law, libraries and archives are authorized to furnish a photocopy or other reproduction. One of these specified conditions is that the photocopy or reproduction is not to be "used for any purpose other than private study, scholarship, or research." If a, user makes a request for, or later uses, a photocopy or reproduction for purposes in excess of "fair use" that user may be liable for copyright infringement,

This institution reserves the right to refuse to accept a copying order if, in its judgment, fulfillment of the order would involve violation of copyright law.

Please Note: The author retains the copyright while the New Jersey Institute of Technology reserves the right to distribute this thesis or dissertation

Printing note: If you do not wish to print this page, then select "Pages from: first page # to: last page #" on the print dialog screen

ABSTRACT

ENGINEERING OF *ESCHERICHIA COLI* 2-OXOGLUTARATE DEHYDROGENASE COMPLEX WITH MECHANISTIC AND SYNTHETIC GOALS

by
Joydeep Chakraborty

The *Escherichia coli* 2-oxoglutarate dehydrogenase complex (OGDHc) compromises multiple copies of three enzymes - 2-oxoglutarate dehydrogenase (E1o), dihydrolipoyl succinyltransferase (E2o), and dihydrolipoyl dehydrogenase (E3). OGDHc is found in the Krebs cycle and catalyzes the formation of the all-important succinyl-Coenzyme A (succinyl-CoA). OGDHc was engineered to understand the catalytic mechanism and optimized for chemical synthetic goals.

Succinyl-CoA formation takes place within the catalytic domain of E2o via a transesterification reaction. The succinyl group from the thiol ester of S8-succinyldihydrolipoyl-E2o is transferred to the thiol group of CoA. Mechanistic studies were designed to investigate enzymatic transthioesterification. His375 and Asp374 was shown to be important in E2o. The magnitude of the rate acceleration provided by these residues suggests a role in stabilization of the symmetrical tetrahedral oxyanionic intermediate by formation of two hydrogen bonds, rather than in acid–base catalysis. Further evidence ruling out a role in acid–base catalysis is provided by saturation mutagenesis studies at His375 and substitutions to other potential hydrogen bond participants at Asp374. The rate constant for reductive succinylation of the E2o lipoyl domain (LDo) by E1o and 2-oxoglutarate (99 s^{-1}) was approximately twofold larger than the rate constant for k_{cat} (48 s^{-1}) for the overall reaction (NADH production). It could be concluded that succinyl transfer to CoA and release of succinyl-CoA is the rate-limiting step. The results suggest a revised mechanism of catalysis for acyl transfer in the superfamily of 2-oxo acid dehydrogenase complexes, thus provide

fundamental information regarding acyl-CoA formation, so important for several biological processes including post-translational succinylation of protein lysines.

OGDHc was converted from a 2-*oxoglutarate* dehydrogenase to a 2-oxo *aliphatic* dehydrogenase complex by engineering consecutive components. OGDHc was reprogrammed to accept alternative substrates by evolving the E1o and E2o components. Wt-ODGHc does not accept aliphatic substrates. E1o was previously engineered to accept a non-natural aliphatic substrate, 2-oxovalerate (2-OV). E2o also required engineering to accept 2-OV in the overall reaction. Hence, saturation mutagenesis libraries of E2o were screened and several variants were identified for 2-OV activity. Variants also displayed activity for larger aliphatic substrates, which demonstrates the potential green synthetic utility.

ENGINEERING OF *ESCHERICHIA COLI* 2-OXOGLUTARATE DEHYDROGENASE COMPLEX WITH MECHANISTIC AND SYNTHETIC GOALS

by
Joydeep Chakraborty

A Dissertation
Submitted to the Faculty of
New Jersey Institute of Technology
in Partial Fulfillment of the Requirements for the Degree of
Doctor of Philosophy in Environmental Science

Department of Chemistry and Environmental Science

August 2019

.

APPROVAL PAGE

**ENGINEERING OF *ESCHERICHIA COLI*
2-OXOGLUTARATE DEHYDROGENASE COMPLEX
WITH MECHANISTIC AND SYNTHETIC GOALS**

Joydeep Chakraborty

Dr. Edgardo T. Farinas, Dissertation Advisor — Date
Associate Professor, Chemistry and Environmental Science, NJIT

Dr. Frank Jordan, Dissertation Advisor — Date
Rutgers Board of Governors Professor of Department of Chemistry,
Rutgers University, Newark

Dr. Somenath Mitra, Committee Member — Date
Distinguished Professor of Chemistry and Environmental Science, NJIT

Dr. Yong Ick Kim, Committee Member — Date
Assistant Professor of Chemistry and Environmental Science, NJIT

Dr. Mengyan Li, Committee Member — Date
Assistant Professor of Chemistry and Environmental Science, NJIT

BIOGRAPHICAL SKETCH

Author: Joydeep Chakraborty

Degree: Doctor of Philosophy

Date: August 2019

Undergraduate and Graduate Education:

- Doctor of Philosophy, Environmental Science
  New Jersey Institute of Technology, Newark, USA, 2019.

- Bachelor of Technology, Biotechnology
  West Bengal University of Technology, India, 2011.

Presentations and Publications:

1. J. Chakraborty, N. Nemeria, F. Jordan and E. Farinas "Catalysis of transthiolacylation in the active centers of dihydrolipoamide acyltransacetylase components of 2-oxo acid dehydrogenase complexes" FEBS OpenBio 8(2018) 880-896.

2. J. Chakrborty, N. Nemeria, X. Zhang, P. Nareddy, M. Szostak, F. Jordan and E. Farinas "Engineering 2-*oxoglutarate* dehydrogenase to a 2-oxo *aliphatic* dehydrogenase complex by optimizing consecutive components" AIChE Journal 2019 (*under review*).

3. J. Chakraborty, N. Nemeria, F. Jordan and E. Farinas "Catalysis of transthiolacylation in the active centers of dihydrolipoamide acyltransacetylase components of 2-oxo acid dehydrogenase complexes" 255th National meeting of the American Chemical Society (ACS), New Orleans, LA March 18-22, 2018.

4. Presented doctoral dissertation work (poster) at the International Society of Pharmaceutical Engineers Cancer conference held at J&J Headquarters, New Brunswick. August 2016.

5. Presented doctoral dissertation work at the Rutgers University, Department of Chemistry open house in 2014, 2015 and 2016.

DEDICATION

চিত্ত যেথা ভয়শূন্য, উচ্চ যেথা শির,
জ্ঞান যেথা মুক্ত, যেথা গৃহের প্রাচীর
আপন প্রাঙ্গণতলে দিবসশর্বরী
বসুধারে রাখে নাই খন্ড ক্ষুদ্র করি,
যেথা বাক্য হৃদয়ের উৎসমুখ হতে
উচ্ছ্বসিয়া উঠে, যেথা নির্বারিত স্রোতে
দেশে দেশে দিশে দিশে কর্মধারা ধায়
অজস্র সহস্রবিধ চরিতার্থতায়–
যেথা তুচ্ছ আচারের মরুবালুরাশি
বিচারের স্রোতঃপথ ফেলে নাই গ্রাসি,
পৌরুষেরে করে নি শতধা নিত্য যেথা
তুমি সর্ব কর্ম চিন্তা আনন্দের নেতা–
নিজ হস্তে নির্দয় আঘাত করি, পিতঃ,
ভারতেরে সেই স্বর্গে করো জাগরিত।

- *রবীন্দ্রনাথ ঠাকুর*

This book has taken seven years in the making, occupying more than one-fifth of my lifespan. I come from a humble family farfetched from a scientific background. As a child, I saw a documentary on melting polar icebergs which was etched in my mind. That somehow drove me towards science to find a way to save our planet one day. This thesis is dedicated to that documentary.

I came into the United States, alone, believing that science can be bread and butter for life. The person, who let me foresee such a notion amidst all adversities, was my father. The person who thought otherwise, but still supported me every step of the way was my mother. This thesis is dedicated to my parents, whose silent sacrifice everyday made this take shape. It is not easy to belong to transition generation into an Indo-American cross-culture, where Indian values have to blend in with the American work-ethics. The strength of my parents is what bound this book together.

Along the way, I lost three of my four grandparents within one-year span. And I hope wherever they are, they would be proud to see this thesis finally coming alive. I dedicate this to my grandparents.

Finally, last but not the least to mention is my wife. We got married in the final year of this thesis. Thus began, the story of two little mice who fell into a bucket of cream. They both struggled so fiercely that the cream churned into butter and they were able to crawl out. I dedicate this thesis to her.

On a closing note I would like to remind everyone reading this thesis that, in the words of Mark Twain, "*Thousands of geniuses live and die undiscovered – either by themselves or by others*". This contribution is dedicated to everyone who believed.

ACKNOWLEDGMENT

I would like to take this opportunity to sincerely thank the Department of Chemistry and Environmental Science at New Jersey Institute of Technology and the Department of Chemistry at Rutgers University, Newark, including all faculty and staff members for all their help along the way.

My heartfelt gratitude goes to my dissertation advisors Dr. Edgardo Farinas and Dr. Frank Jordan for their patience, inputs and guidance throughout my research and dissertation.

I would like to thank all my committee members Dr Somenath Mitra, Dr Yong-Ick Kim and Dr Mengyan Li for their inputs and help.

I am indebted to Dr. Natalia Nemeria for her contributions to this dissertation with invaluable lessons and help with both experiments and writing. I am thankful to have been part of both Farinas and Jordan groups and all my friends/colleagues along the way.

I am grateful for the financial support by the National Science Foundation and National Institutes of Health.

TABLE OF CONTENTS

TABLE OF CONTENTS
(Continued)

Chapter **Page**

TABLE OF CONTENTS
(Continued)

Chapter **Page**

TABLE OF CONTENTS
(Continued)

LIST OF TABLES

LIST OF FIGURES

LIST OF FIGURES
(Continued)

LIST OF FIGURES
(Continued)

LIST OF FIGURES
(Continued)

Figure **Page**

CHAPTER 1
INTRODUCTION

1.1 2-Oxoglutarate Dehydrogenase Complex

The 2-oxoglutarate dehydrogenase complex (OGDHc) or α-ketoglutarate dehydrogenase complex is most commonly known for its role in the Krebs cycle. This enzyme belongs to a family of multienzyme complexes. They are classified on the natural substrate (pyruvate, 2-oxoglutarate (2-OG) or branched-chain α-keto acids) that they utilize (Figure 1.1) [1].

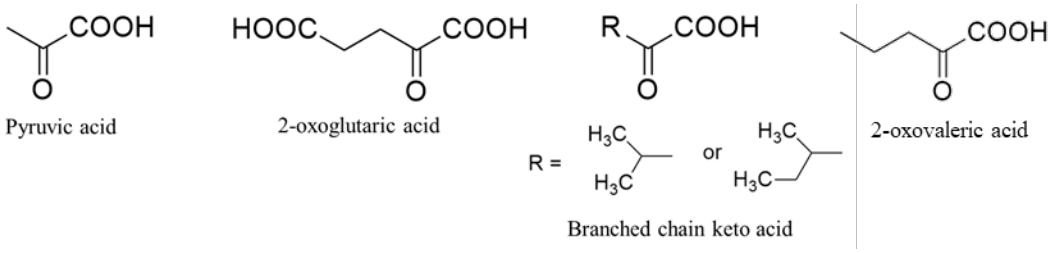

Figure 1.1 α–Keto acid substrates.

This family of multienzyme complexes is important in controlling the carbon flux from carbohydrate precursors and a select group of amino acids into and around the Krebs cycle (Figure 1.2) [2]. This enzyme complex catalyzes the non-equilibrium reaction converting 2-OG, Coenzyme A (CoA) and NAD^+ to succinyl-CoenzymeA (succinyl-CoA), NADH and CO_2.

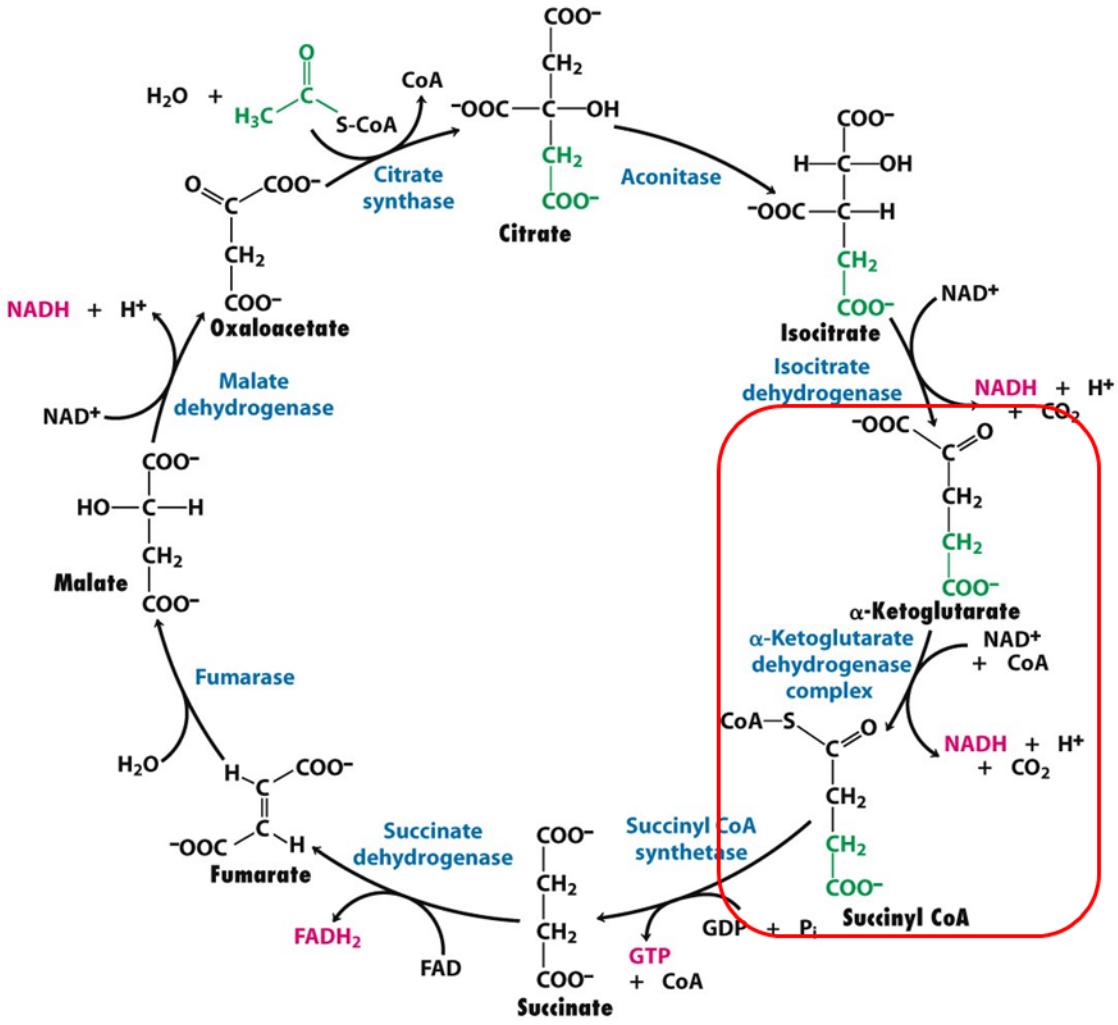

Figure 1.2 Krebs Cycle.
Figure adaptation: Jeremy M. Berg, John L. Tymoczko, and Lubert Stryer Biochemistry, 8th edition, 2015 pp 509 figure 17.15.

The overall reactions require three protein components, which is comprised of a substrate specific dehydrogenase/decarboxylase (E1o EC 1.2.4.2, Figure 1.3a), dihydro-lipoamide succinyl transferase (E2o EC 2.3.1.6, Figure 1.3b), and dihydrolipoamide dehydrogenase (E3 EC 1.8.1.4, Figure 1.3c). The above enzymes respectively require the cofactors thiamine diphosphate (ThDP), lipoic acid and flavin adenine dinucleotide (FAD). In *Escherichia coli,* E1o and E3 exist as homodimers. The E2o component is a trimeric multidomain protein, starting with the amino terminal end a flexible lipoyl

domain (LDo), followed by a long mostly unstructured subunit binding domain for assembly with E1o/E3, then a central nexus catalytic core domain (CDo). The enzyme complex is inhibited by its end products, succinyl-CoA and NADH. It is also regulated by the ATP/ADP ratio, the NADH/NAD^+ ratio, calcium and the substrate availability in the cellular environment [3,4].

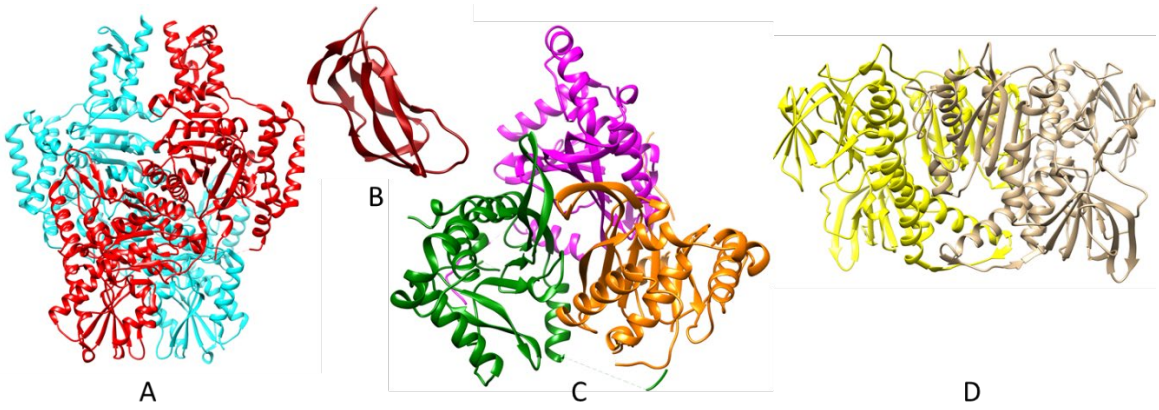

Figure 1.3 Ribbon diagrams for OGDHc components: A. Structure of a truncated variant of E1o (*t*E1o) that is missing the first 77 amino acids on the N-terminus (PDB ID: 2JGD). The structure of *t*E1is homodimer and each chain (105 kDa/subunit) is represented as gold and green ribbons. B. NMR structure of E2o lipoyl domain (21 kDa) (PDB ID: 1PMR). C. Catalytic domain of the E2o is shown as a trimer with each chain (45 kDa/subunit) represented in red, yellow and maroon ribbons (PDB ID: 1C4T).
D. E3 is shown as a homodimer (55 kDa/subunit) (PDB ID: 4JDR).

1.2 Structural Assembly

The quaternary organization of the OGDHc ensures that the products of one reaction are efficiently shuttled to the next active site for the subsequent reaction (called substrate channeling). In almost all instances, E1o and E3 are recruited into their multienzyme complexes through direct interaction with E2o, which is an oligomeric enzyme with structurally distinct domains that are linked by flexible regions [5]. OGDHc complexes are assembled in a tight but noncovalent fashion. This multicomponent and multimeric

nature results in the formation of relatively large complexes with an approximate mass of 2.5 MDa [6,7]. In *E. coli*, the assembly of OGDHc is organized around a 24-meric central core of E2 that exhibits octahedral symmetry (Figure 1.4). The oligomeric E2 core is responsible for tethering and orientating both the E1o and E3 enzymes within the complexes via compact, peripheral subunit-binding domains. The organization of the three component enzymes is crucial for the activity of the complex. The proposed stoichiometry for the *E. coli* complex has been estimated at 12 E1o : 24 E2o : 12 E3. The oligomeric E2o forms the foundation, and it is bound to multiple copies of E1o and E3 [6,8,9].

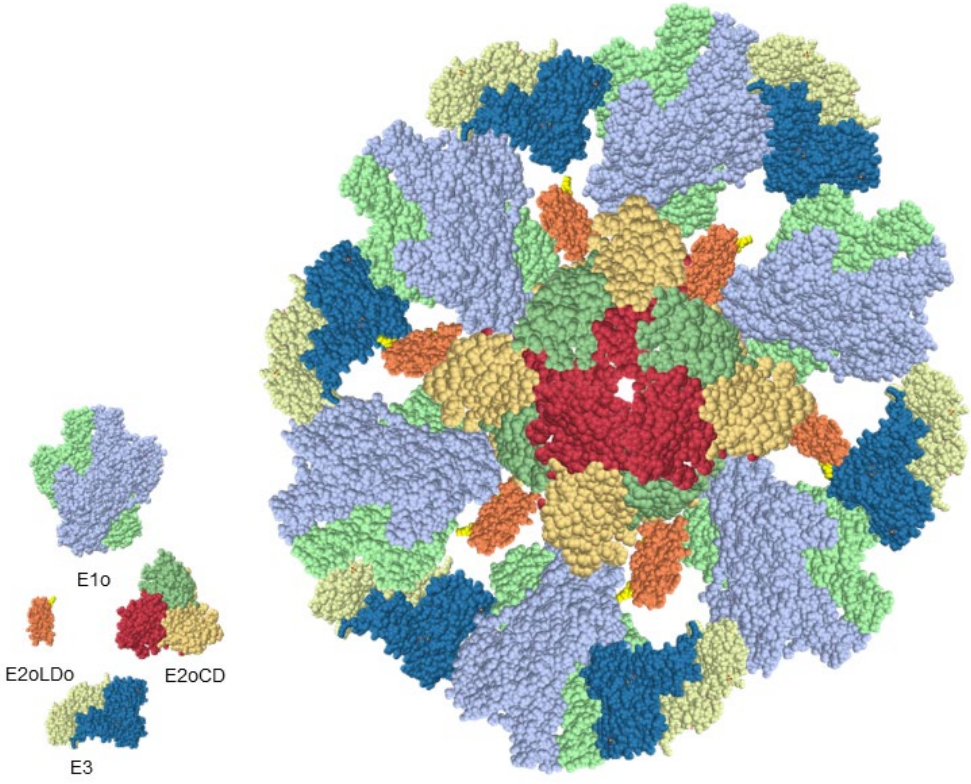

Figure 1.4 Schematic representation of assembled 2-oxoglutarate dehydrogenase multienzyme complex consisting of multiple copies of E1o, E2o and E3 [10].
Figure adaptation: Reginald H. Garrett, Charles M. Grisham Biochemistry, 6th edition, 2017 pp 670 figure 19.21.

1.3 OGDHc Overall Reaction

The overall reaction of OGDHc is as follows (Equation 1.1):

$$\text{2-oxoglutarate} + NAD^+ + CoA \rightarrow \text{succinyl-CoA} + CO_2 + NADH + H^+ \quad (1.1)$$

The steps of the overall reactions are shown in Figure 1.5.

Step 1: E1o component catalyzes the initial decarboxylation of the 2-oxoglutarate, using ThDP as a cofactor.

Step 2: This step is followed by reductive succinylation of the lipoyl group bound to the ε-amino group of a lysine residue in E2o.

Step 3: E2o is a succinyl transferase responsible for transferring the succinyl group to CoA.

Step 4: The reduced dihydrolipoyl group left on E2o is reoxidized to the dithiolane ring by the flavoprotein E3, with NAD^+ as the ultimate proton acceptor [11].

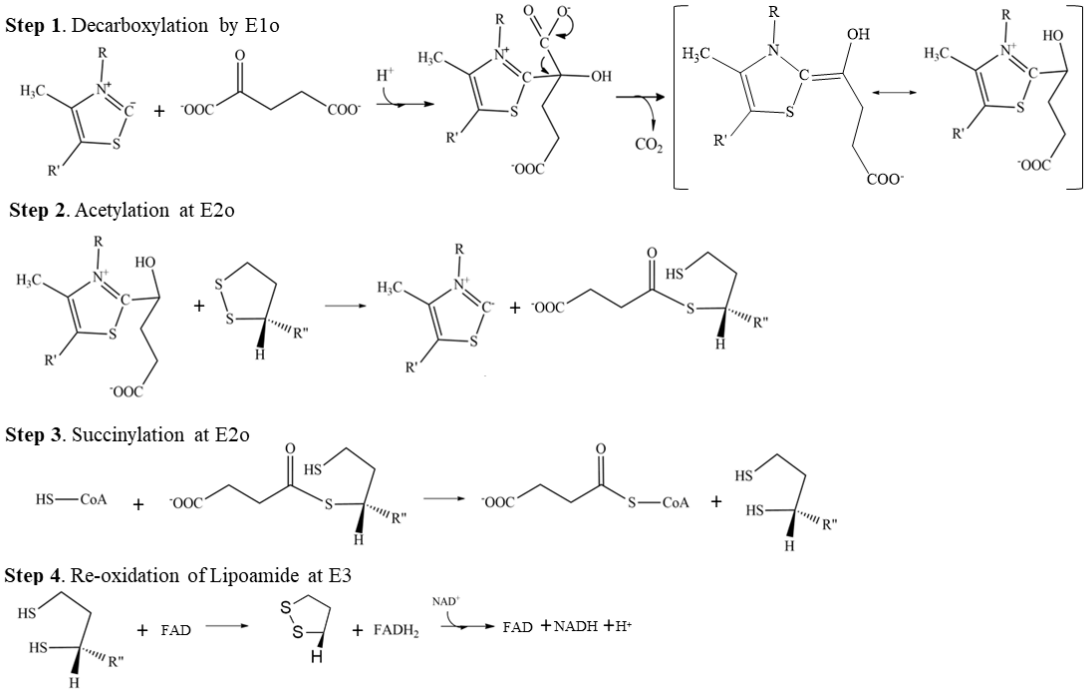

Figure 1.5 The overall reaction mechanism of the complex.

1.4 E1o Component

The thiamin diphosphate (ThDP) dependent E1o component is a dehydrogenase/decarboxylase enzyme. The crystal structure of apo-E1o has been solved to 2.6 Å, and it reveals that the enzyme in *E. coli* is a homodimer (α_2) [12]. The crystal structure (Figure 1.3A) depicts a 190 kDa truncated E1o lacking the first 77 residues from its N-terminus. The truncated enzyme retains decarboxylase activity but it does not form a complex with E2o, suggesting the importance of the N-terminus for E1o-E2o interactions [12]. The E1o active site is lined by three histidine residues at positions 260, 298 and 729 and a serine at position 302 (Figure 1.6). The residues have been proposed to be responsible for substrate specificity. Their proximity to the ThDP thiazolium ring make them likely to define the substrate binding pocket or be of catalytic importance [12,13].

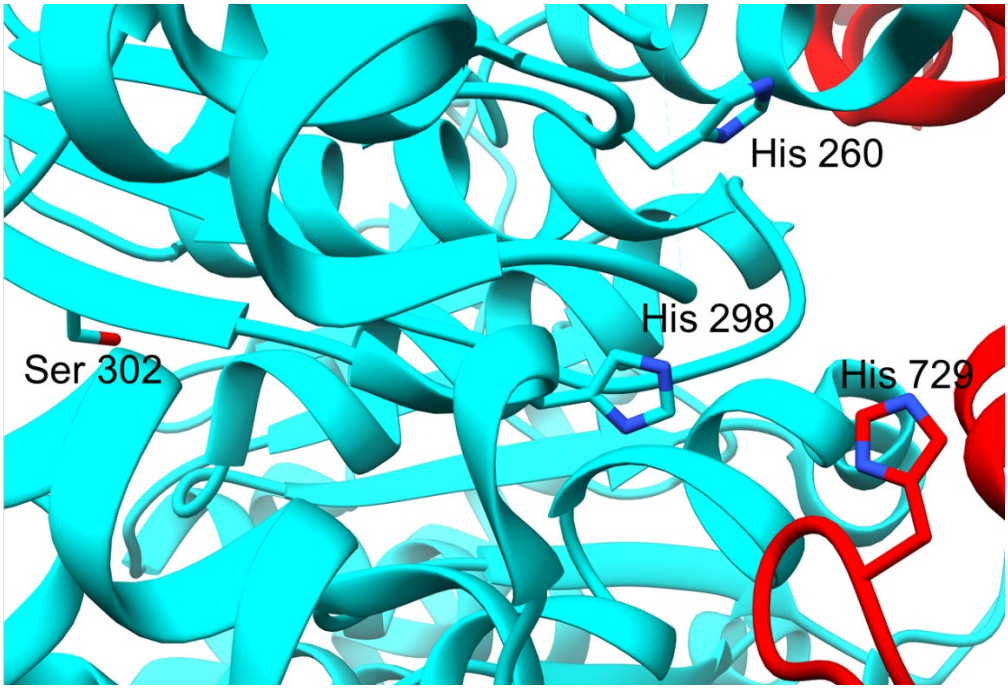

Figure 1.6 Active site of E1o. The active site residues His260, His298 and Ser 302 of chain A (cyan) and His729 of chain B (red) have been shown (PDB ID: 2jgd).

In the active site, the catalytic mechanism has been proposed based on the two histidines at 260 and 298 which behave as a general acid-base catalyst. Substrate channeling occurs through an acidic channel that serves as a proton wire. The catalytic rates of E1o were greatly reduced upon substitution of alanine in place of the His260 and His298, that proved their importance in the reaction [12]. This is consistent with their role in recognition of the distal carboxylate of 2-OG. Previously, the program to alter the substrate specificity of OGDHc to utilize it as a catalyst for green chemical synthesis was initiated by engineering the active site of E1o. In OGDHc, there are three levels of substrate specificity. One occurs at the E1o level and the other two at E2o (LDo and CDo). The active site histidines at 260 and 298 of E1o were identified by structural data as important residues for binding and activity [13]. The goal was to engineer the enzyme to accept a non-natural substrate 2-oxovaleric acid (2-OV). This substrate is a homolog of 2-OG (Figure 1.1), but it lacks the distal carboxyl group (Figure 1.1). The libraries His260X, His298X and His260X/His298X were constructed by saturation mutagenesis and screened for activity towards 2-OV as substrate. Active mutants were identified using a E1o-specific assay (Figure 1.7). The assay is a direct measure of the decarboxylase activity of E1o by an external oxidizing agent 2, 6-dichlorophenolindophenol (DCPIP). Reduction of DCPIP is determined by the loss of absorbance at 600 nm [14] and affirms that decarboxylation to the enamine had taken place.

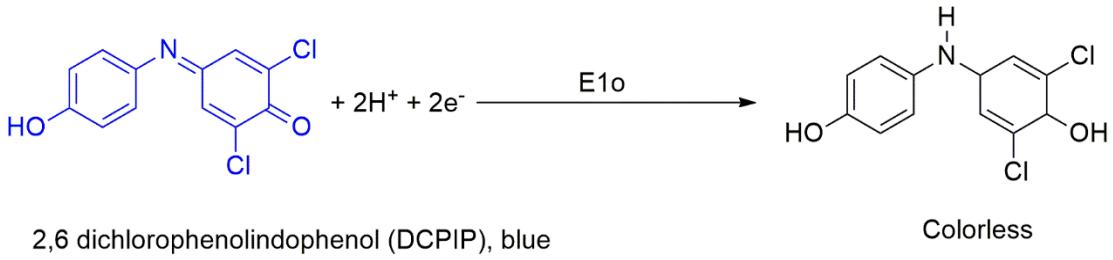

Figure 1.7 DCPIP, an E1-specific, assay reaction.

Results showed that His260 was crucial for substrate binding and most likely has a hydrogen bonding role. The His298 residue when replaced with leucine, threonine, valine or aspartate were all shown to decarboxylate 2-OV (Figure 1.5, Step 1). The E1o-His298Asp was the most active variant showing improvements of catalytic efficiency over the wild type enzyme towards 2-OV [13]. However, NADH production could not be detected in the overall reaction. Mass-spectrometric evidence also showed that there was successful transfer of the E1o-bound hydroxybutyl-ThDP intermediate of substrate (2-OG/2-OV) to the E2o-LDo. This indicated at the E2o level, the second substrate checkpoint, where the succinyl group is transferred from the S-atom of dihydrolipoamide to the S-atom of CoA was blocked towards synthesis of the acyl-CoA derivative derived from 2-OV.

Further, hybrid complexes were also constructed consisting of components from both the OGDHc and the pyruvate dehydrogenase complex (PDHc). The results suggested different components acting as 'gate-keepers' for the specificity for these two multienzyme complexes in *E. coli*. It was shown that E1p determined specificity for pyruvate. However, the same specificity towards 2-OG is determined by E1o and E2o [13].

From this information, it was evident that engineering E2o was necessary to bypass its substrate checkpoint. To broaden the scope of efforts to produce acyl-CoA analogues

and use OGDHc as a synthetic tool, the mechanism at the active site of the catalytic core domain of E2o was further investigated. Also, it was essential to understand the structure-function relationship of the E2o active site residues that contribute to the catalysis of the succinyl-transfer reaction.

1.5 E2o Component

The E2o component consists of, from N-terminal, lipoyl domain, subunit binding domain, and a catalytic domain. The number of lipoyl domains can vary between 1 to 3, which depends on the organism. The domains are connected by flexible linker segments. In *E. coli*, the E2o component consists of only one lipoyl domain (LDo), followed by one E1 and/or E3 binding domain (peripheral subunit binding domain or PSBD), and then by a carboxyl-terminal catalytic or core domain (CDo) (E2o*ec*) [15] (Figure 1.8). The E2o is organized as a 24-mer with octahedral symmetry [16]. The flexibility of the linker segments is thought to inhibit crystallization of the native E2o. Despite that, significant amount of structural information has been published from individual domains (Figure 1.8) [17].

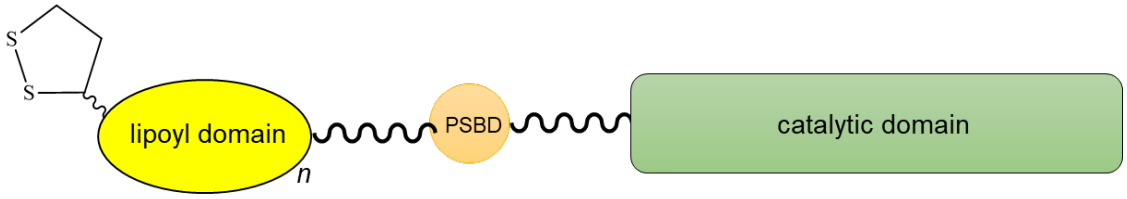

Figure 1.8 Schematic representation of the domains of the E2o component of *E. coli.* The ditholane ring of the flexible lipoyl-lysine arm has been shown on the lipoyl domain (yellow). The value of n = 1, 2 or 3 depends on the organism. For *E. coli*, n = 1. The lipoyl domain is followed by the peripheral subunit binding domain (PSBD) represented in orange. The final catalytic core domain is represented in green.

1.6 E3 Component

The third component of OGDHc is E3 or dihydrolipoamide dehydrogenase. E3 is a flavoprotein that binds FAD and NAD^+ and it is shared between OGDHc and PDHc, and in fact all such complexes in a particular cell share the same E3. In *E. coli,* the E3 interacts with E2o non-covalently at the PSBD. The role of E3 is to reoxidize the dihydrolipoamide of E2o LDo after succinyl transfer (Figure 1.5, Step 3) [18]. Thus, the E3 restores the initial redox states of the E2o LDo lipoamides allowing the multienzyme complex to cycle (Figure 1.5, Step 4). In the other half of the redox reactions, E3 reduces NAD^+ to NADH (Figure 1.9 and Figure 1.5, step 4) [19].

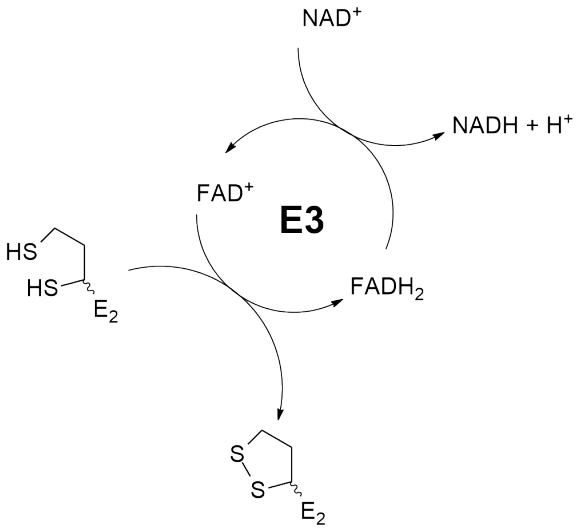

Figure 1.9 E3 catalyzes the restoration of the redox states of the cofactors and the E2 component.

1.7 Applications of OGDHc

1.7.1 As an enzyme for green synthesis

The pharmaceutical, food, detergent, and biofuel industries have reaped the advantages of enzyme catalysis in commercial-scale applications. For complex chemical reactions, the most significant advantages that enzyme catalysis holds over chemical catalysis are the

high regio-, chemo-, and stereoselectivities at which enzymes convert substrate to product [20]. This is the advantage in biological systems; however, they may not be suited for industrial applications. A few common examples of industrially applied enzymes are trypsin, amylase, laccase and lipase in food processing and detergent industries [21–24]. In the pharmaceutical industry, an example of enzyme catalyzed synthesis is sitagliptin, a drug marketed by Merck for type II diabetes treatment [25,26]. The conventional synthesis requires heavy metals, extreme reaction conditions and suffers from low yields. Hence, an R-selective transaminase was evolved to catalyze the synthesis with 99.95% *e.e*. in organic solvent [27–29].

An important example of an intermediate in the organic chemistry and drug industries is CoA linked thioesters. Acyl-CoA and its analogs are important products of α-ketoacid dehydrogenase class of enzymes, such as OGDHc. CoA derivatives are essential and found as intermediates at the crossroads of a variety of metabolic pathways. For example, acetyl CoA is an important link between glycolysis and Krebs cycle [30]. CoA forms thioester linkages with α–keto acid substrates and its terminal thiol. The reactivity of CoA thiol or thioester is diverse. Thiol has a relatively high pK_a (9-10), which makes them good nucleophiles. On the other hand, thioesters are good electrophiles for alcohols, amines, and enolates. Furthermore, a thioester can serve as a nucleophile in its enolate form. This duel character provides versatility for CoA as a cofactor in nature [31]. CoA – linked thioesters can be used as intermediates for organic synthetic purposes. For example, they are precursor to their corresponding carboxylic acid derivatives [32]. Furthermore, they are also key intermediates for peptide coupling [33–35], acyl transfer [36,37], thiol protecting strategies [38] and in organometallic reaction coupling [39]. CoA thioesters are important molecules in the pharmaceutical

industry as reactivity probes, as enzyme inhibitors and as reporter labels [40]. Traditional organic synthetic pathway for acylation of thiols involve the use of acyl sources from carboxylic acids, acid anhydrides or acid chlorides. The reactions proceed in the presence of strong bases such as ethylamine, pyridine or DMAP for refluxing for several hours. The reactions are also supplemented with suitable catalysts such as triflates, CsF, NBS, zeolites, rongalite, lanthanum(III), isopropoxide, Lewis acids, zinc lithium, bis(perfluoroalkylsulfonyl)imide, ionic liquids, titanocene bis(perfluorooctanesulfonate) and dodecylbenzenesulfonic acid for the acylation of thiones. [41]. In conclusion, the synthetic routes are multistep, energy intensive and involve extreme reaction conditions that can be possibly hazardous to the environment.

OGDHc catalyzes the rate limiting step of the Krebs cycle, which is succinyl CoA formation from 2-OG (Figure 2) [2]. As a CoA-dependent enzyme complex it uses the cofactor to bind to carboxylic acids, which are involved in primary and secondary metabolism [31]. OGDHc is able to perform trans-thioesterification as a natural reaction, which is chemically difficult to achieve. The final product of this reaction is a CoA-linked thioester (succinyl-CoA) which is of much interest in pharmaceutical and chemical industries. This makes OGDHc a suitable candidate for one-pot multistep green chemical synthesis under much milder aqueous conditions, thus providing a sustainable and green synthetic chemical pathway. However, being part of a conserved metabolic pathway, such as the Krebs cycle, OGDHc has high substrate specificities at multiple levels at the constituent components. Thus, optimization of the complex is required, to implement it at an industrial level.

1.7.2 Enzyme optimization and engineering

Enzymes catalyze highly specific reactions under mild conditions in aqueous solutions. Therefore, enzymes can be used for environmentally friendly chemical synthesis. However, they require engineering and optimization for industrial process conditions, such as thermostability, organic solvent resistance or altered substrate specificity. Enzyme properties are not coupled. For example, altering the substrate specificity may come at the cost of thermostability. This is especially true for enzymes of conserved pathways, that have specific functions across many species [42,43]. Although the activity and many other properties can be enhanced by accumulation of beneficial mutations over generations of random mutagenesis and screening, it was once believed that it was impossible to create completely novel catalytic activity [44]. One of the earliest approaches to modify enzyme specificity was by rational design [45–47]. This requires in-depth knowledge of crystal structure of the protein and active site configurations. However, the complexity of structure-function relationship of enzymes is a critical limitation to this approach. It is found that enzyme modifications that enhance certain enzyme properties, such as substrate specificity or new catalytic activity, can be located near the active site [48–52]. However, other mutations beneficial for properties such as stability or activity may be far from the active site. It has also been shown that mutations far from the active site can contribute to substrate specificity [53–55]. These mutations would be impossible to predict from rational design.

Directed evolution breaks through this barrier. This idea mimics natural evolution on a single molecule level. First, a parent gene is used to create a library with random mutations. Next, a screening or selection is used to identify protein variants with the

desired properties. Then, the gene is isolated, and it is used as the parent for the next round of laboratory evolution until the optimization is achieved (Figure 1.10).

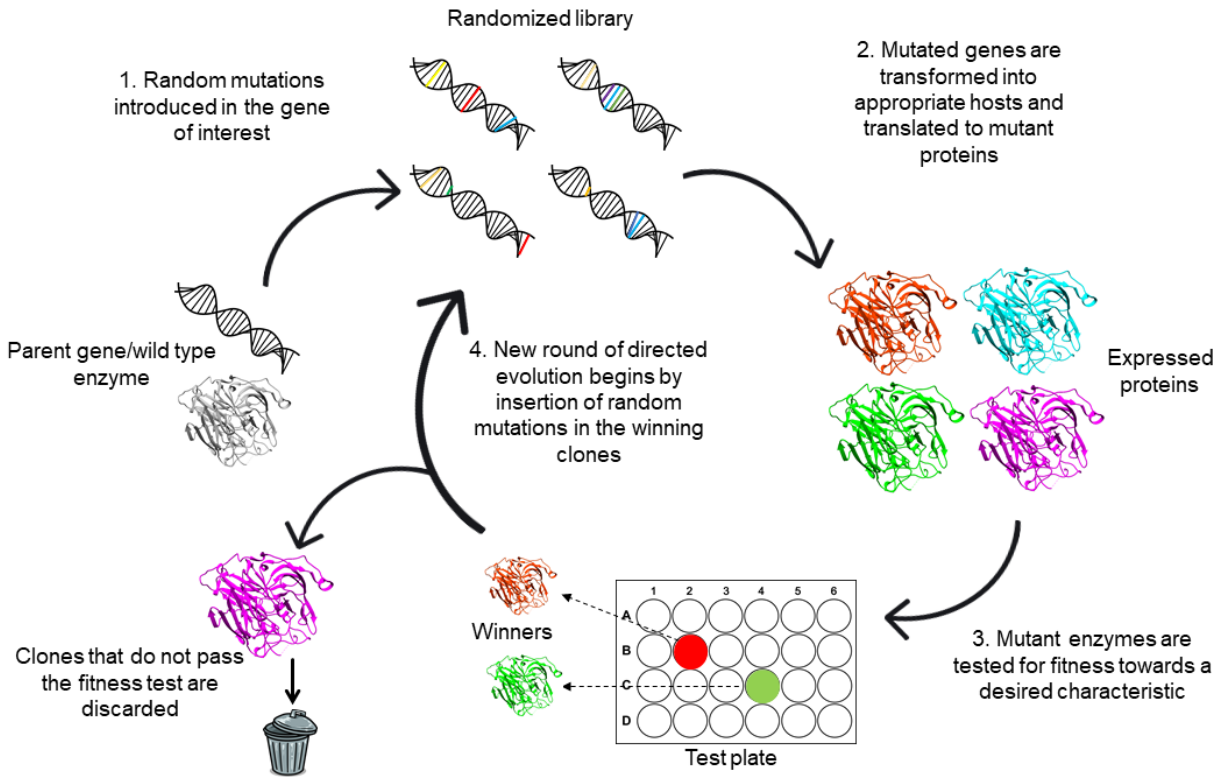

Figure 1.10 Schematic representation of Directed evolution method to evolve proteins.

The major advantage of directed evolution is rapid engineering of enzymes without in-depth structural knowledge. One of the earliest examples was subtilisin evolution in a polar organic solvent dimethyl sulfoxide [56,57]. The final variant had a ~471 fold increased activity over the wild-type under similar conditions [58]. The potential of directed evolution is to be used as a tool to manipulate proteins towards performing reactions that are absent in the biological world. For example, enzymatic formation of carbon-silicon bonds was achieved. This reaction is not found in any biological system. Cytochrome C was evolved to catalyze formation of carbon-silicon

bonds with an efficiency of ~15 times over the best chemical catalyst used for the purpose [59]. In nature, cytochrome C is an electron carrier in the electron transport chain, and it does not perform any catalytic reactions. Rational and directed evolution can complement each other in an engineering strategy. Structure/function knowledge can be used to create focused libraries [60]. For example, saturation mutagenesis can used. Saturation mutagenesis is a method to mutate any amino acid simultaneously to all other 19 amino acids.

1.7 Thesis Objectives

1. Characterization of the critical residues in the active site of E2o catalytic domain that contribute to catalysis and elucidate the mechanism of the succinyl transfer reaction.

The main goal is to understand the contribution of the catalytically important residues in the E2o catalytic domain. It has been established that the human OGDHc activity is linked to Alzheimer's and Parkinson's diseases [61], besides its contribution to cellular disorders related to oxidative stress. The E2o catalytic domain is conserved in all life forms. Mechanistic knowledge provides molecular details of metabolic pathways and the underlining cause of disease.

2. Altering substrate specificity of OGDHc and convert 2-oxo *acid* to a 2-oxo-*aliphatic acid* dehydrogenase complex by engineering E2o.

An important application of OGDHc, is its ability to perform a complex acyl transfer reaction and produce succinyl-CoA. CoA-linked thioester chemical synthesis is a multistep process. Engineered recombinant OGDHc can potentially replace existing synthetic methods with a green method to generate the desired thioester analogs.

CHAPTER 2

CATALYSIS OF TRANS-THIOACYLATION IN THE ACTIVE CENTERS OF DIHYDROLIPOAMIDE ACYLTRANSACETYLASE COMPONENTS OF 2-OXO ACID DEHYDROGENASE COMPLEXES

2.1 Introduction

In the Krebs cycle, the 2-oxoglutarate dehydrogenase complex (OGDHc) catalyzes one of the most important steps, converting 2-oxoglutaric acid (2-OG) to succinyl CoA. OGDHc is composed of multiple copies of three components: (i) 2-oxoglutarate dehydrogenase/decarboxylase (E1o), (ii) dihydrolipoamide succinyl transferase (E2o) and (iii) dihydrolipoamide dehydrogenase (E3). The key metabolic product succinyl-CoA is produced from the catalytic domain of the E2o. In *Escherichia coli*, E2o is a multidomain enzyme: proceeding from the N-terminus it consists of a lipoyl domain(s) (LDo) (~85 amino acids), a peripheral subunit binding domain (PSBD) (~48 amino acids) and a catalytic core domain (CD) (~231 amino acids). The E2o core is composed of 24 subunits that are organized with a 432 point group symmetry, to which both E1 and E3 dimers are attached tightly and non-covalently [1-4]. The organization of the E2 core in OGDHc is specific for each organism [5]. The domains E2o are linked together by flexible 25–30 residue segments rich in alanine, proline, and charged amino acids [62,63]. Chapter 1 outlines the structural organization of the overall complex along with the role of the individual components in the overall reaction. In the current chapter, the kinetic parameters of E2o have been determined to characterize catalysis at the active site of the enzyme.

2.2 E2o Domains

2.2.1 Role of the lipoyl domain

The lipoyl domain is the site of attachment of the prosthetic group, lipoic acid. The attachment of the lipoyl group to the conserved Lys43 at the tip of the protruding β-turn, gives a domain flexibility and reach to the active centres of E1 and E3 (Figure 2.1) [64].

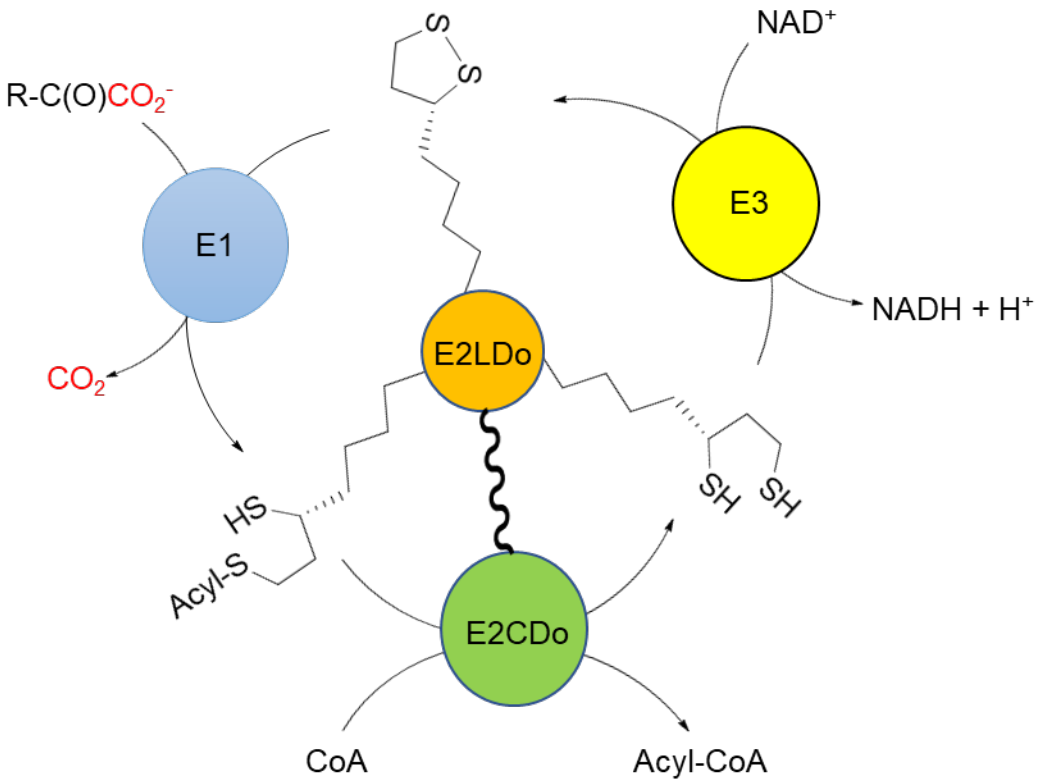

Figure 2.1 General mechanism of the lipoyl domain accessibility to the active sites of E1 and E3 for 2-oxoacid dehydrogenase complexes [65].
The flexible lipoamide arm of the lipoyl domain is able to transport the decarboxylated acyl intermediate from E1 (turquoise) active site to the E2 catalytic domain (green). In the E2CDo, the acyl group is transferred to CoA forming Acyl-CoA. The dithiolane ring of the lipoamide arm gets re-oxidized at E3 (yellow).

The number of lipoyl domain varies from one to three depending on the enzyme complex. In *Escherichia coli* the OGDHc has one lipoyl domain while pyruvate dehydrogenase complex (PDHc) has three [62]. An individual lipoyl domain carries a

lipoyl group in amide linkage with the N-6 amino group of a specific lysine residue forming the swinging arm that ferries substrate (Figure 2.2) [66]. This attachment also limits the diffusion of the dithiolane ring. Only R-enantiomers of the lipoate and dihydrolipoate function with the OGDHc. It is essential for the lipoyl group to be attached to the lipoyl domain for the reductive acylation reaction by the dithiolane ring [11,66]. The ring is at the end of a 1.4 nm swinging arm and is free to rotate with respect to the bulk of the protein.

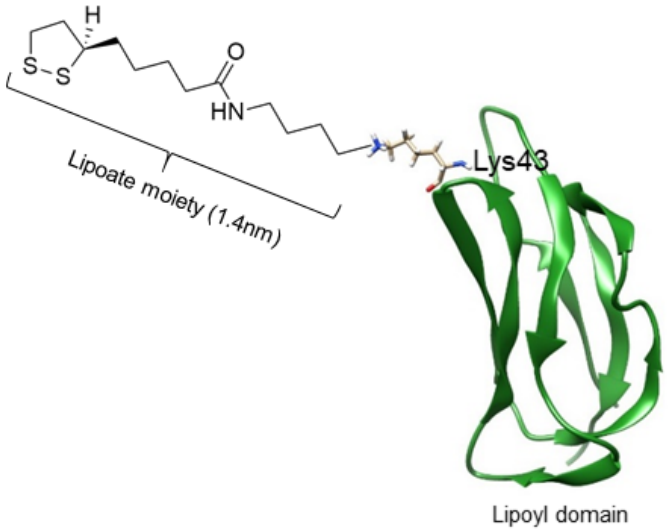

Figure 2.2 Structure of lipoyl domain with the attached lipoyl moiety.
The green ribbon represents a single chain of the lipoyl domain of *E.coli* E2o. The NMR structure is derived from PDB entry 1PMR. The lipoate moiety is shown to be attached with the Lys43 residue of the lipoyl domain. The 1.4nm flexible arm has a dithiolane ring at the end of it.

The enzymes trypsin and lipoamidase have been used as probes to examine the correlation between loss of lipoyl domains or lipoyl moieties versus the loss of overall activity for PDHc and OGDHc. Trypsin digest releases the lipoyl domains that are covalently attached with the lipoyl moieties. In contrast, lipoamidase releases the lipoyl moiety from the lipoyl domain. The results showed that the rate of release of lipoyl

domains (tryptic digests) or lipoyl moieties (lipoamidase digest) was higher than the corresponding rate of loss of overall activity [63,67].

The flexibility of the lipoyl domain confers some process of molecular recognition and interaction between LDo and its cognate E1o component [5]. In recent years, the Farinas and Jordan groups have undertaken studies of the *E. coli* 2-oxoglutarate dehydrogenase complex (OGDHc) with a view to expand the substrate range of the complex and utilize it for green chemo-enzymatic synthesis. The active site of E1o was engineered to accept the non-natural substrate 2-oxovaleric acid (2-OV). However, the overall reaction of the complex did not produce NADH or butyryl-CoA. Mass-spectrometric evidence showed that the E1o active center could reductively acylate the lipoyl domain. This indicated an apparent checkpoint regulation at the active site of E2o catalytic domain. Hybrid complexes with different components of PDHc (E1p, E2p and E3) and OGDHc (E1o, E2o and E3) revealed that E1o could reductively acylate the lipoyl domains of both E2p and E2o. This property was absent in E1p. Hence, it was concluded that substrate recognition occurs at E1p for PDHc and at E1o, E2oLDo and E2oCD for OGDHc [13]. To broaden the synthetic versatility to produce acyl-CoA analogues, it was necessary to bypass the E2o checkpoint. A mechanistic role is proposed for the key catalytic residues at the active site of E2oCD.

2.3 The Catalytic Core Domain of E2o

2.3.1 Active site of E2o core domain

The E2o structure has not been determined. However, the structure of a truncated form (*t*E2o) from *E. coli* has been solved to a 3.0 Å resolution. The *t*E2o structure lacks most of the N-terminal and peripheral domains [9,68]. The *E. coli* E2oCD topology is highly

similar to that of another well-known enzyme of the acyl-transferase family, the chloramphenicol acyl transferase (CAT; EC 2.3.1.28)[69] and *A. vinelandii* E2pCD [15, 16]. Conserved amino acids were found from sequence alignments from various organisms [17].

Structural homology and crystallographic data of CAT and E2oCD suggested a general mechanism of the succinyl transferase reaction occurring at the active site. Also, residues involved in catalysis in the active site had been predicted [71]. An active site histidine (His375) was proposed to be a general-base catalyst. In the first step, His375 was suggested to deprotonate the thiol group of coenzyme A (CoA-SH) [16]. Next, CoA-S^- would attack the carboxylate of the acylated lipoyl moiety (from LDo) to form a tetrahedral intermediate. The collapse of this intermediate results in the transfer of the acyl group to CoA-S^-. The tetrahedral intermediate is stabilized by a threonine residue (Thr323). In addition, an aspartic acid residue (Asp379) assists in the stabilization of the correct tautomer of the catalytically essential histidine (*vide infra*).

The side chain of His375 is oriented 2.5 Å apart with respect to the Thr323 (Figure 2.3b). A salt bridge between Asp374 and Arg376 on the same loop as His375, stabilizes the enzyme-substrate complex. In the E2oCD-CoA complex, the conformation changes the orientation Asp379 to interact with His375 and form a salt bridge with Arg184 of a neighbouring residue. In addition, the side-chain of Arg376 is positioned so that a single hydrogen bond is formed with Asp374 (Figure 2.3b)[16].

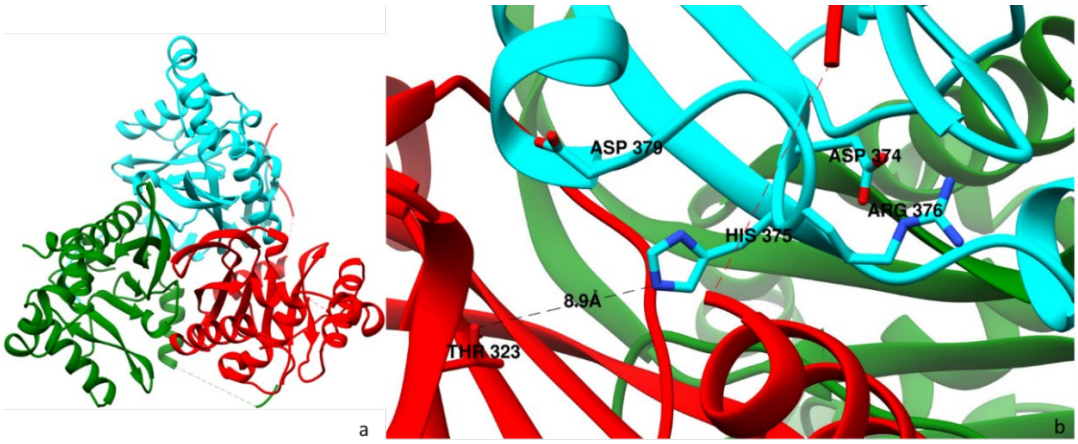

Figure 2.3 *a*, Ribbon drawing showing the crystal structure of the truncated E2o Catalytic Domain trimer with each subunit in a different color ribbon [16]. The three chains of the trimer, viz, chain a, chain b and chain c are represented by red, green and cyan respectively. *b*, active site region at a trimeric subunit interface within the trimer showing positions of active site residues Thr323, Asp374, His375, Arg376 and Asp379 on chain b is shown (PDB ID:1C4T).

2.3.2 Mechanism of the succinyl transferase reaction at the E2o core

Structural homologies

In the superclass family of acyl transferases, sequence alignment studies have been carried out between E2o and E2p derived from the *sucB* and *aceF* genes, respectively. The active site mechanism of these enzymes have been proposed based on their sequence homologies with CAT [71]. The CAT catalyzes the O-acetylation of chloramphenicol in antibiotic resistant bacteria [72,73]. A common feature amongst the CAT, E2o and E2p active sites is the presence of a conserved motif sequence containing the catalytic histidine: His-x-x-x-x-Asp-Gly-x-His (where, x is any amino acid residue).

The catalytically important His375 has been identified in E2o and His602 for E2p, corresponding to the catalytic His195 in CAT (Figure 2.4). The latter has been extensively studied and kinetically characterized by Shaw and Leslie [74,75].

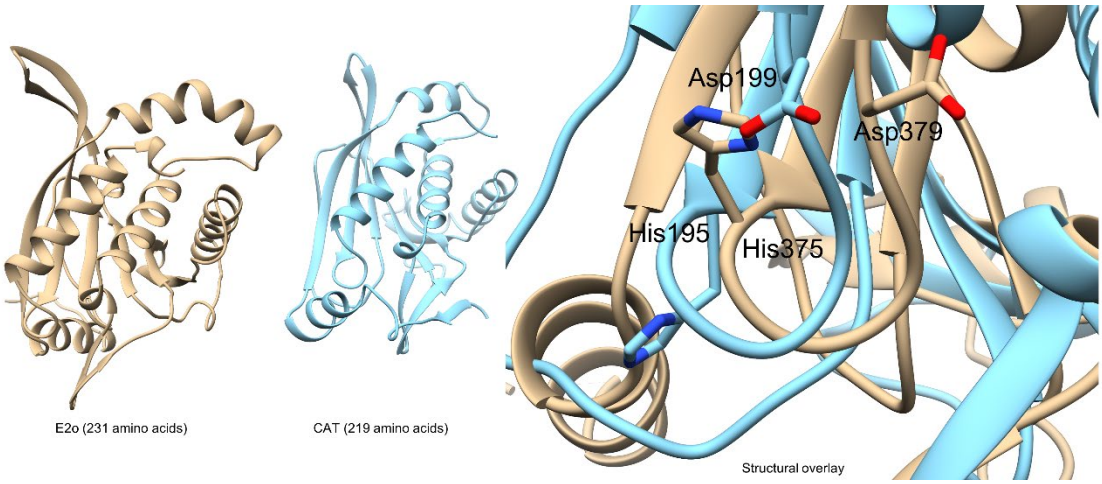

Figure 2.4 Comparison of the crystal structure of monomeric chloramphenicol acetyl transferase (PDB ID: 1CIA) and E2o dihydrolipoamide succinyl transferase catalytic domain, chain a (PDB ID: 1C4T).
The crystal structure superposition of CAT and E2oCD reveals catalytic His195 and Asp199 are located on the same loop for CAT as the corresponding His375 and Asp379 for E2oCD.

2.3.3 Comparative acyl transfer mechanism site of the acyltransferase superfamily

The role of the active site histidine E2o-His375 has been predicted based on CAT-His195, which serves as a general base. Evidence of formation of hydrogen bond between N-1 proton of His195 and the carboxylate of another conserved aspartate residue (Asp199) had been reported [75]. This confers tautomeric stabilization that possibly allows the electron pair at N-3 to abstract a proton from the 3-OH group of chloramphenicol to promote a nucleophilic attack on the thioester of CoA (Figure 2.5, for CAT) [76]. A similar mechanism had been proposed for E2oCD active site catalysis. The conserved E2o-Asp379 plays a similar role as CAT-Asp199 (Figure 2.4). The N-3 of His375-imidazole abstracts a proton from CoA-SH. This triggers the nucleophilic attack on the carbonyl carbon of the dihydrolipoamide succinyl group. This forms the tetrahedral oxyanionic intermediate which is stabilized by a third catalytic residue Thr323 (Figure 2.5 for E2oCD) [71].

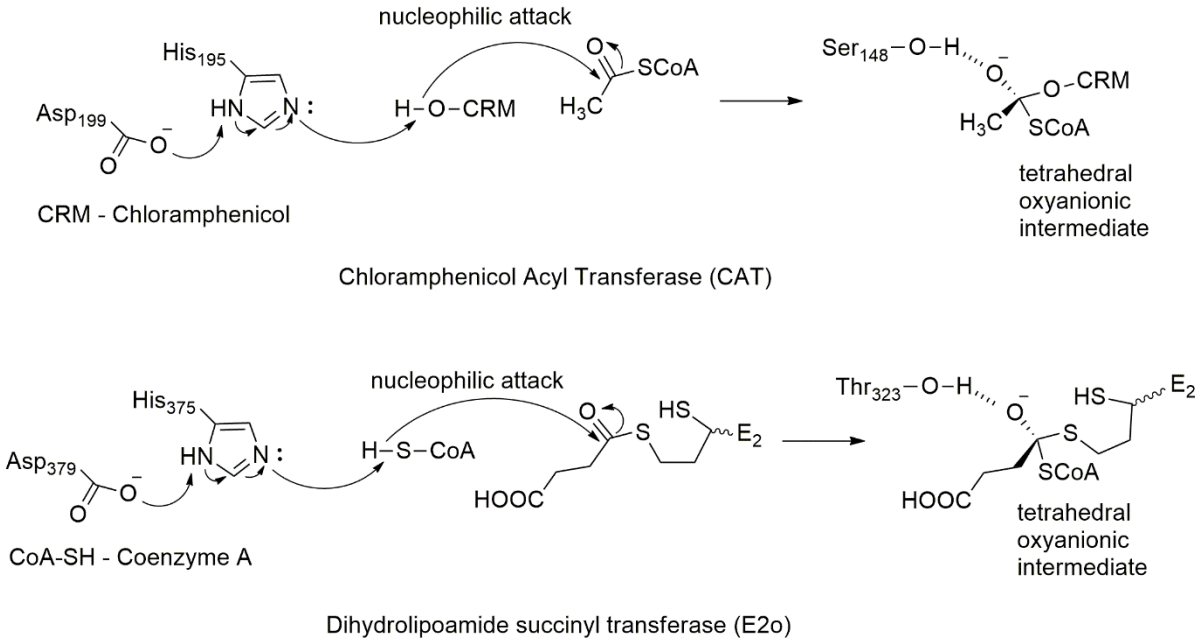

Figure 2.5 *Top*. The proposed mechanism involving the catalytic His375 at the active site of E2o core domain. His375 is proposed to be a general base catalyst in the succinyl transferase reaction.
Bottom. The mechanism of catalytic His195 at the active site of chloramphenicol acyl transferase. His195 is a general-base catalyst in the acyl-transferase reaction [16,72].

2.4 Importance of Studying the E2o-Active Site Mechanism and the Objectives of this Study

Recent studies revealed multiple roles for the mitochondrial OGDHc, and a better understanding of their mechanism could be important for bringing new insight into human diseases. The unique property of the mitochondrial OGDHc to produce the reactive oxygen species superoxide and hydrogen peroxide (H_2O_2) from its substrate 2-OG had been attributed earlier to the flavin cofactor tightly bound to the E3 component [77,78]. Jordan group studies revealed that human E1o (hE1o) can produce the ThDP-enamine radical and superoxide anion from 2-OG and from the next higher homologue 2-oxoadipate (2-OA) by one-electron oxidation of the ThDP-enamine intermediate with dioxygen [79,80]. The efficiency of superoxide/H_2O_2 production by OGDHc was 7 times

larger from 2-OA than from 2-OG making the OGDHc one of the important reactive oxygen species producers among 2-oxo acid dehydrogenase complexes in mitochondria [78,80].

In a role different from its role in the TCA cycle, the OGDHc could also serve as a producer of succinyl groups in neurons and neuronal cell lines for reversible post-translational modification of the cytosolic and mitochondrial enzymes, including those from the TCA, by succinylation, hence playing a role in neurodegenerative diseases [81]. The post-translational modification of histone proteins by succinylation is regarded as very important because it can directly regulate gene expression [82,83]. Recently, evidence of the interaction between the nuclear OGDHc and lysine acetyltransferase 2A displayed a role of lysine acetyltransferase as a carrier of succinyl groups produced by nuclear OGDHc for direct histone H3 succinylation [82].

Studies from the Jordan group suggested that human 2-oxoadipate dehydrogenase (hE1a, also known as *DHTKD1*-encoded protein), which is involved in the oxidative decarboxylation of 2-oxoadipate to glutaryl- CoA on the final degradative pathway of L-lysine, L-hydroxylysine, and L-tryptophan, has recruited the hE2o and hE3 components of the OGDHc for its function [84]. In other words, the hE2o could serve as a source of both succinyl-CoA and glutaryl-CoA in mitochondria and could be linked to the lysine post- translational modification by glutarylation earlier reported [85].

The enzymatic mechanism being studied in this research is responsible for synthesis of important acyl- CoA metabolites involved in post-translational modification of proteins. The results provide important baseline residue-specific contribution to catalysis of succinyl-CoA formation in the active center of the *E. coli* E2o that would be applicable to all E2o components due to high sequence identities reported for all E2o

core/catalytic domains [16,17,19,70,86–88]. The major goal of this study was to address the role of the highly conserved His375 in the active center of the *E. coli* E2o. The His375Ala substitution was found to decrease the catalytic efficiency (k_{cat}/K_m, 2-OG) by 54-fold compared to unsubstituted E2o. This value was approximately 10 000 times smaller than that deter- mined on Ala substitution of the corresponding His195 in chloramphenicol acetyltransferase (CAT, k_{cat}/K_m = 53 x 10^{-4}-fold smaller for the His195Ala variant than wild-type) [75], placing in doubt the earlier deduction of an acid–base catalyst role of His375, assigned by comparison with CAT [71,89]. To gain more insight regarding the function of His375, site-saturation mutagenesis was carried out at this residue, whose results suggested that the His375Trp and His375Gly substitutions at E2o were acceptable, reducing the catalytic efficiency only by two- and five- fold, respectively. Similarly, the Asp374Asn substitution in the E2o active center (10 times less efficient variant) rescued some of the activity displayed by the Asp374Ala substitution (54-times less efficient variant), consistent with participation of Asp374 in hydrogen bond formation. The totality of the current studies suggested that there is no proton transfer in the rate-limiting step in which both His375 and Asp374 participate (Figure 2.6); rather, they may stabilize by hydrogen bonds a transition state, probably resembling a tetrahedral oxyanionic intermediate.

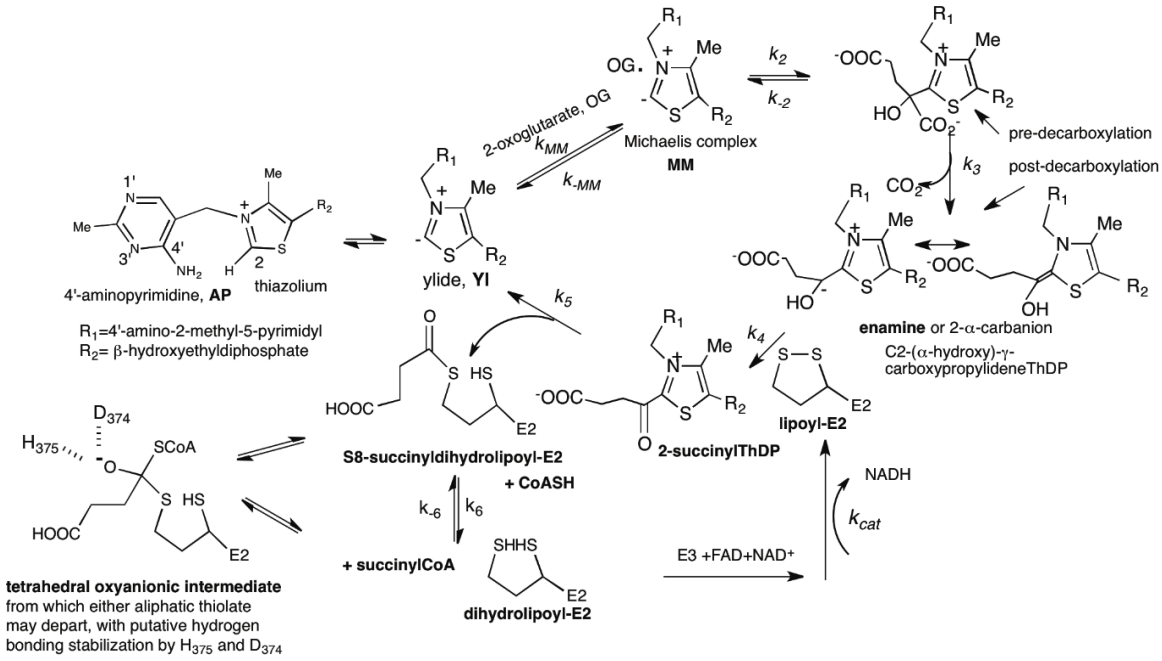

Figure 2.6 Mechanism of 2-oxoglutarate dehydrogenase complex and the putative oxyanionic tetrahedral intermediate suggesting the role of His375 and Asp374 in E2o active center [90].

2.5 Materials and Methods

2.5.1 Reagents

Dithiothreitol (DTT), 2-oxoglutarate, 2-oxovalerate, 2-oxoadipate, and pyruvate were from Sigma-Aldrich (St. Louis, MO, USA). NADH, CoA, isopropyl-β-D-thiogalactopyranoside (IPTG), DNase I, micrococcal nuclease, DL-α-lipoic acid, and ThDP were from Affymetrix (Cleveland, OH, USA). Protease inhibitor cocktail tablets were from Roche Diagnostics GmbH (Mannheim, Germany). Ni-Sepharose 6 Fast Flow and HiPrep^{TM} 26/60 Sephacryl^{TM} S-300 HR column were from GE Healthcare (Pittsburgh, PA, USA). QuikChange Site-Directed Mutagenesis Kit was from Agilent Technologies (Santa Clara, CA, USA). Primers for site-directed mutagenesis were from Fisher Scientific (Pittsburgh, PA, USA). *Escherichia coli* strain JW0715 containing the pCA24N plasmid encoding the E1o component and JW0716 containing pCA24N plasmid

encoding the E2o component were obtained from National Bio Resource Project (NIG, Japan). AG1 cells (Agilent Technologies) were used as host cells.

2.5.2 Protein Expression and Purification

2.5.2.1 Expression and purification of E1o. Expression and purification of E1o was as reported earlier with some modifications [13,91,92]. The E1o component was purified using a Ni-Sepharose 6 Fast Flow column equilibrated with 20 mM KH_2PO_4 (pH 7.5) containing 0.20 M KCl, 0.20 mM ThDP, 1.0 mM $MgCl_2$, 1.0 mM benzamidine·HCl (buffer A) and 30 mM imidazole. After the protein was applied to the column, the column was washed with 500 mL of 30 mM imidazole and then with 500 mL of 50 mM imidazole, both in buffer A. The E1o was eluted with 150 mM imidazole in buffer A and was dialyzed against 2000 mL of 20 mM KH_2PO_4 (pH 7.5) containing 0.35 mM KCl, 0.20 mM ThDP, 1.0 mM $MgCl_2$, and 1.0 mM benzamidine ·HCl for 15 h at 4 ºC. For E1o storage, buffer was exchanged to 20 mM KH_2PO_4 (pH 7.5) containing 0.20 M KCl, 0.20 mM ThDP and 1.0 mM $MgCl_2$ by ultrafiltration using a concentrating unit with a cut-off of 30 kDa. The E1o was stored at -80 ºC.

2.5.2.2 Expression and purification of the E2o and its variants. Expression and purification of E2o was as reported earlier for human E2p with some modifications [18,19]. AG1 cells were grown in LB medium supplemented with 35 μg/mL of chloramphenicol and protein expression was induced by 0.50 mM IPTG for 5 h at 37 ºC. Harvested cells were resuspended in 20 mM KH_2PO_4 (pH 7.5) containing 0.30 M NaCl, 1 mM benzamidine·HCl, 1 mM DTT, and two protease inhibitor cocktail tablets. The resulting cell suspension was incubated with lysozyme (0.60 mg/mL) for 20 min on ice. Next, $MgCl_2$ (5 mM) and 1000 U each of DNase I and Micrococcal Nuclease were

added, and the cells were incubated for an additional 20 min on ice. Cells were then disrupted by ultrasonication at a setting of 6 using 10 s pulse 'on' and 30 s pulse 'off 'for total time of 5 min. PEG-8000 (50% w/v) was added drop-wise to the clarified lysate to 6% (v/v) and the precipitated pellet was dissolved in 20 mM KH_2PO_4 (pH 7.5) containing 0.30 M NaCl, 1 mM DTT, 1.0 mM benzamidine·HCl and 1 mM EDTA. The E2o was purified using a Sephacryl S-300 High Resolution size-exclusion column equilibrated with 20 mM KH_2PO_4 (pH 7.5) containing 0.30 M NaCl, 1 mM DTT, 1.0 mM benzamidine·HCl and 1 mM EDTA. Fractions containing E2o according to PAGE were collected and E2o was precipitated by ultracentrifugation for 4.0 h at 140,000 *g*. The pellet was dissolved in 20 mM KH_2PO_4 (pH 7.5) containing 0.40 M NaCl, 0.50 mM EDTA, 1,0 mM DTT and 1.0 mM benzamidine·HCl for 15 h at 4 ^oC. The clarified E2o was stored at -80 ^oC.

The E2o variants with Thr323Ala, Thr323Ser, Asp374Ala, Asp374Asn, His375Ala, His375Cys, His375Asn, Arg376Ala, and Asp379Ala substitutions were created using the pCA24N-E2o plasmid as a template and two synthetic oligonucleotide primers complementary to the opposite strands of the DNA with Quik-Change site-directed mutagenesis kit and Protocol supplied by the manufacturer (Stratagene, La Jolla, CA). The following oligonucleotide primers and their complements were used (mismatched bases are underlined, and mutated codons are shown in boldface type):

5'-AACTTCACCATC**G**C**G**AACGGTGGTGTGTTCGGTTCC-3**'** (Thr323Ala),

5'-AACTTCACCATCA**G**CAACGGTGGTGTGTTCGGTTCC-3' (Thr323Ser)

5'-CTGGCGCTGTCCTAC**GCG**CACCGTCTGATC-3' (Asp374Ala)

5'- GGCGCTGTCCTAC**A**A**C**CACCGTCTG-3' (Asp374Asn)

5'-GCGCTGTCCTACGAT**GCG**CGTCTGATCGAT-3' (His375Ala)

5’-GCGCTGTCCTACGAT**TG**CCGTCTGATCGAT-3’ (His375Cys)

5’-GCTGTCCTACGAT**A**ACCGTCTGATCG-3’ (His375Asn)

5’-TCCTACGATCAC**GCG**CTGATCGATGGTCGC-3’ (Arg376Ala)

5’-CACCGTCTGATC**GCG**GGTCGCGAATCCGTG-3’ (Asp379Ala)

5’-GGCGCTGTCCTACGAT**NNS**CGTCTGATCG-3’ (His375X) where N = A/T/G/C and S = G/C

The presence of substitutions was verified by DNA sequencing with specific primers at the Molecular Resource Facility of Rutgers New Jersey Medical School (Appendix B).

2.5.2.3 Expression and purification of LDo and E2o $^{1\text{-}176}$ didomain. Expression and purification of the E2o lipoyl domain (LDo, residues 1-105 in E2o) and E2o$^{1\text{-}176}$ didomain was as reported earlier for *E. coli* LDp and E2p$^{1\text{-}190}$ [19,93]. The representation of the individual domains that were used for the experiments are described in Figure 2.7. To ensure full lipoylation of the LDo and E2o$^{1\text{-}176}$ di-domain, these E2o derived domains were lipoylated *in vitro* by an *E. coli* protein lipoyl ligase as reported earlier [91]. Lipoylation of each E2 derived domain was confirmed by FT-MS (data not shown).

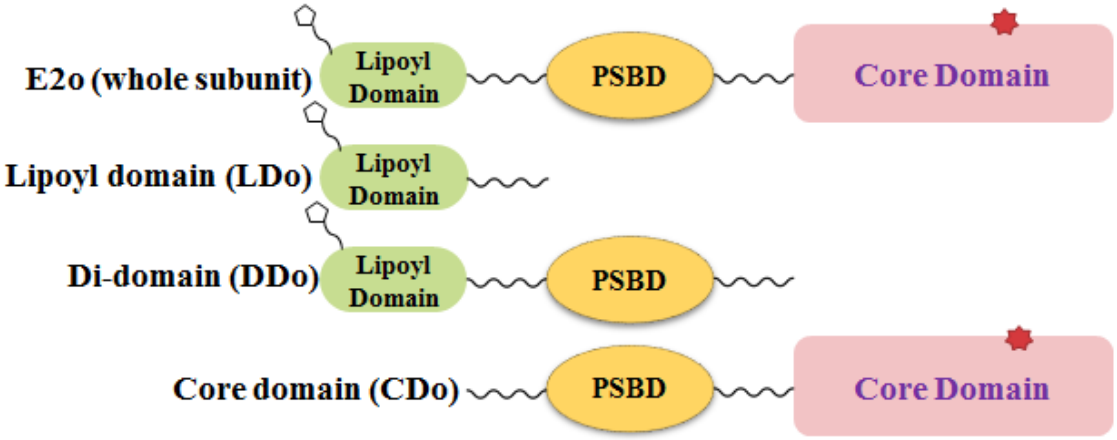

Figure 2.7 E2o Constructs that were used for the experiments. Each of the constructs were expressed separately, and the recombinant proteins were purified before subsequent activities were measured.

2.5.2.4 Expression and purification of the E2o catalytic domain and its His375Ala and Asp374Ala variants. For expression of the CDo, DNA encoding residues 93 – 404 corresponding to catalytic domain (Figure 2.7) [16], subunit binding domain and linker connecting them in wt-E2o was synthesized and was cloned into pD451-SR vector by DNA 2.0 Inc. (Menlo Park, CA). DNA encoding CDo with His_6 tag at the C-terminal end was introduced into BL21 (DE3) cells (Novagen) and cells were grown in LB medium supplemented with 35 μg/mL of kanamycin at 37 ºC overnight. 15 mL of the overnight culture was inoculated into 800 mL of the LB medium supplemented with kanamycin (35 μg/mL) and cells were grown to OD_{600} of 0.5-0.6 at 37 ºC, and then IPTG (0.5 mM) was added, and cells were grown for an additional 5 h at 37 ºC. The cells were then washed with 50 mM KH_2PO_4 (pH 7.5) containing 0.15 M NaCl and were stored at -20 ºC. The harvested cells were resuspended in 20 mM KH_2PO_4 (pH 7.5) containing 0.30 M NaCl, 1 mM benzamidine·HCl, 1 mM DTT, and two protease inhibitor cocktail tablets. Cells were treated with lysozyme (0.6 mg/mL) at 4 ºC for 20 min and then with DNase I (NEB) and Micrococcal Nuclease (NEB) (1,000 units of each) for an additional 20 min at 4 ºC. Cells were disrupted by a sonic dismembrator with 10 s pulse "on" and 30 s pulse "off" for 5 min. The supernatant was centrifuged at 30,000 *g* for 20 min. The clarified lysate was loaded onto a 10 ml Ni-Sepharose 6 Fast Flow column (GE Healthcare) pre-equilibrated with 20 mM KH_2PO_4 (pH 7.5) containing 0.30 M NaCl, 1.0 mM benzamidine·HCl and 10 mM imidazole. The column was first washed with 35 mM imidazole in the same buffer solution. The CDo was eluted with 150 mM imidazole. The fractions containing CDo were dialyzed against 2,000 ml of 20 mM KH_2PO_4, containing 0.45 mM NaCl and 1.0 mM benzamidine·HCl by overnight at 4 ºC. The CDo was

concentrated by ultrafiltration with a 10 kDa MW cut off concentrating unit and was stored at -80 ^{o}C.

For construction of Asp374Ala and His375Ala CDo variants, the pD451-SR plasmid encoding CDo was used as a template, and the amplification primers 5'-GCGCTGTC-CTACGAT**GCG**CGTCTGATCGAT-3' (for His375Ala) and 5'-CTGGCGCTGTCCTA-C**GCG**CACCGTCTG ATC-3' (for Asp374Ala) and their complements were used for site-directed mutagenesis (the mismatched bases are underlined and mutated codons are shown in boldface type). The QuikChange site-directed mutagenesis kit was used for single-site substitution (Figure 2.7) (Stratagene, La Jolla, CA).

2.5.2.5 Expression and purification of E3. Expression and purification of E3 was carried out exactly following published protocols by the Jordan group [18].

2.5.3 Enzyme Activity Measurement

Overall OGDHc activity was measured in the reaction assay as reported earlier [13]. For OGDHc assembly, E1o in 20 mM KH_2PO_4 (pH 7.0) containing 0.15 M NaCl was assembled with independently expressed E2o and E3 components with a mass ratio of E1o:E2o:E3 of 1:1:1 (μg/μg/μg) for 20 min at 25 ^{o}C. Reaction was initiated by 2-OG (2 mM), or pyruvate (25 mM), or 2-OV (45 mM), and CoA (0.13 mM).

In the OGDHc assay with CDo and LDo replacing E2o, the E1o (60 μg, 1.4 μM subunits) in 50 mM KH_2PO_4 (pH 7.0) was first preincubated with independently expressed CDo or CDo variants (60 μg, subunits 4.9 μg) and E3 (60 μg, 2.9 μM subunits) at a mass ratio of 1:1:1 (μg: μg: μg) at 25 ^{o}C. An aliquot with 5 μg of E1o (0.11 μM subunits) was then withdrawn and was mixed with varying concentrations of LDo in a

cuvette containing all components needed for OGDHc assay. After 1 min of equilibration at 30 ºC, the OGDHc reaction was initiated by the addition of 2-OG (2 mM) and CoA (0.13 mM) as above.

2.5.4 Site Saturation Mutagenesis in the E2o Core Domain on the His375 Residue

Creation of the mutagenic library.

The site saturation mutagenesis technique was used to create a library at the His375 position in the E2o core domain using a modified procedure for QuikChange Site directed mutagenesis kit and using NNS primers:

5'-GGCGCTGTCCTACGAT**NNS**CGTCTGATCG-3' (His375X) where N = A/T/G/C and S = G/C. The pCA24N-E2o wild-type plasmid DNA was used as template. A typical 50 mL reaction contained 10x PfuUltra buffer, dNTP (0.2 mM) and PfuUltra DNA polymerase (1U), pCA24N encoding E2o as template, and NNS primers listed above. The PCR reaction consisted of 16 cycles at 95 °C for 30 s, 55 °C for 1 min and 68 °C for 10 min. After the PCR, *Dpn*I was added to the reaction mixture and then PCR product was transformed into *E. coli* BL21 (DE3) competent cells and plated on LB-agar plate containing 30mg/ml chloramphenicol and was incubated overnight at 37 ºC. The transformants were emulsified and stored as 20% glycerol frozen stocks at -80 ºC.

Growth and expression

The library was plated onto an LB-Agar plate containing chloramphenicol antibiotic (50 µg/ml) to obtain single colonies. Approximately 270 single colonies were picked and inoculated into a 96-well plate containing LB medium and chloramphenicol (50 µg/ml) to make master plates. The master plates were incubated at 37 ºC at 250 RPM. Next, duplicate plates were constructed by inoculating (50x dilution) deep well plates that

contained 1 ml LB media, chloramphenicol, *d,l*-lipoic acid (0.3 mM) and IPTG (1 mM) for E2o. The deep-well plates were incubated at 37 ºC at 250 RPM. The cells were centrifuged at 1600 *g* and the media was discarded. The cell pellets were stored -20 ºC until use. The cell pellets were resuspended and lysed in a buffer containing KH_2PO_4 (20 mM), NaCl (0.15 M), DTT (1 mM), protease inhibitor cocktail tablet, lysozyme (1 mg/ml), DNAse (0.1 mg/ml) and incubated for 1 h at 37 ºC. The lysate was centrifuged twice at 1600*g* for 30 min and the clarified supernatant was used for the subsequent steps.

The E1o and E3 components were over-expressed separately each in 1.6L culture medium following published protocols and lysed [18]. The lysates of E1o, E2o and E3 were reconstituted in a 96 well plate (total volume 300 µl) buffer containing KH_2PO_4 (20 mM), NaCl (0.15 M), $MgCl_2$ (1 mM) and ThDP (0.1 mM) in a ratio of 1:2:1 as per OD_{600nm}/µl for 1 h and mixed well. The first column on the plate was the wild-type OGDHc complex as shown in the Figure 2.8, represented by the screen section.

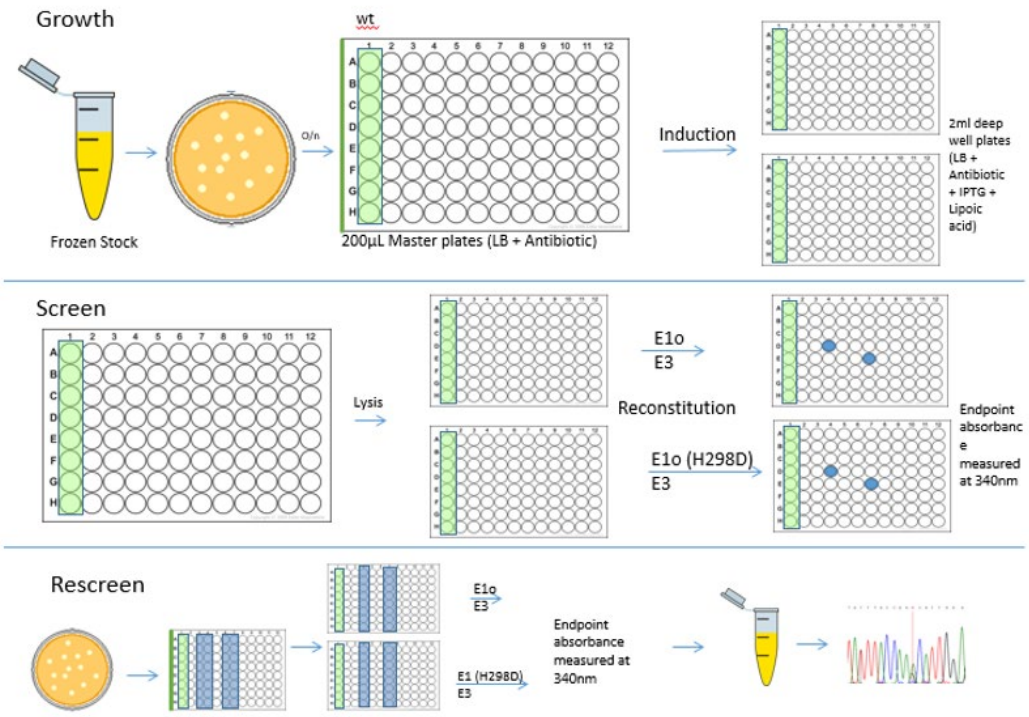

Figure 2.8 Schematic representation of the steps followed for high-throughput screening assay.

Screen and validation

The overall activity was measured in a 200 µl flat-bottomed 96-well plate containing 0.1 M Tris-HCl (pH 8.0), $MgCl_2$ (1 mM), ThDP (0.1 mM), DTT (2.6 mM), NAD^+(2.5 mM), CoA (0.13 mM) and substrate OG (5-10 mM). NADH production was measured by the initial rate of reaction at 340 nm. The reaction was initiated using 60 µl of the reconstituted complex. The endpoint at 340 nm was measured with a plate reader (Spectramax ® M2 UV-Vis) after 2, 5, 7 and 10 min.

Those E2 variants were chosen that had similar or higher activity than the wild-type [(OD 340 $_{\text{final variant x}}$ - OD340 $_{\text{initial variant x}}$) / (OD340 $_{\text{final wt}}$ - OD340 $_{\text{initial wt}}$)]. The candidates were re-screened, and the positive variants were sequenced.

The rescreening conditions were identical to the screening assay with a minor modification (Figure 2.8, re-screen). First, identified clones were traced back to the master plate and re-streaked on an LB-agar plates containing chloramphenicol (50 μg/ml). The first column was reserved for wild-type and 2 columns or 16 colonies from a single E2-variant were inoculated into a 96 well plate containing LB medium and antibiotic. The false positives were discarded (Figure 2.8). The positive clones were sequenced, overexpressed, and purified following the same protocol for E2o as described above. Next, the purified E2 variants were reconstituted with purified E1o and E3 and kinetic parameters were determined.

2.5.5 Fluorescence Spectroscopy

To determine the dissociation constant of CoA and succinyl-CoA with the E2o His375Trp variant, to the protein (0.24 mg/mL, concentration of active centers of 3.5 μM) in a mixture of 50 mM KH_2PO_4 and 50 mM Tris (pH 8.0), containing 0.1 M NH_4Cl, 1 mM DTT and glycerol (1% v/v) was added CoA (3-570 μM) or succinyl-CoA (5-380 μM), and the fluorescence spectra were recorded after each addition at 25 °C using a Cary Eclipse spectro-fluorimeter. The excitation wavelength was 295 nm, and the emission spectra were recorded in the range of 300-450 nm in 3 mL quartz cuvettes. The K_d values for CoA were calculated using Equation 2.1.

$$(F_o - F_i) / F_o = (\Delta F_{max} / F_o[\text{CoA}]^n) / (S_{0.5}{}^n + [\text{CoA}]^n) \quad (2.1)$$

where $(F_o - F_i) / F_o$ is the relative fluorescence quenching following the addition of CoA or suc-CoA, n is the Hill coefficient, and for $n = 1.0$, the value of $S_{0.5}$ is equal to K_d.

2.5.6 Reductive Succinylation of the LDo by E1o and OG

For this experiment, the LDo (100 μM) was incubated with E1o (0.015 μM) in 35 mM $(NH_4)_2CO_3$ (pH 7.5) containing 0.50 mM $MgCl_2$ and 0.1 mM ThDP. The reaction was started by addition of 2 mM of 2-OG. Aliquots of 10 μL were withdrawn at times of 5-600 s and were diluted into 1 mL of 50% methanol and 0.1% formic acid to stop the reaction. Samples were analyzed by ESI FT-MS. The fraction of succinylated LDo at different times was determined by taking a ratio of the relative intensity of the mass of the succinylated form to the total relative intensity (sum of unsuccinylated and succinylated LDo). The time dependence of this fraction was plotted, and the data were fitted to a single exponential (Equation 2.2) using Sigma Plot 10.0. The rate constant was calculated from the linear fit to the initial rate conditions.

$$f = f_o + f_1 \times (1-e^{-kt}) \quad (2.2)$$

2.5.7 Succinyltransferase Reaction of the CDo and its His375Ala and Asp374Ala Variants in the Reverse Direction

The following protocol outlines simultaneous detection of succinylated and unsuccinylated LDo forms when CDo was used as catalyst in the reverse reaction. The reaction mixture in 300 μL of the 35 mM NH_4HCO_3 (pH 7.5) contained the following: 40 μM LDo lipoylated *in vitro*; 0.10 mM TCEP to keep LDo in the reduced form; 0.15 mM succinyl-CoA, and 0.05 μM CDo. The reaction was started by addition of CDo after 40 s of equilibration of the reaction assay and was conducted at 30 ^oC. Aliquots of 20 μL were withdrawn at times of 5-120 s and were diluted into 1 mL of 50% methanol and 0.1% formic acid to quench the reaction. Samples were analyzed by ESI FT-MS. The fraction of succinylated LDo at different times was determined by taking a ratio of the relative

intensity of the mass corresponding to the succinylated form to the total relative intensity (sum of intensities for the unsuccinylated and succinylated LDo). The time dependence of this fraction was plotted, and data were fitted to a single exponential (Equation 2.2) using Sigma Plot 10.0. The rate constant was calculated from the linear fit to the initial rate conditions.

2.6 Results and Discussion

2.6.1 Reductive Succinylation of the Lipoyl Domain by E1o and 2-OG is not the Rate-Limiting Step in the OGDHc Reaction

Reductive succinylation of the lipoyl moiety covalently attached to the lipoyl domain on E2o is the final step involving ThDP-bound covalent intermediates formed on the first E1o component of the OGDHc. It is a concomitant oxidation of the 2-OG derived enamine and reductive acylation of E2o (Figure 2.7, for C-terminally truncated E2o proteins created by DNA manipulations and employed in these experiments). According to Figure 2.6, the S8-succinyldihydrolipoyl-E2o is the product of the reductive succinylation of the lipoyl-E2o by E1o and 2-OG [94]. Next, transfer of the succinyl group from the thiol ester of S8-succinyldihydrolipoyl-E2o to CoA takes place exclusively at the E2o core domain active centers (Figure 2.3), so there is no oxidation–reduction involved in succinyl transfer, rather it represents a conversion of one thiol ester to another.

Earlier, an appropriate model reaction was developed [91] to study the rate of reductive acetyl transfer from *E. coli* pyruvate dehydrogenase (E1p) to the lipoyl domain of the dihydrolipoyl transacetylase (E2p), which maintains both the chemistry and the intercomponent communication due to its specific recognition of E1p [95–97]. The

method developed takes advantage of the ability to detect and quantify LD-E2p and acetyl-LD-E2p simultaneously in the quenched reaction mixtures using Fourier transform mass spectrometry (FT-MS). Analogously, the reductive succinylation of LDo by E1o and OG under steady-state conditions here examined provides an appropriate model reaction to study the communication between the E1o and E2o components. The LDo employed in these studies was fully lipoylated *in vitro* by *E. coli* lipoyl protein ligase (see Materials and methods), and lipoylation was con- firmed by FT-MS [91]. Two LDo forms were identified by FT-MS: an LDo form with mass of 11421.2 Da that correlates well with the theoretical mass of LDo = 11420.4 Da, and an LDo form with mass of 11435.2 Da that differs from the previous form by 14 Da, possibly due to methylation of His_6-tag as reported in the literature [98]. Both LDo forms could be nearly completely reductively succinylated by E1o and OG (>90% succinylation) (Figure 2.9a), leading to an LDo form with mass of 11523.2 Da (increase in mass by 102 Da on succinylation, the theoretical mass = 11522.4 Da), and LDo form with mass of 11537.2 Da. An average (based on three experiments) rate constant of 99 s^{-1} could be calculated from a steady-state experiment for reductive succinylation of LDo (see Fig. 2.9a for a typical experiment) and was approximately twice as large as the k_{cat} of 48 s^{-1} determined from the overall OGDHc activity measurements in Table 2.1. These data indicate that with a sufficient amount of LDo in the reaction assay, the succinyl transfer from E1o to E2o is not a rate-limiting step (48 s^{-1} is k_{cat} for overall activity vs. 99 s^{-1} for reductive succinylation). Importantly, the substrate analogues, 2-OA ($k_{glutarylation}$ = 22 s^{-1}), 2-OV ($k_{butyrylation}$ = 0.0084 s^{-1}), and pyruvate ($k_{acetylation}$ = 0.048 s^{-1}), could also be used by E1o as substrates for reductive acylation of LDo; however, their efficiency was lower than that with 2-OG (see Figures 2.9a for 2-OG and 2.9b for 2-OA). Finally, this model reaction is

an important control to assure that the acyl group derived from 2-OG on E1o could be transferred to LDo before acyl-CoA formation in the active centers of E2o and could lead to determination of the catalytic rate constants for acyl transfer.

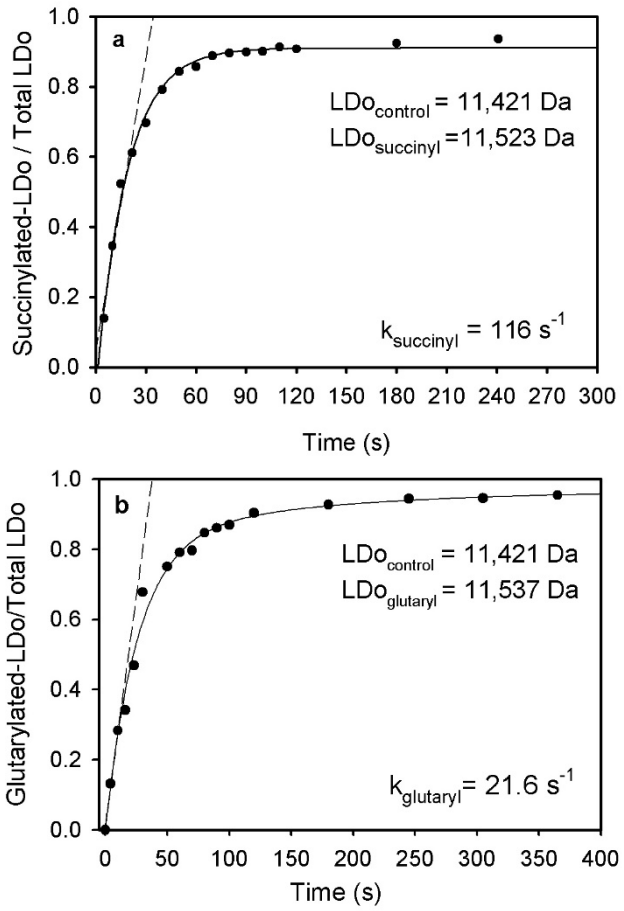

Figure 2.9 Time dependence of the reductive acylation of LDo by E1o and 2-oxoglutarate or 2-oxoadipate.

a. The reductive succinylation of the LDo by E1o and OG. LDo (100 μM), E1o (0.048 μM active centers), 0.1 mM ThDP, and 0.5 mM $MgCl_2$ in 35 mM NH_4HCO_3 (pH 7.5) were mixed with 2 mM OG. At time interval (5- 240 s), aliquots of 10 μL were withdrawn and were quenched into 1 mL of 50% methanol and 0.1% formic acid. Samples were analyzed by FT-MS. **b.** The reductive glutarylation of the LDo by E1o and OA. The LDo (100 μM), E1o (0.075 μM active centers), 0.10 mM ThDP and 0.5 mM $MgCl_2$ in 35 mM NH_4HCO_3 (pH 7.5) were mixed with 2.5 mM OA. Samples were analyzed by FT-MS. The relative intensity of the acylated *versus* total LDo (sum of acylated and unacylated) was plotted *versus* time. The trace is a nonlinear regression fit to a single exponential rise to maximum (see Equation 2.3), and the *dashed line* represents a linear fit to initial rate conditions. The rate constants were calculated from the initial slope.

Table 2.1 Kinetic Parameters of E2o and its Active Center Variants Assembled into OGDHc

E2o Variant	OGDHc activity [a] ($\mu mol \cdot min^{-1} \cdot mg^{-1}$)	k_{cat} (s^{-1})	k_{cat}/K_m ($M^{-1}\ s^{-1}$)	E1o- activity [b] ($\mu mol \cdot min^{-1} \cdot mg^{-1}$)	K_m, 2-OG (mM)	K_m, CoA (mM)
wt E2o	13.7 ± 2.5 (100%)	48.0	$1.07x10^6$	0.35 ± 0.01	0.05 ± 0.011	0.0204
Thr323Ala	6.2 ± 0.30 (45%)	21.7	$0.48x10^6$	0.36 ± 0.01	0.095 ± 0.03	0.0233
Thr323Ser	5.9 ± 0.50 (43%)	20.7	$0.46x10^6$	0.29 ± 0.03	ND	ND
Asp374Ala	0.28 ± 0.01 (2.1%)	0.98	$0.02x10^6$	0.32 ± 0.02	0.077	ND
Asp374Asn	1.33 ± 0.03 (9.7%)	4.7	$0.10x10^6$	0.40 ± 0.07		
His375Ala	0.29 ± 0.03 (2.1%)	1.0	$0.02x10^6$	0.30 ± 0.01	0.082	ND
His375 Cys	0.13 ± 0.01 (1.0%)	0.46	$0.01x10^6$	0.33 ± 0.04		
His375Asn	0.07 ± 0.01 (0.5%)	0.26	$0.006x10^6$	0.44 ±0.01		
His375Trp*	8.137 ± 0.4 (59.4%)	28.8	$0.52\ x10^6$	0.33 ± 0.04	0.07 ± 0.02	0.0133
His375Gly*	1.76 ± 0.15 (12.6%)	5.76	$0.18\ x10^6$	0.37 ± 0.08	0.04 ± 0.006	0.0206
Arg376Ala	7.7 ± 0.08 (56%)	27.0	$0.60x10^6$	0.31 ± 0.04	0.14 ± 0.007	0.0198
Asp379Ala	1.3 ± 0.07 (9.5 %)	4.6	$0.10x10^6$	0.29 ± 0.01	ND	0.0211

[a)] OGDHc was assembled from E1o, indicated E2o variants and E3 at a mass ratio of 1:1:1 (μg: μg: μg). Activity was calculated per mg of E1o. No OGDHc activity was detected for E1o or E3 in the absence of E2o.

[b)] E1o-specific activity of the assembled OGDH complexes was measured in a DCPIP assay and was calculated per mg of E1o[1]. All assays were carried out in triplicates. The E2o* variants are the mutants picked on site-saturation mutagenesis.

2.6.2 Residues Asp374 and His375 are the key E2o active site residues

Next, the residue-specific contribution to catalysis of succinyl-CoA formation in the active center of the *E. coli* E2o was studied. Results of this study would be applicable to all E2o components due to high sequence identities reported for all E2o core/catalytic domains [16,17,19,70,87,88,99]. Putative residues from the active center of the E2o involved in succinyl transfer and substrate binding were identified based on the X-ray structure of the truncated cubic core of the *E. coli* E2o, known as the E2o catalytic domain (Figure 2.3a) [16,17]. The following E2o active center variants were created to determine their individual contributions toward the catalytic efficiency of the OGDHc complexes assembled from E1o, E2o (or its active center variants) and E3: Thr323Ala, Thr323Ser, Asp374Ala, Asp374Asn, His375Ala, His375Cys, His375Asn, Arg376Ala and Asp379Ala (Figure 2.3b, Table 2.1). The activity of the assembled OGDHc variants was measured in the overall assay for NADH production and in an E1-specific assay to study 2-OG oxidation by OGDHc in the presence of the artificial electron acceptor 2,6-dichlorophenolindophenol (DCPIP). The E1-specific activity does not need the presence of the E2o and E3 components; however, substitutions in E2o could potentially affect assembly into OGDHc.

As shown in Table 2.1, the Thr323 E2o substitutions to Ala or Ser do not significantly affect the NADH production as 45% (Thr323Ala E2o) and 43% (Thr323Ser E2o) of E2o activities were detected. From these results, it is unlikely that Thr323 in E2o is a catalytically important residue, contrary to the suggestion made based on the X-ray studies [16]. Similarly, the Arg376Ala E2o substitution led to 56% OGDHc activity remaining. In contrast, the Asp374Ala and Asp374Asn E2o substitutions revealed 2.1% and 9.7% of OGDHc activity remaining, respectively. Approximately, 9.5% of the

OGDHc remaining activity was detected for Asp379Ala substituted E2o (Table 2.1). The His375Ala, His375Cys and His375Asn E2o substitutions at the highly conserved histidine residue in all 2-oxo acid dehydrogenase complexes, led to 2.1%, 1.0% and 0.5% activity remaining, respectively, but did not abolish the OGDHc activity.

These findings are in in agreement with data reported from Rutgers earlier for amino acid substitutions in His339 for *E. coli* pyruvate dehydrogenase complex (PDHc) which is analogues to His375 in E2o [100]. The activity of the *E. coli* PDHc was reduced to approximately 5.6% with the His399Ala and 2.8% with the His399Cys substitution, clearly indicating that cysteine substitution led to a lower activity of both E2's as compared with the Ala substitution [100]. When OGDH complexes assembled with E2o and its variants were tested with pyruvate (25 mM) or 2-OV (45 mM) as potential substrates for chemo-enzymatic synthesis of acyl-CoA analogues, no NADH production was detected, indicating that neither acetyl-CoA nor butyryl-CoA could be produced (data not presented). It is also noteworthy that neither the E1o-specific activity of the reconstituted OGDH complexes, nor indeed the complex assembly itself, was affected by the indicated E2o substitutions (Table 2.1).

The following could be concluded: two residues, Asp374 and His375 from the E2o active center are catalytically important, as substitution of either residue for Ala impaired E2o catalytic efficiency by 54-fold, while a 107-fold reduction was observed for the His375Cys E2o variant. Compared to the wild type E2o, the His375Asn substitution lowered the catalytic efficiency by 178-fold, while the Asp374Asn E2o substitution lowered it by only 11-fold. The rate retardation resulting from Ala substitution of all five active center residues here tested is ~125,000 fold [this number represents the product of $(k_{cat}/K_m)_{\text{wild type}}$ / $(k_{cat}/K_m)_{\text{variant}}$] for each Ala substituted variant. This number could be

compared to the 30,000-fold rate acceleration for acyl transfer between two aliphatic thiols reported by Hupe and Jencks in model systems [101].

2.6.3 Functional importance of Asp374 and His375 in independently expressed E2o catalytic domain

An alternative approach to study coupling of the E2o active center with the peripheral E1o and E3 components was developed by the Jordan group recently [19]. It employs independently expressed E2o catalytic domain (CDo) in combination with a lipoyl domain source originated from E2o, such as lipoyl domain by itself (LDo) or C-terminally truncated E2o proteins, such as $E2o^{1-176}$ didomain, which consists of LDo, an E1o and E3 binding domain (peripheral subunit binding domain, PSBD) and flexible linkers connected them (see Figure 2.7). For this approach, first, the functional competence of the independently expressed CDo in the overall OGDHc reaction needed to be proved. As shown in Figures 2.10 and 2.11, on mixing of the CDo with varying concentrations of the LDo (0-70 μM) (Figure 2.10a), or of $E2o^{1-176}$ didomain (0 –16 μM) (Figure 2.11), with E1o and E3 components to complete the OGDH-like complex, production of NADH could be detected. While the rate of NADH production was proportional to the concentration of the lipoyl domain source, no evident saturation could be reached with either LDo or $E2o^{1-176}$ didomain. Nor could saturation be reached with the Asp374Ala and His375Ala CD variants (Figure. 2.10b, 2.10c). In the absence of saturation apparent in Figures 2.10 and 2.11, the values of the second order rate constants k_{cat}/K_m could be calculated from the initial slope for NADH production: 0.124×10^6 M^{-1} s^{-1} (CDo+LDo domains); 0.192×10^6 $M^{-1}s^{-1}$(CDo + $E2o^{1-176}$ di-domain); 0.028×10^6 M^{-1} s^{-1} ($CDo^{Asp374Ala}$ + LDo) and 0.019×10^6 M^{-1} s^{-1} ($CDo^{His375Ala}$ +LDo) in comparison with

$1.07x10^6$ M^{-1} s^{-1} for E2o by itself (Table 2.2). Again, the catalytic efficiency of Asp374Ala and His375Ala CDo variants was 4.4- and 6.5- fold, respectively, lower than that for unsubstituted CDo. These results confirm the contribution of Asp374 and His375 to E2o catalysis. Another important conclusion from this study is that the reaction intermediates could be transferred between active centers of E1o, CDo and E3 in the presence of lipoyl domain source in the reaction assay with no covalent bond linking CDo and lipoyl domain source. This is the second example from Rutgers, as similar findings were reported earlier for the *E. coli* E2p [19]. In support of these striking conclusions, the following controls were performed: (i) No OGDHc activity was detected for LDo on its own in the absence of CDo; (ii) Negligible or no OGDHc activity could be detected for a mixture of E1o, E3 and CDo, but in the absence of LDo, thereby excluding any contamination from intrinsic wild-type OGDHc. The results indicate that it will be sufficient to use independently expressed E2o domains for future active center engineering of E2o.

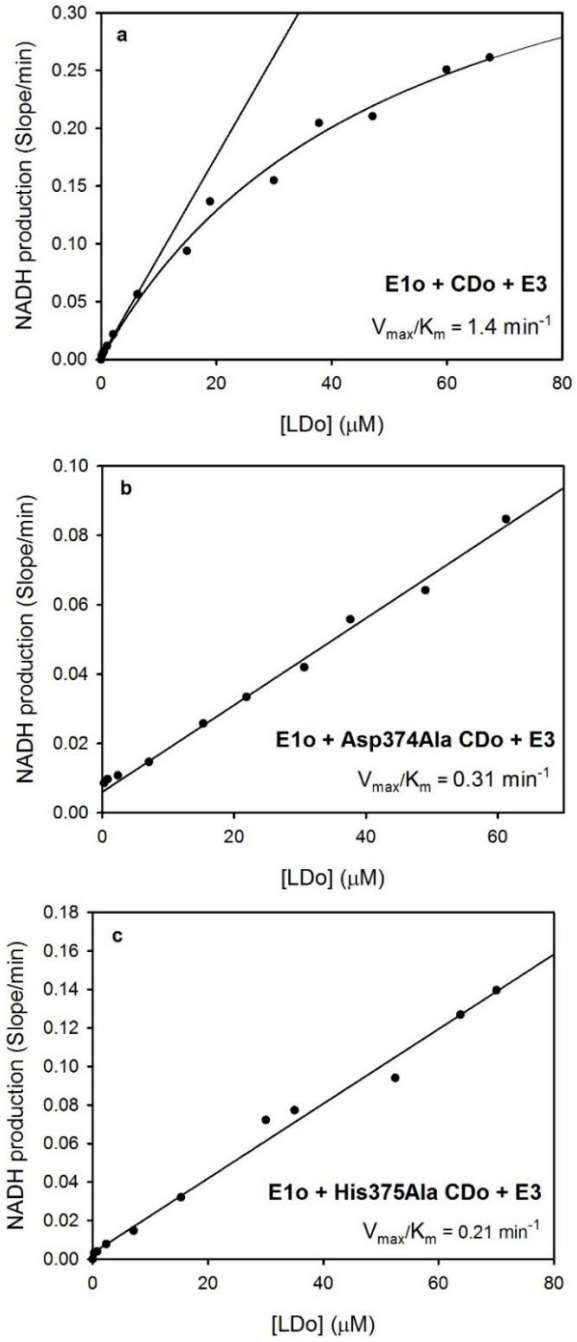

Figure 2.10 Dependence of the OGDHc Activity on Concentration of the Lipoyl Domain in the Overall Assay with CDo and LDo replacing E2o.

a. The E1o (3 μg, 0.028 μM subunits), E3 (3 μg, 0.06 μM subunits) and CDo (3 μg, 0.1 μM subunits) were mixed at a mass ratio of 1:1:1 (μg:μg:μg) in 0.1 M Tris-HCl (pH 8.0) containing $MgCl_2$ (1.0 mM), ThDP (0.2 mM), NAD^+ (2.5 mM) and different concentrations of the LDo (0-67.5 μM) at 30 °C. After 5 min of equilibration, the reaction was initiated by OG (2 mM) and CoA (0.13 mM) and NADH production was recorded at 30 °C for 5 min. **b.** The Asp374Ala CDo and LDo were used to replace E2o. **c.** The His375Ala CDo and LDo were used to replace E2o. Condition of experiment for **b** and **c** were similar to that presented above for **a**.

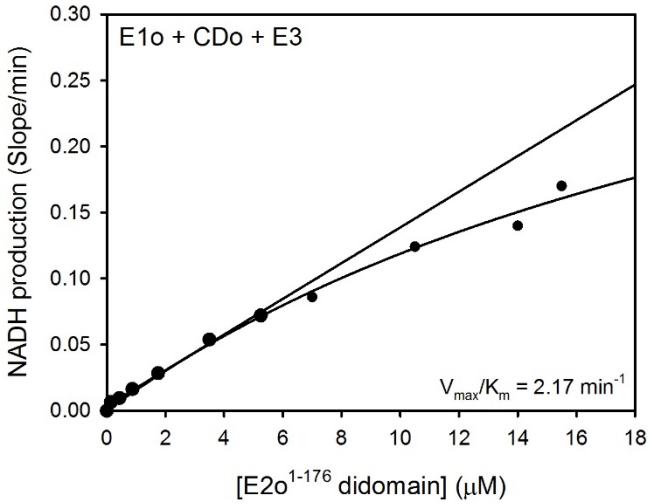

Figure 2.11 Dependence of the OGDHc activity on concentration of the $E2o^{1-176}$ Didomain in the Overall Assay with CDo and $E2o^{1-176}$ Didomain replacing E2o.
For experimental conditions, see figure legend to Figure 2.10.

Table 2.2 The Second Order Rate Constants for NADH production in the Overall Assay where E2o was substituted by its indicated Catalytic Domain Variants and Lipoyl Domain in comparison with E2o

E2o source	k_{cat}/K_m (M^{-1} s^{-1})[a] forward direction	k_{cat} (s^{-1})[b] reverse direction
E2o[a]	$1.07x10^6$	n/a
CDo+LDo	$0.124x10^6$	19.9
$CDo^{Asp374Ala}$ +LDo	$0.028x10^6$	1.86
$CDo^{His375Ala}$ +LDo	$0.019x10^6$	4.9

[a] Activity was measured in the NADH assay in the physiological direction. [b]Activity was measured in the reverse direction. The concentrations of dihydro-LDo were: 35 μM for Asp374Ala CDo and 40 μM for both His375Ala CDo and for wild-type CDo. For details on activity measurement see Materials and Methods section.

2.6.4 Further evidence for the catalytic importance of Asp374 and His375 from the rate of succinyl transfer catalyzed by the E2o catalytic domain

To further substantiate the role of the His375Ala and Asp374Ala substitutions in the catalytic domain of E2o, an experiment was designed to study the succinyl transfer *per se* in the reverse reaction as shown in Equation 2.3, enabling us to determine rate constants for the reaction taking place in the E2o active center exclusively. A mixture of dihydro-LDo [LDo reduced by tris(2-carboxyethyl)phosphine, TCEP] and CDo or its variants, was reacted with succinyl-CoA according to Equation 2.3 where CDo or variants are the catalysts for the reaction.

$$\text{succinyl-CoA + dihydro-LDo} \overset{\text{CDo}}{\leftrightarrows} \text{succinyldihydro-LDo + CoA} \qquad (2.3)$$

Direct measurement of the masses of dihydro-LDo and succinyldihydro-LDo by FT-MS was used to quantify the rate of succinyl transfer from succinyl-CoA to the dihydro-LDo. At concentrations of dihydro-LDo (40 μM), succinyl-CoA (0.15 mM), and CDo (0.05 μM), the dihydro-LDo is a substrate, CDo is a catalyst, and succinyldihydro-LDo is a product in Equation 2.3. The reaction was stopped at different times (5–120 s) by diluting into 50% methanol and 0.1% formic acid, and the samples were analyzed by FT-MS. The ratio of succinyldihydro-LDo / total LDo (the sum of succinyldihydro-LDo and dihydro-LDo) was plotted versus time (Figure 2.12a). As seen from Figure 2.12a, approximately 60% of dihydro-LDo is converted to succinyldihydro-LDo with a rate constant of 19.9 s^{-1} as calculated from a linear fit to the initial rate of succinyldihydro-LDo formation (Table 3). It should be noted that some time-dependent formation of succinyldihydro-LDo was detected by FT- MS even in the absence of CDo in the reaction assay. While this nonenzymatic reaction was insignificant with unsubstituted CDo, the

slope of this nonenzymatic reaction was taken into account when rate constants were calculated for the His375Ala and Asp374Ala CDo variants (Figure 2.12 b,c). As seen in Figure 2.12 and Table 2.2, the rate constant of 1.86 s^{-1} (Asp374Ala) and of 4.9 s^{-1} (His375Ala) was 11 times and 4 times smaller, respec- tively, compared to the rate constant of 19.9 s^{-1} for unsubstituted CDo. A ratio of succinyldihydro-LDo/total LDo of ~ 0.55–0.60 (reproducible with wild-type and variant CDo's in Fig. 6) was observed. The data above, and presented in Table 2.2, support the conclusion that Asp374 and His375 are important residues for succinyl transfer in both directions, as they need to be, while also suggesting an equilibrium constant near unity for the reaction in Equation 2.3.

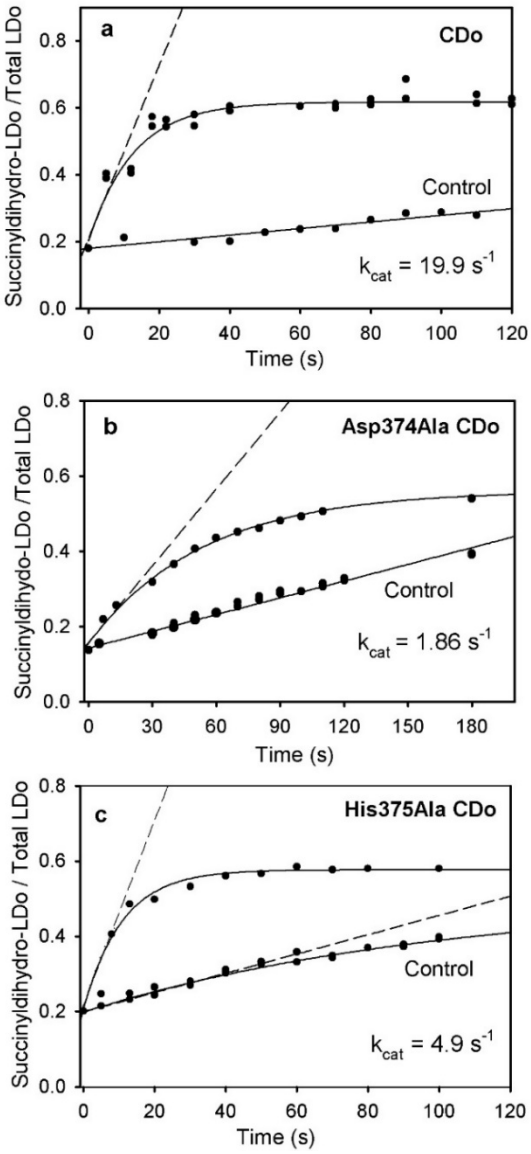

Figure 2.12 Kinetics of Succinyldihydro-LDo formation by CDo and variants in the Reverse Succinylltransferase Reaction.

a. The dihydro-LDo (40 μM), 0.10 mM TCEP and 0.05 μM CDo in 35 mM NH_4HCO_3 (pH 7.5) were mixed with 0.15 mM succinyl-CoA. The reaction was stopped by addition of 50% methanol and 0.1% formic acid and samples were analyzed for the presence of succinyldihydro-LDo and dihydro-LDo by FT-MS. The relative intensity of succinyldihydro-LDo *versus* total intensity (sum of succinyldihydro- and dihydro-LDo) was plotted *versus* time. A control experiment was performed in the absence of CDo. **b.** Progress curves of succinyldihydro-LDo formation by Asp374Ala CDo. The reaction assay in 0.30 ml of 35 mM NH_4HCO_3 (pH 7.5) contained the following: 35 μM dihydrolipoyl-LDo, 0.35 mM TCEP and 0.15 mM succinyl-CoA. After 40 s of pre-incubation, the reaction was started by addition of 0.10 μM Asp374Ala CDo. **c.** Progress curves of succinyldihydro-LDo formation by His375Ala CDo. The reaction assay was similar to that in **b** except of 40 μM dihydrolipoyl-LDo was used. The traces are the nonlinear regression fit to a single exponential rise to maximum, and the *dashed line* represents a linear fit to initial rate conditions. For rate constants calculation in **b** and **c**, the slope in the control experiment was subtracted from that in the experiment.

2.6.5 Site saturation mutagenesis on the E2o active center His375

To gain further insight into the possible role of His375, out site-saturation mutagenesis was carried out on this residue and screened for possible variants that display OGDHc activity.

The following His375 variants were identified: His375Trp E2o with a significant retention of the overall NADH activity (60%); and His375Gly E2o with significantly reduced NADH activity (13%) compared to unsubstituted E2o (Table 2.1). Steady-state kinetic experiments revealed an approximately twofold reduction in k_{cat} for the His375Trp E2o (29 s^{-1}) and about eightfold reduction for the His375Gly E2o (6 s^{-1}) compared to E2o (48 s^{-1}) (Table 2.1; Figures 2.13 a,b,c). No significant changes in values of K_m with respect to 2-OG or CoA were detected for the variants in comparison to the unsubstituted E2o (Table 2.1, Figure 2.14a). To further test whether His375 participated as a general acid–base catalyst, the pH dependence of the overall NADH activity of the His375Trp E2o and of the unsubstituted E2o, both assembled with the E1o and E3 components, was com- pared and revealed no difference in their shapes. The pK_{app} for the alkaline limb of the curve was 8.8 for E2o and 8.7 for the E2o-His375Trp variant (Figure 2.14b). This parallel behavior of the pH dependence with His or Trp effectively rules out an acid–base role for His375.

As there is no tryptophan residue in the E2o active center, the intrinsic fluorescence could be utilized of the newly installed Trp in position 375 of the His375Trp E2o variant to determine the nearly equal K_d of CoA (61.2 μM) and succinyl-CoA (47 μM) from quenching of fluorescence on addition of either compound (Figure 2.15). As control, the E2o experienced no fluorescence quenching, thus also confirming substitution at the active center. In view of the modest decrease in k_{cat}/K_m with the Trp substitution at

position 375, these K_d values are appropriate for the unsubstituted E2o, and indicate similar binding affinity of E2o for CoA and succinyl-CoA, where both succinyl and CoA moieties appear to contribute to binding.

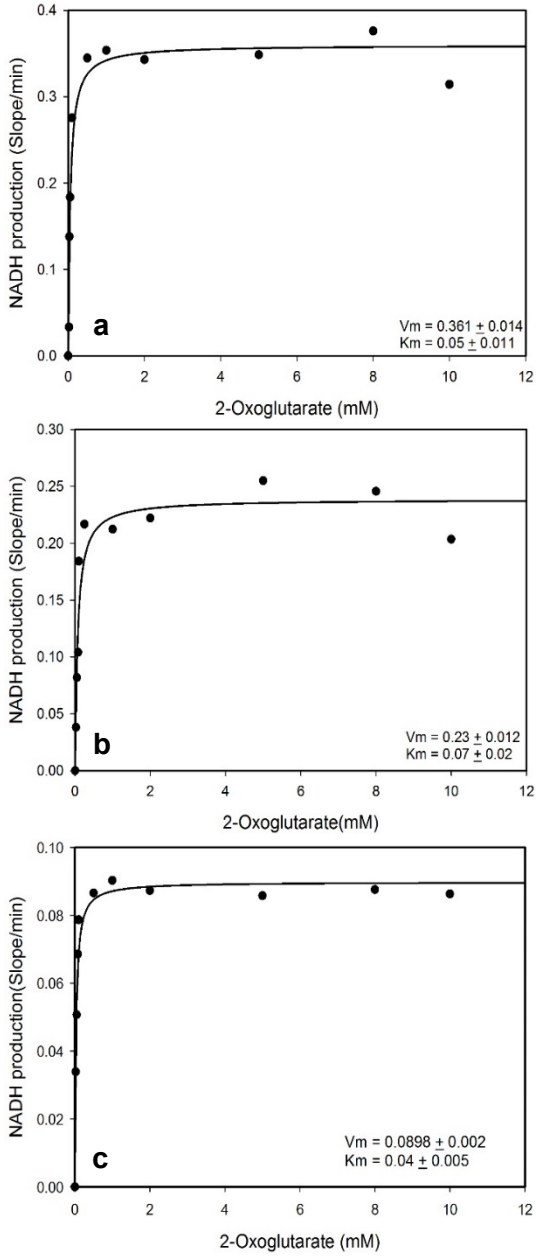

Figure 2.13 Dependence of the NADH production in the OGDHc reaction on concentration of the 2-oxoglutarate substrate for the (a) wild type complex, (b) E2 mutant His375Trp and (c) His375Gly.

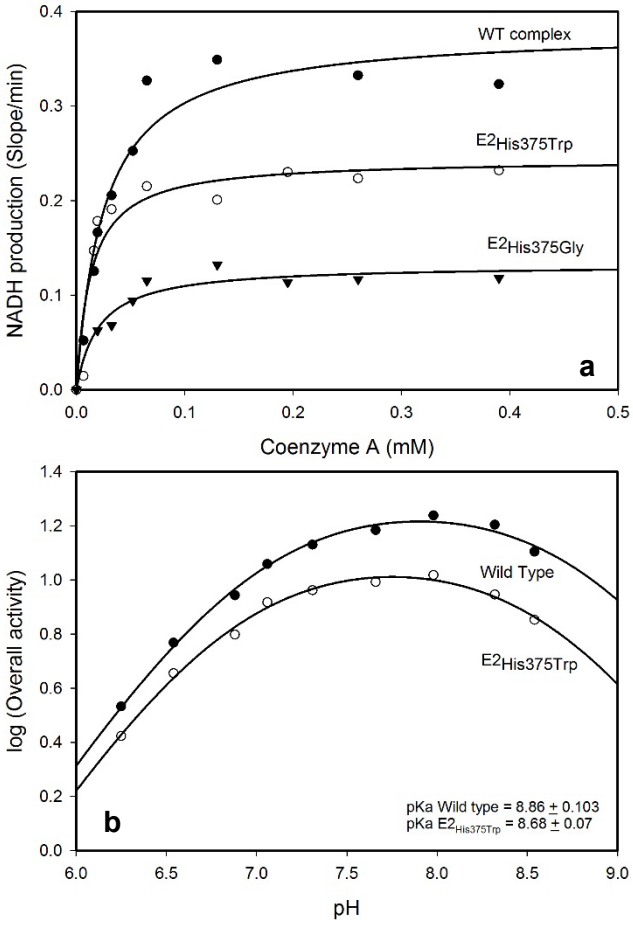

Figure 2.14 (a) Dependence of the NADH production in the OGDHc reaction on concentration of the Coenzyme A.
NADH assay with wild type E2o, $E2_{His375Trp}$ and $E2_{His375Gly}$.

(b) pH dependence of the OGDHc activity for wild-type E2o and His375Trp E2o variant.
The E1o (3 μg, 0.028 μM subunits), E3 (3 μg, 0.06 μM subunits), and wild-type E2o (3 μg, 0.1 μM subunits) or His375Trp E2o were mixed at a mass ratio of 1 : 1 : 1 (μg: μg: μg) in the reaction assay containing 0.05 M Tris/HCl, 0.05 M KH_2PO_4, $MgCl_2$ (1.0 mM), ThDP (0.2 mM), and NAD^+ (2.5 mM) with pH of the reaction assay varied from 6.28 to 8.5. The reaction was initiated by CoA (0.13 mM) and OG (2 mM) and NADH production was recorded at 30 °C for 1 min. The values of activity were plotted to a curve defined by one ionizing group according to Equation (2.4).

$$\log(\text{activity}) = \log(\text{activity}_{max}) - \log(1+10^{pK1-x}) \quad (2.4)$$

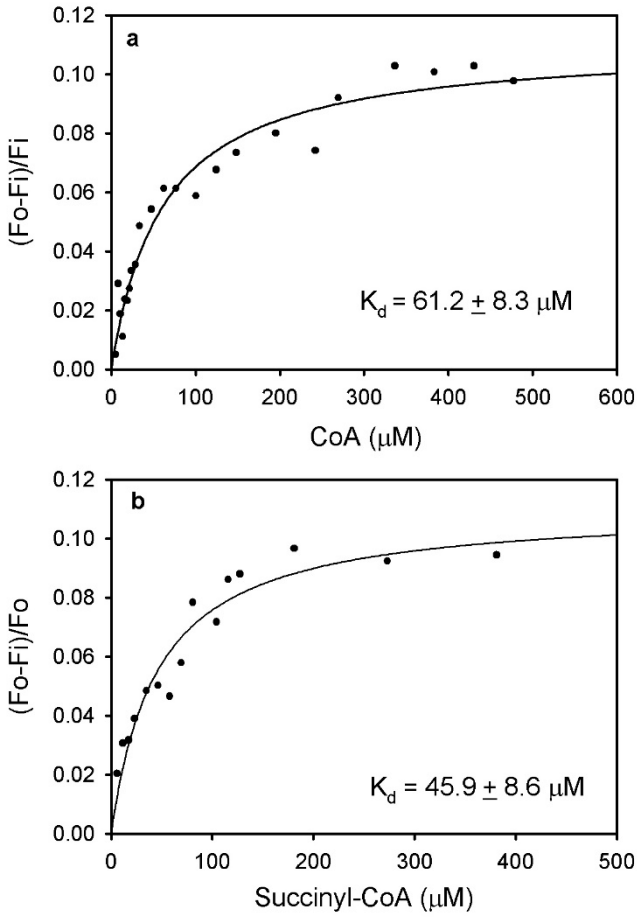

Figure 2.15 Quenching of the intrinsic fluorescence of the His375Trp E2o by CoA and succinyl-CoA.
a. The top panel shows the dependence of the relative fluorescence quenching on the concentration of CoA. His375Trp E2o (0.24 mg/mL, concentration of active centers of 3.5 μM) in a mixture of 50 mM KH_2PO_4 and 50 mM Tris (pH 8.0) containing 0.15 M NH_4Cl, 1 mM DTT and 1% glycerol was titrated with CoA (3−570 μM). **b.** The bottom panel shows the dependence of the relative fluorescence quenching on the concentration of succinyl-CoA (5−380 μM). Data points in **a** and **b** were fit to Hill Equation (2.1); the lines are the regression fit trace.

2.7 Conclusions

This chapter is directed to an elucidation of the fundamental mechanism of the transthioesterification reaction carried out by the E2o of the *E. coli* OGDHc that would be applicable to all E2o components due to high sequence identities reported for the E2 catalytic domains [16,17,19,70,87,88,99]. Important classes of enzymes carrying out similar reactions include inteins in expressed protein ligation [102] and many reactions

on the polyketide pathways [103]. Based on the studies, the following important results emerged.

(a) Identification of catalytically important Asp374 and His375 residues of the E2o catalytic domain and the rate acceleration provided by these residues. The other residues tested displayed much smaller contribution to catalysis. Using the E2o variants substituted by alanine at the putative catalytic center for transthioesterification, NADH production as a measure of the complex activity indicated that the five residues tested accounted for 2.23 (Thr323Ala), 54 (Asp374Ala and His375Ala each), 1.78 (Arg376Ala), and 11 (Asp379Ala)-fold rate accelerations for a total of ~125,000-fold. This is the first identification of partial catalytic rate constants for this important reaction and raises the question: Which likely mechanism is consistent with the results?

(b) A closer look at the transthioesterification mechanism was provided by the use of independently expressed E2o domains (LDo, $E2o^{1–176}$, and CD) that allowed to the conclusion that both Asp374 and His375 are important residues for succinyl transfer in both the physiological and in the reverse direction.

(c) The rate of reductive acylation of LDo by a number of substrate analogues (2-oxoadipate, 2-oxovalerate and pyruvate) signals that communication between E1o and E2o is not fatally compromised by the alternative substrates. The rate constant of 99 s^{-1} for reductive succinylation of the LDo by E1o and 2-OG (the rate constant for the reaction starting with free enzyme and culminating in reductive succinylation of E2o, resulting in formation of S8-succinyldihydrolipoyl-LDo) compared to the k_{cat} of 48 s^{-1} (NADH formation by OGDHc).

(d) These results raise the question: Which likely mechanism of transthiolacylation is consistent with the experimental findings? Based on numerous precedents, there are two

prominent likely mechanisms to account for the transfer of acyl group between two thiols depicted by the step characterized by the rate constants k_6 and k_{-6} in Figure. 2.6. A general acid–base mechanism would suggest that the His375 converts the thiol of the attacking nucleophile (CoA-SH) to a thiolate anion (CoAS-) as depicted on pathway B in Figure 2.16. The activated thiolate then attacks the carbonyl atom of the succinyldihydrolipoyl-E2 to form a tetrahedral intermediate, which is stabilized by the hydroxyl side chain of Thr323 [17]. This notion was long accepted based on analogy with a mechanism developed for chloramphenicol acetyltransferase (CAT) [69,71,75]. When the analogous His195 in chloramphenicol acetyltransferase was replaced by Ala, a $9x10^5$-fold decrease in k_{cat} and virtually no change in K_m was observed, that is, a $(k_{cat} / K_m)_{\text{wild-type CAT}}/(k_{cat} / K_m)_{\text{His195Ala CAT}} = 500\ 000$ [19]. In contrast, the $(k_{cat} / K_m)_{\text{unsubstituted E2o}}/ (k_{cat} / K_m)_{\text{His375Ala E2o}} = 54$. This difference strongly suggests different functions for the highly conserved active center histidine on the two enzymes.

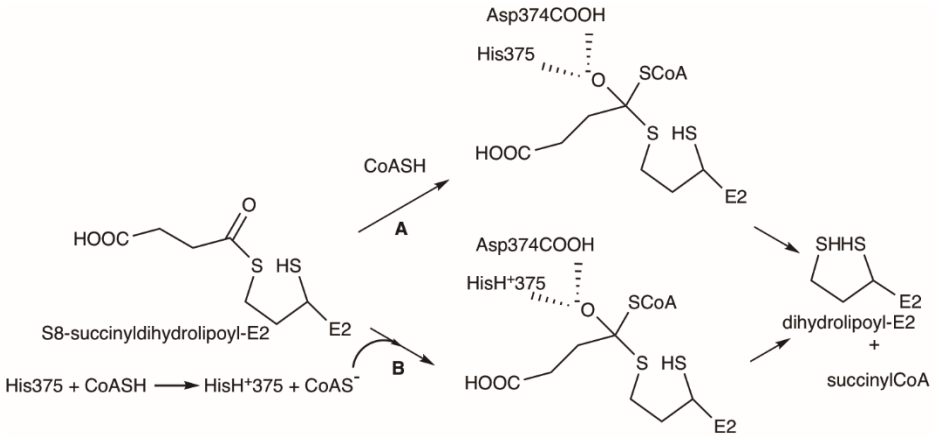

Figure 2.16 Likely mechanisms of succinyl transfer from dihydrolipoamide-E2o to CoA-SH.

Pathway A: direct attack by the conjugate base thiolate anion of CoASH assuming a low pK_a for the CoASH, or by the thiol form itself. Pathway B: initial proton transfer from CoASH to His375 forming the conjugate base $CoAS^-$, which is the attacking agent. Both pathways then proceed by an oxyanionic tetrahedral intermediate consistent with model studies [101].

As a ‘gold standard’ for acid–base catalysis by a histidine side chain, comparison with the much studied His64 at the catalytic triad of the subtilisin family of serine proteases, where the His64Ala substitution led to a reduction of 10^6-fold in k_{cat}/K_m, a number similar to that observed for CAT [104] is also presented.

As an alternative to acid–base catalysis, for a protein with a pK_a for the cysteine thiol group near pH 7.0, one could envision direct attack by a thiolate anion on the thiol ester carbon, forming an essentially symmetrical tetrahedral oxyanionic intermediate, in which the central carbon atom is flanked by two C–S bonds, where either C–S bond has nearly equal probability for cleavage (Figure 2.6, lower left and Figure 2.16 pathway A) [101]. It can be suggested that the nearly equal magnitude of the rate acceleration provided by the His375 and the Asp374 residues, more likely, reflects their roles in stabilizing the oxyanion by two hydrogen bonds (Figure 2.16, pathway A), in other words creating a so-called ‘oxyanion hole’.

It had been demonstrated some years ago that in subtilisin, where a putative transition state stabilizing oxyanion hole is created by one main chain hydrogen bond donor and one side chain hydrogen bond donor (Asn155), substitution of Asn155 to Leu had small effect on the K_m but reduced the k_{cat} by a factor quoted as 200- to 300-fold [105]. This is very similar in magnitude to the k_{cat}/K_m reductions observed (54 for each) with the Asp374Ala and His375Ala substitutions reported in this study (again no change in K_m was observed). These results also concur with homology modelling studies between the enzymes chloramphenicol acetyl transferase and dihydrolipoamide acetyl transferase about existence of a His-Asp-Gly consensus in the catalytic core which is likely to play an important role [71].

While well accepted, it has been difficult to obtain experimental proof for the existence of an oxyanion in solution; as an example, proton inventory solvent kinetic isotope effect studies, a very subtle method, failed to do so [106].

The proposed hydrogen bond donation by Asp374 and His375 was tested by studying the alternative Asp374Asn substitution in E2o that allows hydrogen bond donation similar to His375 (Table 2.1). The His375Asn substitution led to 4.0-fold further reduction in the E2o catalytic efficiency (to 0.5% of the remaining activity) compared to the His375Ala substitution (to 2.1%). In contrast, the Asp374Asn substitution partially rescued the E2o catalytic efficiency (9.7%) compared to Asp374Ala E2o (2.1% activity) and suggested that Asp374 is more likely to be involved in hydrogen bond formation. The result also raises an important implication that the carboxyl group of Asp374 has an unusually elevated pK_a as only in the conjugate acid form could it serve as a hydrogen bond donor. As this step appears to be part of rate limitation, it can be further speculated that the alkaline limb of the two activity–pH profiles (parallel for His375 or Trp375), and the deduced pK_a of 8.7–8.8 pertains to a highly perturbed Asp374 environment.

The His375 residue appears to be more sensitive to substitutions, suggesting a more complicated scenario. Therefore site-saturation mutagenesis was carried out on this residue and screened for substitution-tolerant active variants. Informatively, the His375Trp and His375Gly variants were found to have intermediate activity (60% and 13%, respectively). Steady-state kinetic analysis of the enzymes harbouring these substitutions revealed only modest changes in K_m. But, the two-fold decrease in the k_{cat} for E2o-His375Trp compared to the wild-type E2o is inconsistent with the earlier suggestion that His375 acts as a proton donor for protonation of the leaving group. These

results are consistent with studies by McLeish's laboratory on the ThDP-dependent enzyme benzoylformate decarboxylase, where similar changes were observed on site-saturation mutagenesis studies based on the active site His281, by finding that the His281Phe and His281Trp variants displayed significant activity [107], and also arguing strongly against acid–base catalytic activity. Additional argument against an acid–base role of His375 is provided by the similar activity–pH profiles of unsubstituted E2o and its His375Trp variant.

Given the results with the E2o- His375Trp variant, assigning a role to the His375 side chain need to be done cautiously: rather than a direct participation in a hydrogen bond as suggested in Figure 2.16, perhaps the imidazole ring provides a physical barrier protecting the hydrogen bonding unit, a role that could also be played by the indole side chain of Trp. Of course, there is also the possibility that the indole NH of Trp375 is the hydrogen bond donor for oxyanion stabilization.

Using a variety of experiments, the accumulated evidence allowed the conclusion that the rate-limiting step on OGDHc is succinyl transfer to CoA in the E2o active center. In contrast, on the *E. coli* PDHc, the rate-limiting step is the initial addition of substrate to the E1p component forming the first covalent pre-decarboxylation intermediate [26]. The results also provide crucial information for further engineering of the E2o component for producing a variety of acyl-CoA analogues.

CHAPTER 3

ENGINEERING 2-*OXOGLUTARATE* DEHYDROGENASE TO A 2-OXO *ALIPHATIC* DEHYDROGENASE COMPLEX BY OPTIMIZING CONSECUTIVE COMPONENTS

3.1 Introduction

Multienzyme complexes are attractive for one-pot sequential step chemical synthesis of complex molecules. Enzymes catalyze reactions with high yield and enantioselectivity under mild conditions [108–112], which makes them desirable for fine chemical, pharmaceutical, and agricultural industries [59,113]**.** Next, they facilitate the formation enzyme-substrate complex for improved catalytic efficiency. For example, the substrate is channeled from one catalytic center to the next one. This prevents intermediates from diffusing into the cytoplasm. Furthermore, cellular damage is avoided, which may be caused from toxic byproducts [114,115].

Multienzyme complexes are found in conserved metabolic pathways across all kingdoms [116]. It is believed that their primitive ancestors were once promiscuous. They performed a multitude of bond forming/breaking reactions with a variety of mechanisms [116,117]. Hence, a relatively small set of enzymes supported numerous pathways to sustain life. As time marched forward, gene duplication and divergence led to enzymes with exquisite catalytic efficiency in particular metabolic pathways [118]. Therefore, metabolic pathways have been reprogrammed for survival of the organism. This necessitates conversion of a specialist for a particular substrate to a generalist with broad substrate specificity, then back to a specialist with a new function**.** Optimizing a multienzyme complex requires engineering the component for each individual reaction,

which may include two or more proteins. This can be achieved via laboratory or directed evolution, which have become the method of choice for protein design [44,119–122].

The *Escherichia coli* 2-oxoglutarate dehydrogenase (OGDHc) multienzyme complex was converted into a 2-oxoaliphatic acid dehydrogenase with broader substrate specificity. The natural substrate for OGDHc is 2-oxoglutarate (2-OG) and the enzyme was engineered to accept 2-oxovalerate (2-OV) (Figure 3.1).

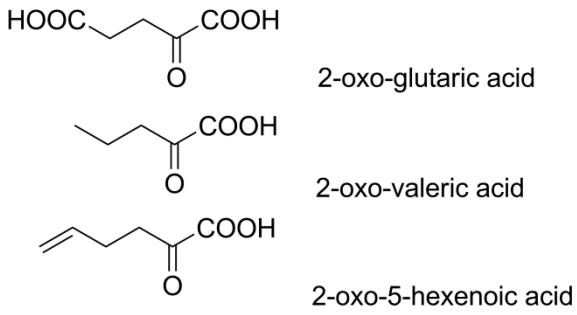

Figure 3.1 Substrate structures.

The OGDHc catalyzes a rate-limiting step in the Krebs cycle and it belongs to the super-family of 2-oxo acid dehydrogenase complexes [3,12]. The Krebs cycle commences with condensation of oxaloacetate with acetyl-Coenzyme A, the latter being a product of the pyruvate dehydrogenase member of the super-family, while pyruvate is the end product of glycolysis. OGDHc is composed of three components: (1) the thiamin diphosphate (ThDP)-dependent 2-oxoglutarate dehydrogenase/decarboxylase (E1o, EC 1.2.4.2, 105 kDa/subunit), (2) dihydrolipoylsuccinyl transferase (E2o, EC 2.3.1.6, 45 kDa/subunit), and (3) dihydrolipoyl dehydrogenase (E3, EC 1.8.1.4, 55 kDa/subunit). In *E. coli*, E1o and E3 exist as homodimers. The E2o component is a trimeric multidomain protein, starting with the amino terminal end a flexible lipoyl domain (LDo), followed by

a long mostly unstructured subunit binding domain for assembly with E1o/E3, then a central nexus catalytic core domain (CDo). The proposed complex contains 12 E1o: 24 E2o :12 E3 (total mass of 2.5 MDa) [6,7]. The OGDHc has three substrate specificity checkpoints: one is in E1o and other two in E2o (CDo and LDo)[13]. The overall reaction of OGDHc proceeds according to Equation 3.1. While the detailed reactions proceed by a succession of reactions (Equations 3.2-3.5).

$$\text{2-OG} + \text{CoASH} + NAD^+ \rightarrow \text{succinyl-CoA} + CO_2 + \text{NADH} + H^+ \quad (3.1)$$

$$RC(=O)COOH + \text{E1o-ThDP} \rightarrow CO_2 + \text{E1o-ThDP=C(OH)R (an enamine)} \quad (3.2)$$

$$\text{E1o-ThDP=C(OH)R} + \text{lip(S-S)-E2o} \rightarrow \text{E1o-ThDP} + \text{RC(=O)S-lip(SH)-E2o} \quad (3.3)$$

$$\text{RC(=O)S-lip(SH)-E2o} + \text{HS-CoA} \rightarrow \text{R(C=O)-S-CoA} + \text{lip}(SH)_2\text{-E2o} \quad (3.4)$$

$$\text{lip}(SH)_2\text{-E2o} + \text{E3-FAD} + NAD^+ \rightarrow \text{lip(S-S)-E2o} + \text{NADH} + H^+ + \text{E3-FAD} \quad (3.5)$$

[R = $-(CH_2)_2$-COOH, ThDP = thiamin diphosphate, lip(S-S) = oxidized lipoate on E2o, $\text{lip}(SH)_2$ = reduced lipoate]

The OGDHc controls the carbon flux through the Krebs cycle [2]. OGDHc catalyzes formation of CoA linked thioesters via trans-thioesterification, which makes it a suitable candidate for green chemical synthesis. Thioesterification reactions are of importance in both organic chemistry and chemical biology[123,124]. For example, they are found in antibiotics and natural products [36,125]. Thioester derivatives are also useful for the synthesis of heterocyclic compounds and molecules containing carbonyl functional groups[126–128]. Hence, thioester synthesis is essential in the industrial, and pharmaceutical industries. Traditional thioester synthesis requires an acyl source available from carboxylic acids, acid anhydrides, or acid chlorides. The reaction conditions are harsh and energy intensive, often requiring strong bases, long reflux

conditions, and toxic heavy metals[41]. Thus, recombinant engineered OGDHc may be provide a green alternative method to chemical synthesis of acyl-CoenzymeA thiolesters.

The *Escherichia coli* OGDHc was converted into a 2-oxoaliphatic acid dehydrogenase. The natural substrate for OGDHc is 2-OG. The E1o and E2o of the complex were engineered to accept 2-oxovalerate (2-OV) (Figure 3.1). The E1o His298Asp variant was identified from saturation mutagenesis libraries to be active towards 2-OV. The catalytic efficiency of E1o His298Asp variant increased 4.4-fold for 2-OV, while a 1200-fold decrease for 2-OG resulted in the E1o-specific assay (assay with DCPIP, 2,6-dichlorophenolindophenol)[13]. However, when the E1o-His298Asp was reconstituted with wt-E2o and E3, it did not display overall activity (NADH production) with 2-OV. Mass spectrometric evidence showed that wild-type and E1-His298Asp transfers the ThDP-bound decarboxylated intermediate of 2-OG or 2-OV to the E2o lipoyl domain (Equation 3.2). However, the lack of overall activity for 2-OV indicated that butyryl-coenzyme A was not formed in the E2o-CD. Hence, the reaction was halted in the E2o-LDo at the S8-butyryldihyrdolipoyl-E2o intermediate. It became evident that the E2o-CD active center required engineering to complete the reaction. The X-ray structure of the *E. coli* E2o-CD indicated that the residues Ser330, Ser333 and His348 may interact with the succinyl carboxylate of the LDo substrate intermediate[16,17] (Figures 3.2a, 3.2b). The side chains of Ser330, Ser333, and His348 were proposed to form a hydrogen bond with the terminal carboxylate of the 2-OG. Amino acid substitutions at these positions may result in accepting a hydrophobic substrate (Figure 3.2b). Hence, these amino acids were targeted for saturation mutagenesis. The libraries were screened for overall activity with 2-OV and E2o-Ser333Met, E2o His348Phe, E2o His348Gln and E2o His348Tyr were identified to be active towards 2-OV. In addition,

the variant complexes could also accept a larger and more hydrophobic substrate, 2-oxo-5-hexenoic acid (2-OHe) (Figure 3.1).

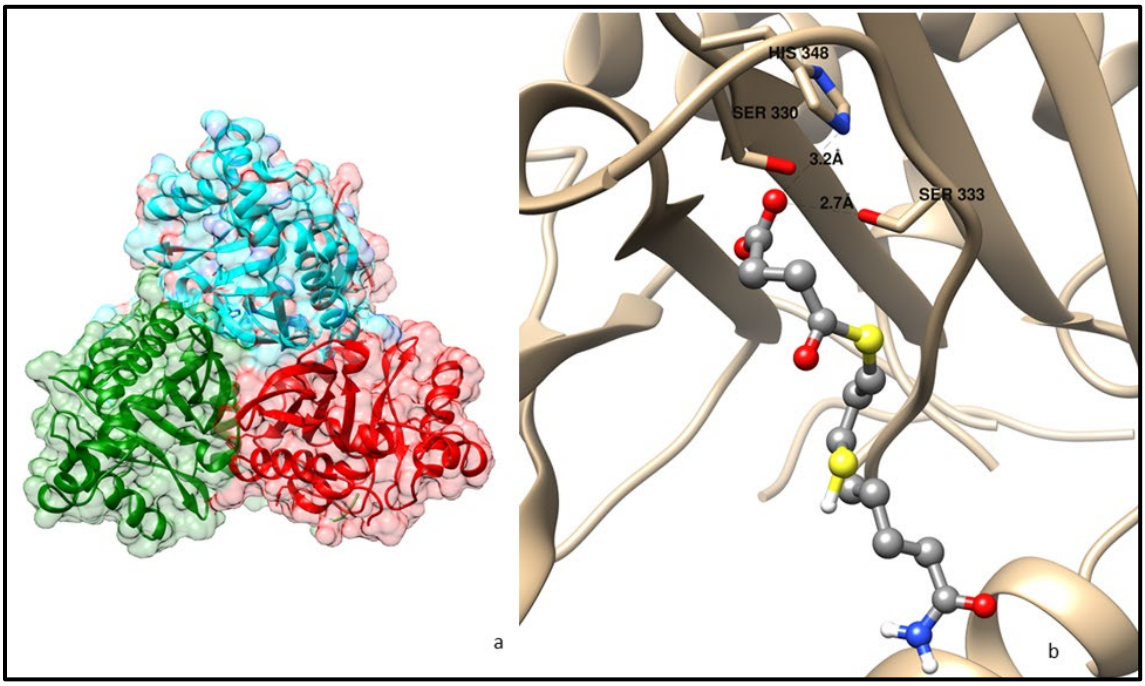

Figure 3.2 E2oCD structure and active site. **(a)** The E2o-core depicted as a trimer with the surface area shown.
The ribbons of three colors cyan, red and green represents chains a, b and c respectively (PDB id: 1c4t).

(b) The active-site binding pocket of the E2oCD trimer is represented. Ser330, Ser333 and His348 are shown to be lining the active site.
S8-succinyl dihydrolipoamide (ligand) was docked into the active site pocket of the E2oCD (receptor). The docking calculations were performed with AutoDock Vina v.1.1.2 using Chimera to visualize [129,130]. The terminal carboxylate oxygen of S8- succinyl dihydrolipoamide is at a distance of 3.2 Å from the His348 imidazole-N(3) and 2.7 Å from the Ser333 sidechain-OH.

3.2 Materials and Methods

3.2.1 Reagents

Dithiothreitol (DTT), 2-oxoglutarate (2-OG), 2-oxovalerate (2-OV), butyryl-CoA were from Sigma Aldrich (St. Louis, Mo). NADH, CoA, isopropyl-β-D-thiogalactopyranoside (IPTG), DNase I, Micrococcal Nuclease, DL-α-lipoic acid and ThDP were from

Affymetrix (Cleveland, OH). Protease inhibitor cocktail tablets were from Roche Diagnostics GmbH (Germany). Ni Sepharose 6 Fast Flow and HiPrep^{TM} 26/60 Sephacryl^{TM} S-300 HR column were from GE Healthcare (Pittsburgh, PA). QuikChange Site-Directed Mutagenesis Kit was from Agilent Technologies (Santa Clara, CA). Primers for site-saturation mutagenesis were from Fisher Scientific (Pittsburgh, PA). *E. coli* strain JW0715 containing the pCA24N plasmid encoding the E1o component and JW0716 containing pCA24N plasmid encoding the E2o component were obtained from National Bio Resource Project (NIG, Japan). AG1 cells (Agilent Technologies) were used as host cells. DNA sequencing was carried out by Molecular Resource Facility at New Jersey Medical School, Rutgers University.

3.2.2 Creation of the saturation mutagenesis library and screen

Site-directed saturation mutagenesis libraries for E2o at positions Ser330, Ser333 and His348 were constructed using a modified QuikChange procedure, very similar as described in Chapter 2. A typical 50 μL reaction contained 10x PfuUltra buffer, dNTP (0.2 mM) and PfuUltra DNA polymerase (1U), pCA24N encoding E2o as template, and NNS primers listed as in Table 3.1. The PCR reaction consisted of 16 cycles at 95 °C for 30 s, 55 °C for 1 min and 68 °C for 10 min. After the PCR, *DpnI* was added to the reaction mixture and then PCR product was transformed into *E. coli* BL21 (DE3) competent cells and plated on LB-agar plate containing 30μg/ml chloramphenicol and was incubated overnight at 37 ºC. The transformants were emulsified and stored as 20% glycerol frozen stocks at -80 ºC. The libraries were restreaked on an LB-Agar plate with chloramphenicol antibiotic.

Table 3.1 List of Primers used for Saturation Mutagenesis

Primers[a]	Sequence[b]
Ser330X	5'- GGTGGTGTGTTCGGTNNSCTGATGTCTACGCCG -3'
Ser333X	5'- GGTTCCCTGATGNNSACGCCGATCATCAACCCG -3'
His348X	5'- GCGCAATTCTGGGTATGNNSGCTATCAAAG -3'

[a] X represents any amino acid.
[b] N refers to an equal mixture of A, T, G and C; S refers to an equal mixture of G and C.

E2o libraries (Ser330X, Ser333X and His348X) were screened. First, a sample from the frozen stock of each of the E2-libraries was applied onto an LB-Agar plate containing 30 μg/ml chloramphenicol. Next, approximately 270 colonies of each library were picked onto a 96-well plate (200 μl volume) containing LB media with 30 μg/ml chloramphenicol and shaken overnight at 250 rpm and 37 ºC. The first column was inoculated with wt-E2o single colonies as control. The plates were covered with breathable cover films to minimize evaporation. Next, the plate was replicated into 96 deep-well plate (2 ml volume) containing 1 ml LB media, 30 μg/ml chloramphenicol, 0.3 mM lipoic acid and 1 mM IPTG. This master plate was stored at -80 ºC. The plates were induced for 16 h at 250 rpm, at 37 ºC in triplicates. The OD_{600nm}/μl was normalized for the culture and the cells were harvested by centrifugation at 2000 *g* for 15 min at 4 ºC. The residual supernatant was discarded, and the cell pellets containing the expressed mutant proteins were frozen at -20 ºC.

The cell pellets were resuspended in 300 μl lysis buffer (20 mM KH_2PO_4, 0.2 M NaCl, 1 mM DTT, 1 mM benzamidine-HCl), protease inhibitor (2 tablets/50 ml), lysozyme (1 mg/ml), DNAse (0.1mg/ml) and incubated for 40 min at 37 º C. After incubation, the suspension was centrifuged at 2000 *g* for 25 min at 4 ºC. The supernatant

was used as the E2-lysate for assembly and the pellet was discarded. All subsequent steps were performed on ice.

The complex was assembled by the following procedure. E1o and E3 expression was previously described and cell lysates were used in the assay[13,18]. The expression was based on cell density and normalized. The lysates of E1o, E2o and E3 were reconstituted in a 96 deep-well plate (2 ml volume). The total reaction volume was 300 µl [240 µl E1:E2:E3 of 1:2:1 (v:v:v); 60 µl buffer (20 mM KH_2PO_4, 0.2 M NaCl, 1 mM $MgCl_2$ and 0.2 mM ThDP)]. The first column was E1o-His298Asp/E2o/E3 for control. The plate was mixed on a plate shaker for 10 min at room temperature and stored on 4 ^oC for 30 min.

The activity assay volume was 200 µl. The wells contained 135 µl of assay buffer (0.1 M Tris-HCl (pH 8.0), 0.15 M NaCl, 1 mM $MgCl_2$, 0.2 mM ThDP, 2.6 mM DTT and 2.5 mM NAD^+). Next, 50 µl was transferred from the above lysate solution to each well. The plates were equilibrated at 30 ^oC. Then, the reaction was initiated using 0.13 mM CoA and 10 mM 2-OV. Next, the endpoint (2, 5, 7, and 10 min) was measured at 340 nm at 30 ^oC. The plate contents were mixed between readings. Positive clones were identified as those that were 20 % above the control lane.

A rescreen was performed to eliminate false positives. The positive clones were streaked on an LB-agar plate containing chloramphenicol (30 µg/ml) from the corresponding master plate. The plate was incubated for 12 h at 37 ^oC. 16 colonies were picked for each positive clone and they were placed into a 96-well plate (200 µl volume) containing LB media with chloramphenicol (30 µg/ml). Wild-type E2o was used on the same plate as the control. The activity procedure is similar to the screening assay. The

His348X library screen identified eight positive clones which were re-screened and sequenced (Figure 3.3). The positive variants from the preliminary screen was validated in a rescreen. The graph represents end-point absorbance at 340nm plotted with time. Each point is an average of 16 E2 colonies for each clone reconstituted with E1o-H298D and E3. The complex formed with wild-type E2o (E1o-H298D: E2o: E3) was used as control. The complexes containing E2o-His348Phe, E2o-His348Gln and E2o-His348Tyr were expressed and purified to verify the screening results. One positive clone was identified from Ser333X library. Sequencing revealed the variant to be Ser333Met. However, No positive clones were identified from the Ser330X library that were active towards 2-OV.

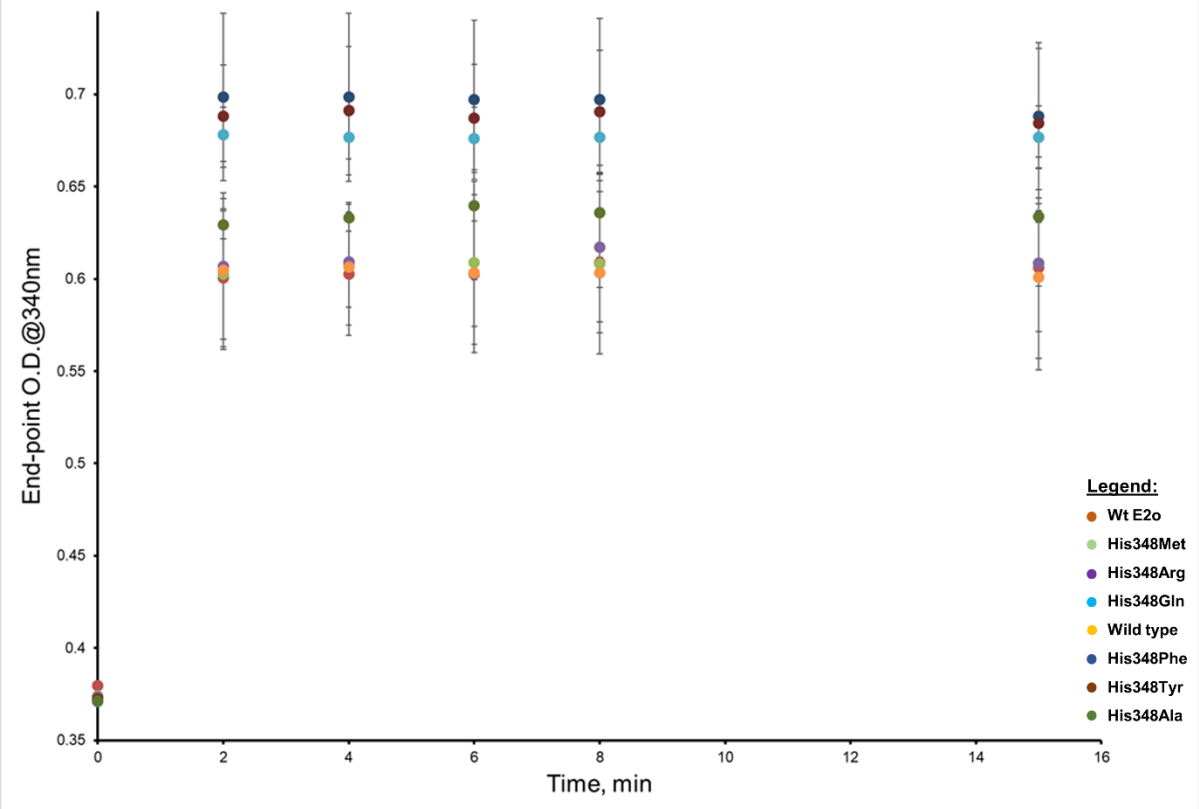

Figure 3.3 Rescreen of E2His348X library.

3.2.3 Expression and purification of E1o, E2o, E3 and variants

E1o, E2o, E3 and variants were expressed and purified following published procedures [13,18,90].

3.2.4 Enzyme activity measurements.

Overall activity was measured in triplicate with purified proteins. The kinetic parameters were determined following published procedures [13,90]. The E1o/E2o/E3 ratios were optimized at substrate saturation conditions prior to determining the kinetic parameters of the OGDHc variant complexes. The mass ratios (μg: μg: μg) for E1o-His298Asp:E2o-His348Phe:E3, E1o-His298Asp:E2o-His348Gln:E3, and E1o-His298Asp:E2o-His348Tyr:E3, were 1:8:1, while E1o-His298Asp:E2o-Ser333Met:E3 was 1:10:1.

3.2.5 Modelling of solvent accessible surface

The solvent accessible substrate binding channel was generated by the 3 V (Voss-Volume-Voxelator) server. First, the structure of E2o CDo was prepared by deleting all non-standard and non-complexed residues using the UCSF Chimera tool. This structure was entered as input in the 3V server. The outer probe radius was set to 9 Å and the inner probe radius was set to 1.5 Å. The final solvent accessible volume was generated as a solid surface accessing into the protein substrate binding pocket. The server also gives output about the volume and surface area of the binding channel [131]. This is an mrc file extension, which is viewable in the UCSF Chimera software.

Further, the Rotamer tool in Chimera was used to generate the mutants in the E2o active site. The amino acid substitution calculations provide results with a number of orientations of the side chain with the corresponding probability. The orientation with the

maximum probability in the active site pocket without the substrate bound is chosen. This conformer is further overlaid with the wild-type E2o chain, to generate any visual changes in the active site pocket.

3.2.6 Receptor-ligand docking of substrate into E2oCD with Chimera

Ligand

The ligand (S8-succinyl dihydrolipoamide) was created using Chemdraw Ultra 12.0 software. Next, the translated canonical SMILE string of the 2D structure was used to generate a 3D structure of the ligand with a -1 charge. This structure was saved as mol2 file and used as ligand for docking.

Receptor

The receptor (E2oCD) was obtained from RCSB PDB (1c4t). First, the nonstandard and unbound solvent atoms were removed from the structure. Then, the Dockprep tool was used on the receptor to minimize the structure. The necessary hydrogens and charges were added. This structure was saved into a new PDB file and used for docking.

Docking

The Autdock Vina plugin was used to perform the docking. The search volume was set for a cube with edge length 15Å. The cube occupied the proposed active site pocket. The docking results returned 10 possible orientations of the ligand with the receptor. The orientations were scored based on the energy (kcal/mol) and RMSD values. The orientation of the ligand with the highest score with respect to the receptor was chosen.

3.2.7 Enzymatic synthesis of the butyryl-CoA by OGDHc assembled from His298Asp E1o with E2o variants with substitutions in the trans-thiolacylation active center, and with E3

For enzymatic synthesis of the butyryl-CoA, the E1oHis298Asp was reconstituted with E2o variant (His348Phe, His348Tyr, His348Gln or Ser333Met) and E3. The complex was assembled in 0.1 mL buffer containing 0.1M Tris (pH 7.5)0.3M NH_4Cl, 0.5 mM ThDP and 2.0 mM $MgCl_2$. For OGDHc assembly, the His298Asp E1o (0.035 mg) was mixed with the E2o variant (0.24 mg) and E3 (0.059 mg) at a mass ratio of 1: 6.9: 1.7, a ratio that was selected from kinetic experiments where NADH production by the variant complexes from 2-OV was measured at OD_{340}. After 30 min of incubation of the assembled components at 25 ºC, the reaction medium containing 0.1M Tris·HCl (pH 8.0), 0.5 mM ThDP, 2.0 mM $MgCl_2$, 2.6 mM DTT and 2.5 mM NAD^+ was added to each reaction mixture to a total volume of 0.4 mL. Next, 2-OV (4 mM final concentration) was added to each reaction mixture followed by equilibration for 1 min at 30 ºC in a thermomixer (Eppendorf). The enzymatic reaction was initiated by addition of CoA (300 μM final concentration). After one h or overnight incubation at 30 ºC, the samples were acidified to pH 2.0 by additon of 2.5% trifluoroacetic acid (TFA) to a final concentration of 0.1% and were filtered through a 10-kDa membrane (Amicon Ultra-0.5 mL centrifugal filters, Millipore Sigma) to separate proteins from the reaction mixture.

The CoA esters were purified by solid phase extraction with Sep-Pak® Vac tC_{18} cartridges (Waters) equilibrated with 0.1% TFA[132]. Briefly, the cartridges were washed with 3 vol of 0.1% TFA (v/v) and CoA esters were eluted with 0.1% TFA containing 50% acetonitrile (v/v). Solvent was partially removed by centrifugation on a Speed-Vac concentrator. The samples were concentrated to a volume of ~100 μL.

3.2.8 Analysis of product using MALDI TOF/TOF Mass Spectrometry

Butyryl-CoA (Sigma Aldrich) and CoA (Sigma Aldrich) were used as external standards. The matrix was CHCA (α-cyano-4-hydroxycinnamic acid from Sigma) which was dissolved in 70% acetonitrile/0.1% TFA. Approximately 1 μL of the sample was withdrawn and was mixed with1 μL of α-cyano-4-hydroxycinnamic acid matrix in the tube and then 1μL of the mixture was spotted on the plate. The samples were analyzed with a 355 nm laser in the negative mode on the ultrafleXtreme MALDI TOF/TOF spectrometer (Bruker Daltonics, Bremen, Germany). For each spectrum, 5 subspectra with 400 laser shots with 400 Hz frequency were acquired. The spectra were analyzed using flexAnalysis 3.0 software (Bruker Dlatonics, Bremen, Germany) and were smoothed using by the Savitzky-Golay algorithm after the baseline subtraction.

3.3 Results and Discussion

This is the first report in which the 2-oxoglutarate dehydrogenase complex is converted into a 2-oxo *aliphatic* dehydrogenase complex by consecutive engineering of the E1o and E2o components. The natural substrate for OGDHc is 2-OG, which contains a terminal carboxylate group. Variants of the multienzyme complex were screened for overall activity towards 2-OV, which has a terminal methyl group (Figure 3.1). We were able to bypass the three stages of substrate recognition, namely the E1o active site, the lipoyl domain of E2o, and the catalytic domain of E2o.

The E2o variants were overexpressed, purified, and assembled with E1o-His298Asp and E3. The kinetic parameters were evaluated for the 2-OV. Wild-type E1o/E2o/E3 does not show detectable overall activity (NADH production) towards 2-OV. Previously, E1o-His298Asp was demonstrated to be active for 2-OV in an E1o-specific assay.

However, E1o-His298Asp/E2o/E3 does not show overall activity towards 2-OV[13]. This indicated additional engineering at E2o was required for altering substrate specificity in the overall reaction. The residues Ser330, Ser333, and His348 were proposed to be important in substrate recognition in E2o[16]. Hence, saturation mutagenesis libraries of these residues were constructed (E2-Ser330X, E2-Ser333X or E2-His348X) and assembled with E1o-His298Asp and E3, and the overall activity was screened with 2-OV. Positive clones were identified that displayed approximately 20% activity above the wild-type control for 2-OV. The E2o variants with the His348Phe, His348Tyr, His348Gln, or Ser333Met substitution were identified in the screen to be active towards 2-OV in the overall activity assay (NADH formation).

3.3.1 Computational analysis of substrate channel and surface-volume measurements

There are three proposed binding sites in the trimer. Each site is formed at the interface of two monomers[9,16]. For example, the cyan and green E2o CD monomers together form the substrate binding pocket and the water accessible volume is represented in solid magenta (Figure 3.4). The substrate accessible volume was computed by rolling a 1.5 Å sphere, and it is represented in a magenta solid (Figure 3.4) [131]. The volume was determined to be 2265 $Å^3$ of the wt-E2o CD (Figure 3.4A). E2o His348Phe and His348Tyr have similar volume when compared to wt-E2o CD (Figure 3.4B and 3.4D). On the other hand, the E2o CD His348Gln and Ser333Met variants have smaller volumes of 18 $Å^3$ and 90 $Å^3$, respectively (Figure 3.4C and 3.4E).

The ligand S8-succinyl dihydrolipoamide (SLM) was modelled substrate binding channel of E2oCD and its variants. The H-bond distances were calculated between the

amino acid side chains of residue lining the active site pocket of the receptors (E2oCD) and terminal carboxylate of SLM. The wild type E2oCD was docked with SLM as control (Figure 3.5A).

It has been proposed that the His348 and Ser333 residues are able to identify the terminal carboxylate of SLM by forming a H-bond [16]. The wild type docking results show that the distances of the carboxylate of SLM and the His348-N2 and Ser333-0H is 3.2 Å and 2.7 Å, respectively (Table 3.2). These distances fall under moderately strong H-bond category.

The side chains for E2oCD-His348Tyr side chains of residues are 3.4 and 3.0 Å for Tyr348 and Ser333, respectively (Figure 3.5D, Table 3.2). Also, kinetic experiment results show that E2oCD-His348Tyr is the most active variant (k_{cat}/K_m: 38.5% with respect to the wt-E2oCD) towards 2-OG. This variant has similar hydrogen bond distances and binding site volume. Hence, it is most active for 2-OG.

The side chains for E2oCD-His348Phe are 4.6 and 3.1 Å for Phe348 and Ser333, respectively (Figure 3.5B, Table 3.2). The Van der Waals volume of Phe side chain (135 $Å^3$) is slightly larger than His (118 $Å^3$). Phe fulfills a volume constraint, which is accompanied by lower catalytic efficiency (28% of wt-E2oCD).

The side chains for E2oCD-Ser333Met side chains are 3.5 and 4.0 Å for His348 and Met333, respectively (Figure 3.5E, Table 3.2). Moreover, the side chains for E2oCD-His348Gln are 3.4 and 4.7 Å for Gln348 and Ser333, respectively (Figure 3.5C, Table 3.2). The substrate-channel volumes decrease by 90 $Å^3$ and 18 $Å^3$ for both Ser333Met and His348Gln variants. This decrease is attributed to a change in the orientations of the amino acids side chains at position 333 for both the mutants which is reflected in a poor interaction with the substrate (Table 3.2). A cumulative unfavorable environment leads to

a decrease in catalytic efficiency (24% and 17% w.r.t. wt-E2oCD) for both Ser333Met and His348Gln variants.

Table 3.2 Comparison of E2oCD Amino Acid Side Chain Distances with Catalytic Efficiency towards 2-OG

E2oCD substitution	k_{cat}/K_m, ***2-OG*** **($M^{-1}s^{-1}$)**	**Residue 348[a] (Å)**	**Residue 333[b] (Å)**
none	875 x 10^3 (100%)	3.2	2.7
His348Tyr	337.5 x 10^3 (38.5%)	3.4	3.0
His348Phe	244 x 10^3 (28%)	4.6	3.1
Ser333Met	210 x 10^3 (24%)	3.5	4.0
His348Gln	149 x 10^3 (17%)	3.4	4.7

[a] Denotes the distance between terminal carboxylate of S(8)-succinyl dihydrolipoamide and side chain of the respective residue at position 348.
[b] Denotes the distance between terminal carboxylate of S(8)-succinyl dihydrolipoamide and side chain of the respective residue at position 348.

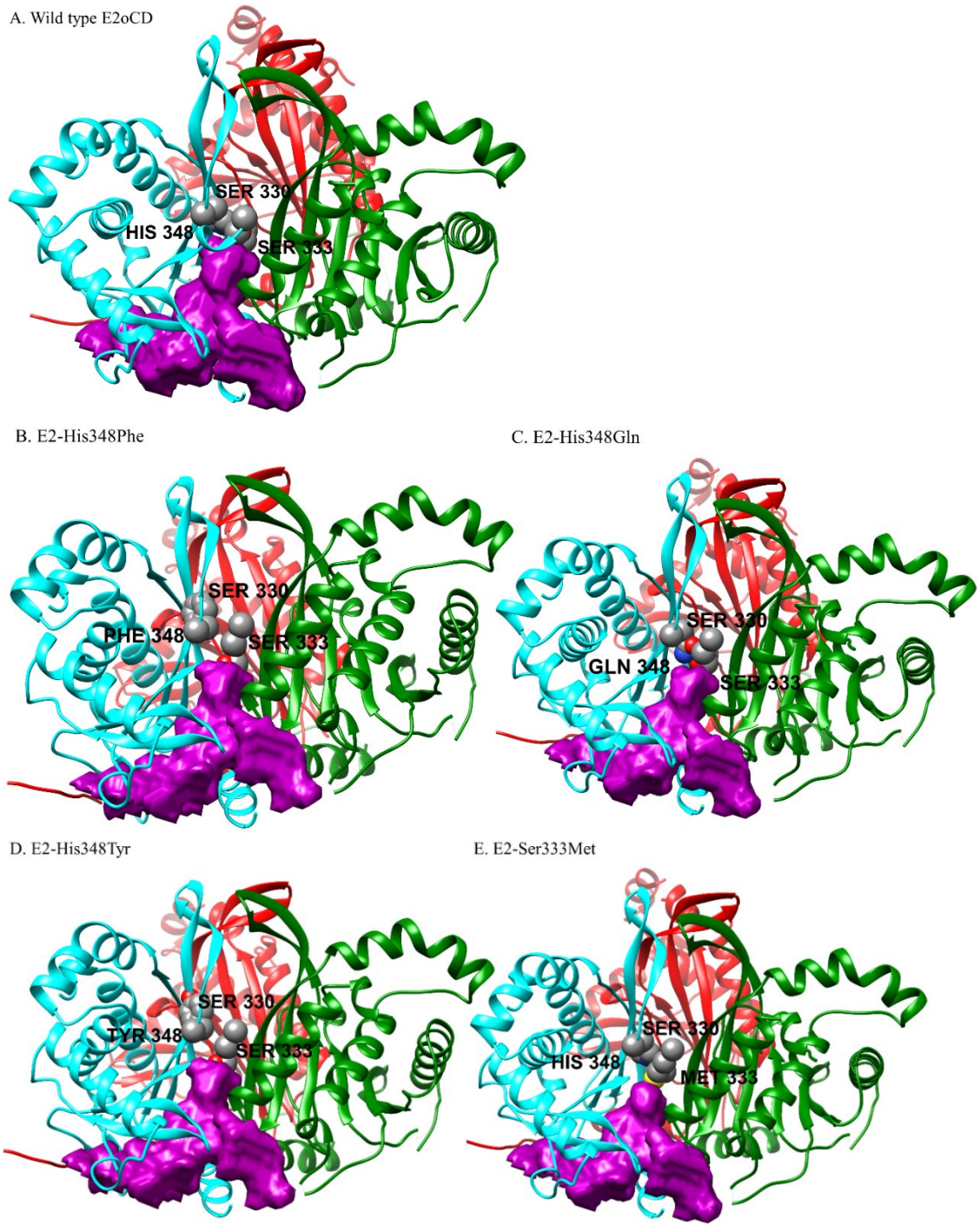

Figure 3.4 The solvent-accessible substrate channel modelled into the trimeric E2oCD. The substrate channel is shown in magenta. The trimer is represented by three different ribbon colors (red, green and cyan). Only one of the available three channels have been represented. S330, S333 and H348 are depicted as grey spheres. A. Wild type; B.His348Phe; C. His348Gln; D. His348Tyr; E. Ser333Met.

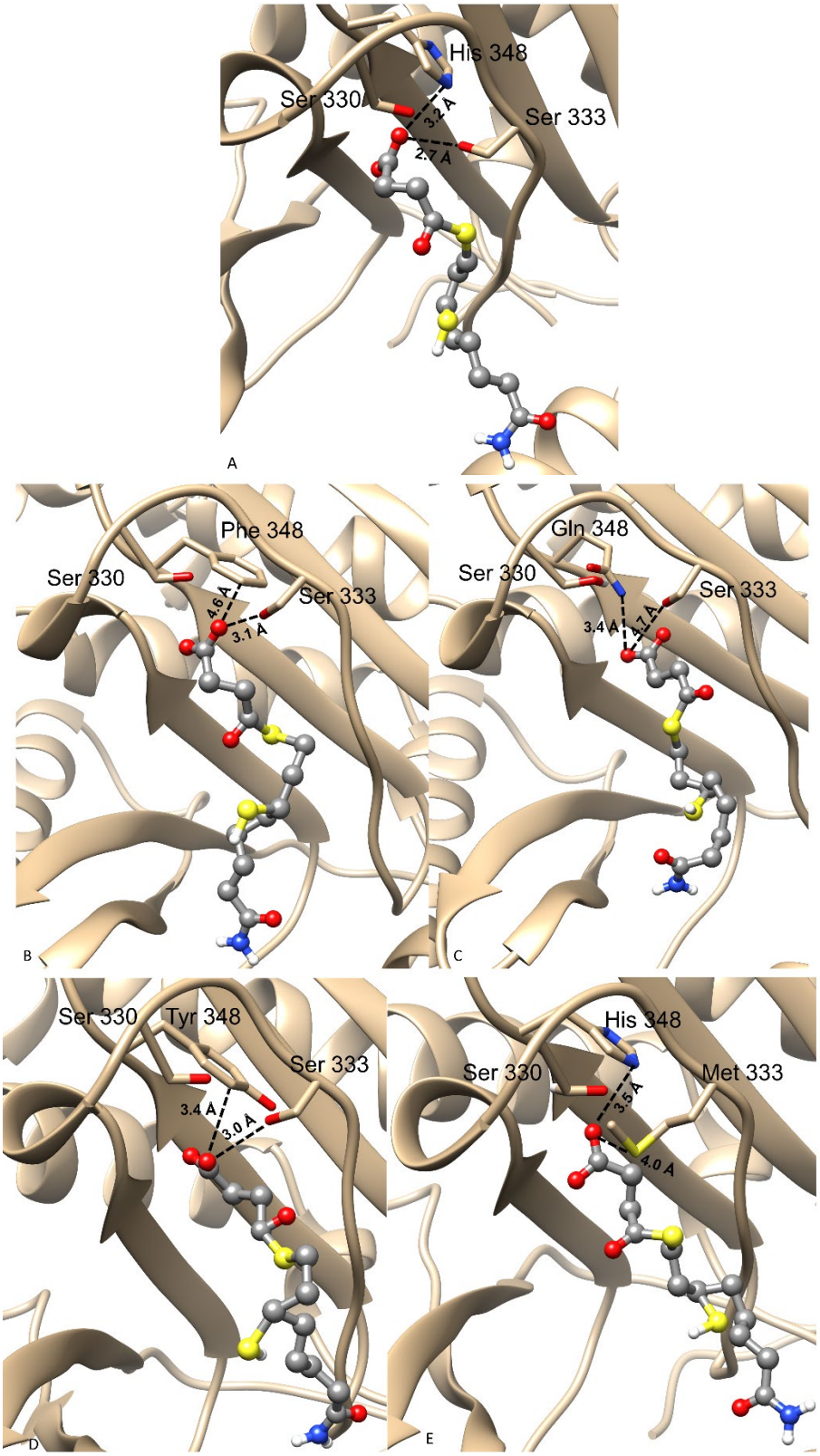

Figure 3.5 The active-site binding pocket of the E2oCD trimer and its variants docked with the substrate is represented.

S8-succinyl dihydrolipoamide (ligand) was docked into the active site pocket of the E2oCD (receptor) and variants: A. wildtype E2oCD B. E2oCD-His348Phe C. E2oCD-His348Gln D. E2oCD-His348Tyr E. E2oCD-Ser333Met. The docking calculations were performed with AutoDock Vina v.1.1.2 using Chimera to visualize [129,130]. The distances between the terminal carboxylate oxygen of S8- succinyl dihydrolipoamide and nearest the side-chain atom of the corresponding amino acid receptor has been shown.

3.3.2 Assembly of E1o-His298Asp/E2o-variants/E3 complex active with 2-OV

The overall activity ratio for the $[E1o\text{-}His298Asp/E2o\text{-}His348Gln/E3]_{2\text{-}OV}$, $[E1o\text{-}His298Asp/E2o\text{-}Ser333Met/E3]_{2\text{-}OV}$, $[E1o\text{-}His298Asp/E2o\text{-}His348Tyr/E3]_{2\text{-}OV}$, $[E1o\text{-}His298Asp/\ E2o\text{-}His348Phe/E3]_{2\text{-}OV}$, were 1.8%, 2.1%,, 3.0% and 5.6%, respectively, when compared to $[E1o\text{-}His298Asp/E2o/E3]_{2\text{-}OG}$ (Table 3.3). E1o-His298Asp and E3 assembled with E2- His348Phe, E2- His348Gln, or E2- His348Tyr had a K_m between 0.01- 0.05 mM (Figures 3.6 a,b; 3.7a,b; 3.8a,b and 3.9a,b). On the other hand, the K_m for E1o-His298Asp/E2o/E3 could not be determined because it has no activity towards 2-OV.

Table 3.3 Kinetic Characterization of the Different Complexes with Substrates 2-Oxoglutaric Acid, 2-Oxovaleric Acid and 2-Oxo-5-Hexenoic Acid (continued)

2-oxoglutaric acid

E2 substitution	Overall activity (μmol/min/mg E1)	K_m (mM)	k_{cat} (s^{-1})	k_{cat}/K_m ($M^{-1}s^{-1}$)
none[a]	18.2 ± 0.6 (100%)	0.04 ± 0.01	35	875 x 10^3
none[b]	5.35 ± 0.11 (29.4%)	0.03 ± 0.007	21.1	703.3 x 10^3
His348Phe[b]	2.06 ± 0.04 (11.3%)	0.03 ± 0.011	7.32	244 x 10^3
His348Gln[b]	2.94 ± 0.1 (16.1%)	0.07 ± 0.01	10.45	149.3 x 10^3
His348Tyr[b]	1.90 ± 0.02 (10.6%)	0.02 ± 0.005	6.75	338 x 10^3
Ser333Met[b]	2.37 ± 0.03 (13.02%)	0.042 ± 0.01	8.4	210 x 10^3

2-oxovaleric acid

E2 substitution	Overall activity (μmol/min/mg E1)	K_m (mM)	k_{cat} (s^{-1})	k_{cat}/K_m ($M^{-1}s^{-1}$)
none[a]	No activity detected	-	-	-
none[b]	No activity detected	-	-	-
His348Phe[b]	0.30 ± 0.1	0.01 ± 0.004	0.81	81 x 10^3
His348Gln[b]	0.096 ± 0.03	0.05 ± 0.01	0.34	6.8 x 10^3
His348Tyr[b]	0.161 ± 0.02	0.01 ± 0.007	0.57	57 x 10^3
Ser333Met[b]	0.107 ± 0.006	0.08 ± 0.012	0.38	4.7 x 10^3

Table 3.3 (continued) Kinetic Characterization of the Different Complexes with Substrates 2-Oxoglutaric Acid, 2-Oxovaleric Acid and 2-Oxo-5-Hexenoic Acid

2-oxo-5-hexenoic acid

E2 substitution	Overall activity (μmol/min/mg E1)	K_m (mM)	k_{cat} (s^{-1})	k_{cat}/K_m ($M^{-1}s^{-1}$)
none[a]	No activity detected	-	-	-
none[b]	No activity detected	-	-	-
His348Phe[b]	0.279 ± 0.0012	0.5 ± 0.14	0.99	1.98×10^3
His348Gln[b]	0.182 ± 0.005	1.1 ± 0.2	0.65	0.59×10^3
His348Tyr[b]	0.243 ± 0.033	0.73 ± 0.25	0.86	1.17×10^3
Ser333Met[b]	0.50 ± 0.12	0.11 ± 0.023	1.68	15.3×10^3

[a] Wild type E1o/E2o/E3 in a mass ratio of 1:1:1 (μg: μg: μg).
[b]The mutant complex is comprised of E1oHis298Asp, indicated E2o-X (X=Phe, Gln, Tyr or, Met) and E3 with a mass ratio of approximately 1:8:1 (μg: μg: μg). Activity was calculated per mg of E1His298Asp.

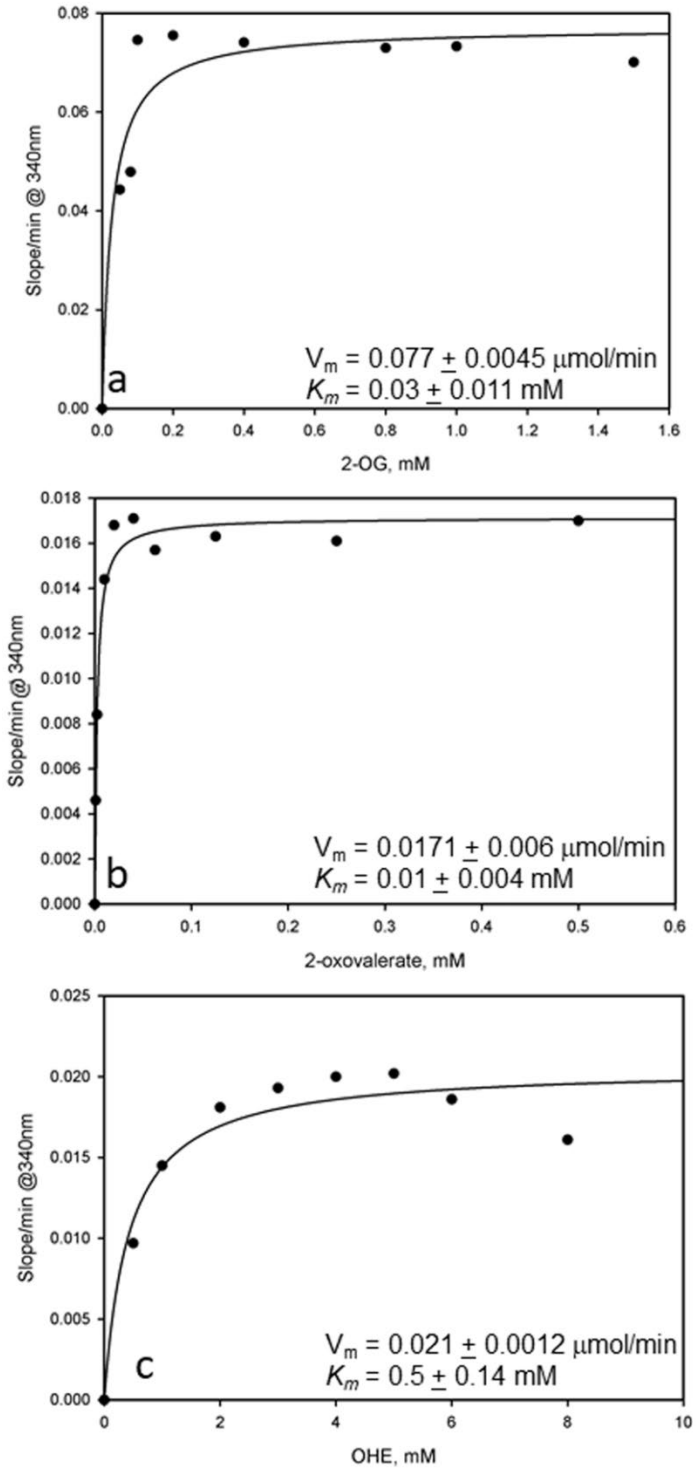

Figure 3.6 Michaelis Menten curves for the overall activity of the complex constituted of E1oHis298Asp:E2oHis348Phe:E3 in a mass ratio of 1:8:1 (µg: µg: µg).

The Y axis is represented by the rate of reaction shown by slope/min at absorbance 340nm. The X axis is represented by the corresponding substrate. For plot a. substrate 2-oxoglutarate is used. For plot b. substrate 2-oxovalerate is used and for plot c. substrate 2-oxo-5-hexenoic acid is used.

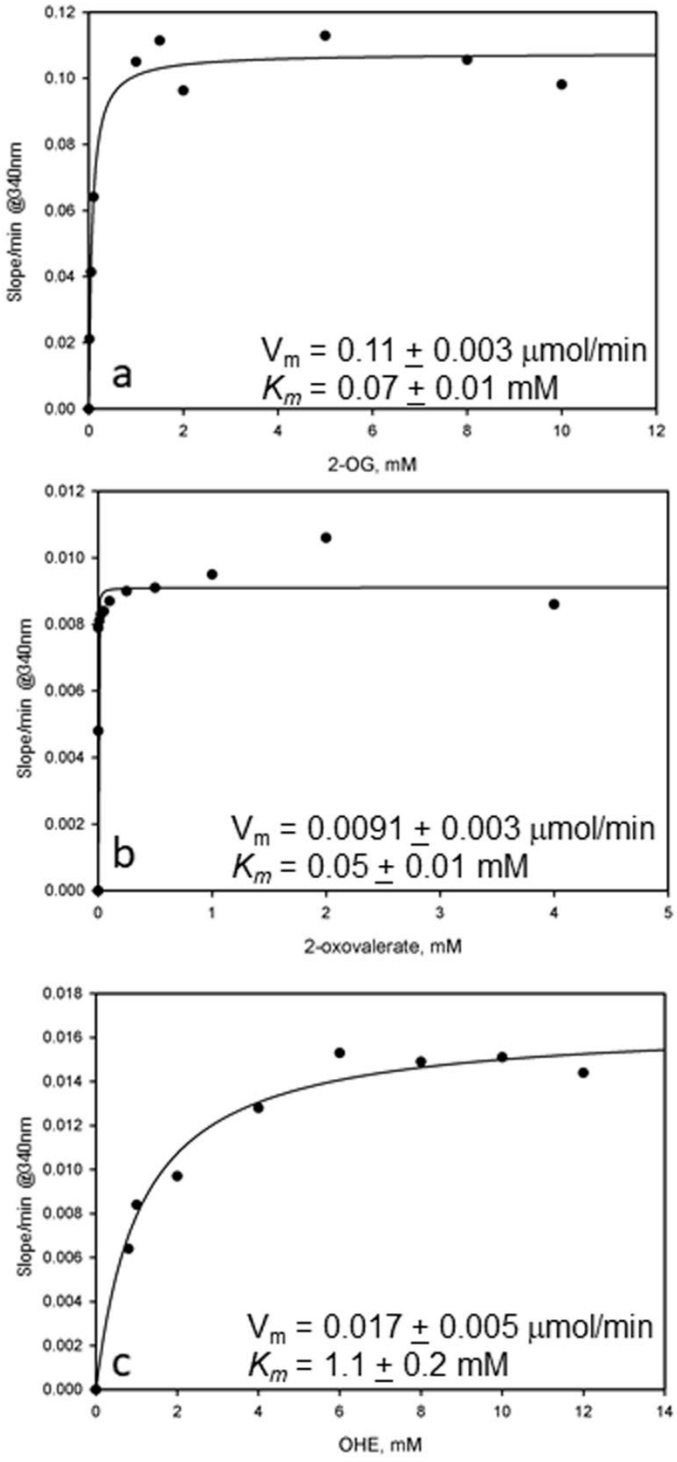

Figure 3.7 Michaelis Menten curves for the overall activity of the complex constituted of E1oHis298Asp:E2oHis348Gln:E3 in a mass ratio of 1:8:1 (µg: µg: µg).

The Y axis is represented by the rate of reaction shown by slope/min at absorbance 340nm. The X axis is represented by the corresponding substrate. For plot a. substrate 2-oxoglutarate is used. For plot b. substrate 2-oxovalerate is used and for plot c. substrate 2-oxo-5-hexenoic acid is used.

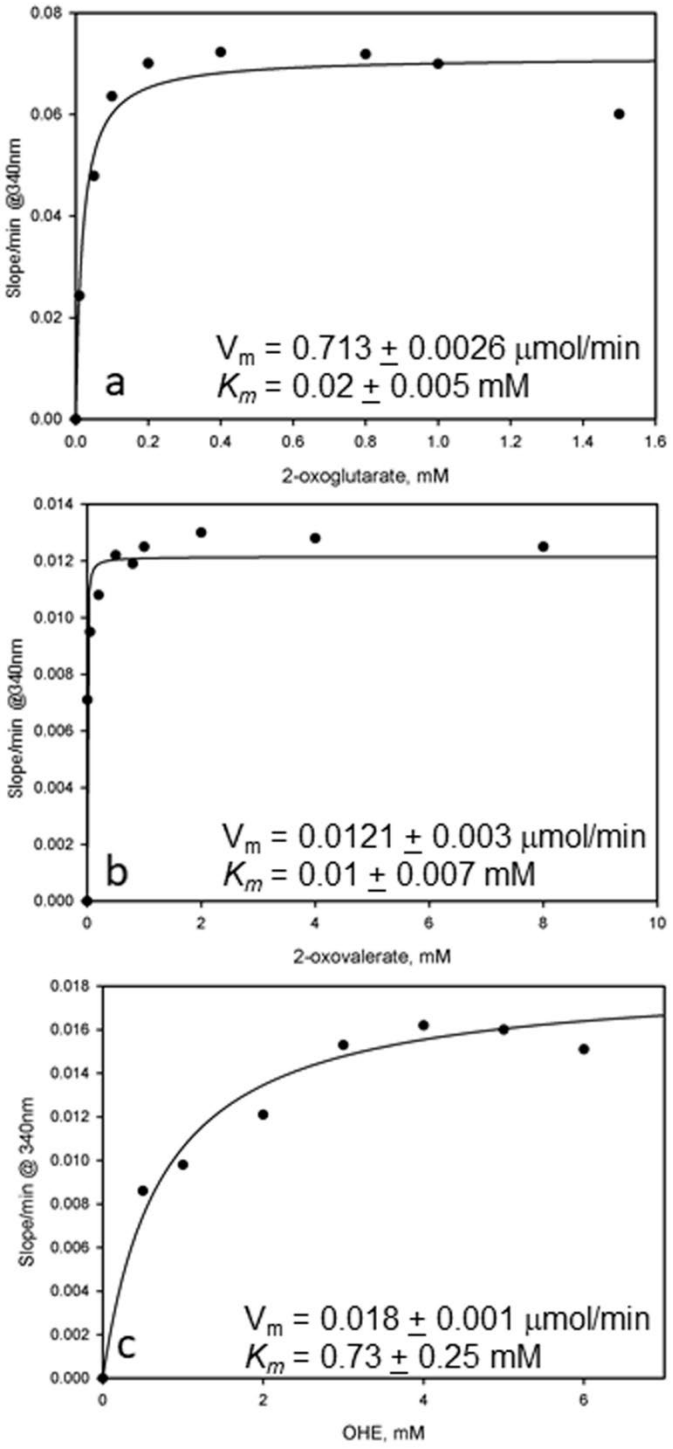

Figure 3.8 Michaelis Menten curves for the overall activity of the complex constituted of E1oHis298Asp:E2oHis348Tyr:E3 in a mass ratio of 1:8:1 (µg: µg: µg).

The Y axis is represented by the rate of reaction shown by slope/min at absorbance 340nm. The X axis is represented by the corresponding substrate. For plot a. substrate 2-oxoglutarate is used. For plot b. substrate 2-oxovalerate is used and for plot c. substrate 2-oxo-5-hexenoic acid is used.

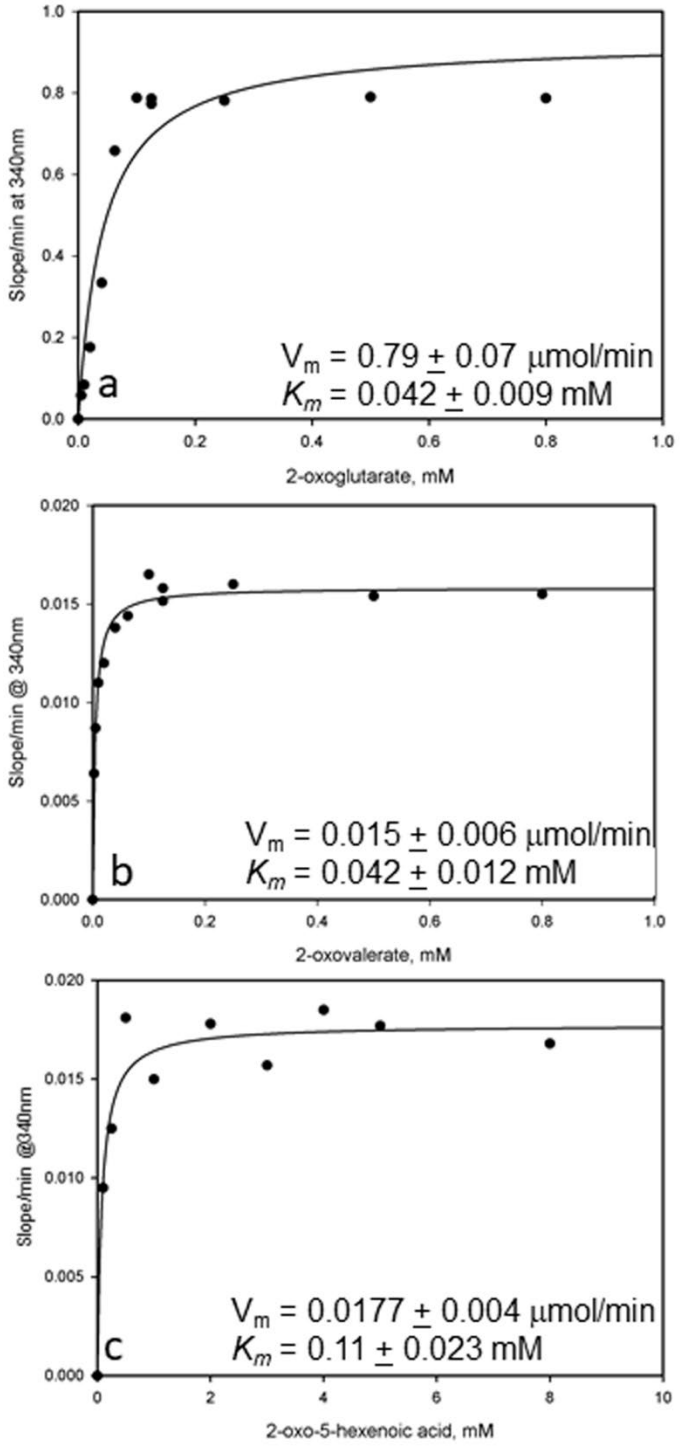

Figure 3.9 Michaelis Menten curves for the overall activity of the complex constituted of E1oHis298Asp:E2oSer333Met:E3 in a mass ratio of 1:10:1 (µg: µg: µg).
The Y axis is represented by the rate of reaction shown by slope/min at absorbance 340nm. The X axis is represented by the corresponding substrate. For plot a. substrate 2-oxoglutarate is used. For plot b. substrate 2-oxovalerate is used and for plot c. substrate 2-oxo-5-hexenoic acid is used.

The k_{cat}/K_m was 81.0, 57.0, 6.8, and 4.7 $mM^{-1} \cdot s^{-1}$ for [E1-His298Asp/E2-X/E3] (X = His348Phe, His348Tyr, His348Gln, or Ser333Met) with 2-OV, respectively. The residue histidine 348 is conserved in a broad range of species [16,17]. This residue was proposed to interact with the distal carboxylate of 2-OG for substrate recognition. It could be predicted that a hydrophobic amino acid substitution is required for 2-OV recognition and E2-His348Phe was most active towards 2-OV. The phenylalanine substitution does not alter the volume. It may enhance favorable hydrophobic interactions with the distal $–CH_3$ group of 2-OV to accommodate the substrate in the pocket (Figures 3.4B, 3.5B and 3.10A). The tyrosine amino acid substitution does not alter the solvent accessible volume. However, the hydrophobic character of the phenol ring furnishes complementary interactions with 2-OV that are not available with histidine. The histidine and glutamine have similar size, which are 114 and 118 Å, respectively. The His348Gln has a smaller solvent accessible volume than wt-E2o CD (Figures 3.4C, 3.5C and 3.10B). It is possible that a reduced pocket size favors the accommodation of the smaller 2-OV. Furthermore, the hydroxyl group of serine at position 333 has been proposed to H-bond with the distal carboxylate of succinyl dihydrolipamide [16]. Finally, similar to His348Gln, the Ser333Met substitution results in a smaller volume for 2-OV. Hence, methionine can interact favorably with the distal $-CH_3$ (Figure 3.4E, 3.5E and 3.10D).

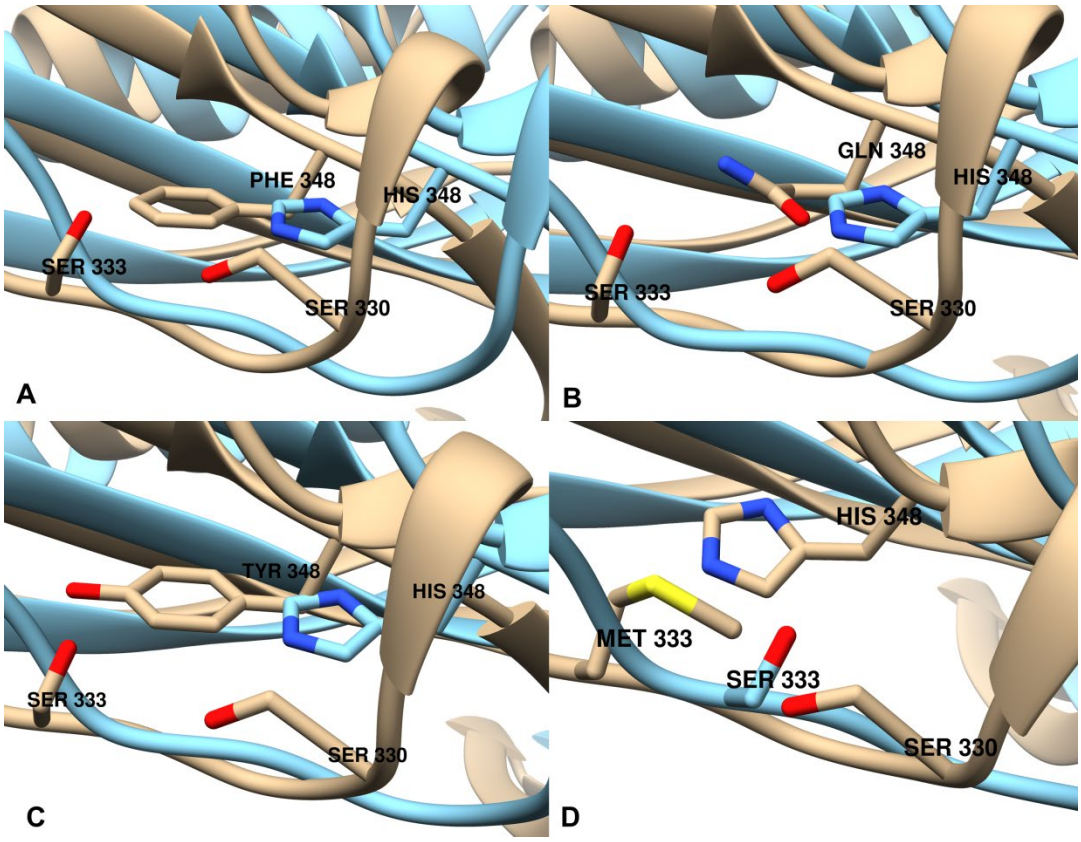

Figure 3.10 Substrate binding pocket of 2-OV binding variants. The amino acid substitution is superimposed over the wild-type residue.
Wt-E2o is represented by cyan ribbon. The orange ribbon represents the mutants A. H348F B. H348Q C. H348Y and D. S333M (PDB ID 1c4t).

The variant complexes show substrate inhibition with higher concentrations of 2-OV (Figure 3.11), the His348Gln < His348Phe < Ser 333Met. The complex assembled with E2-Ser333Met shows maximum inhibition with 2-OV, while the His348Gln variant shows the least inhibition. The complex assembled with E2o-His348Tyr, however, remained unaffected by higher concentrations of 2-OV.

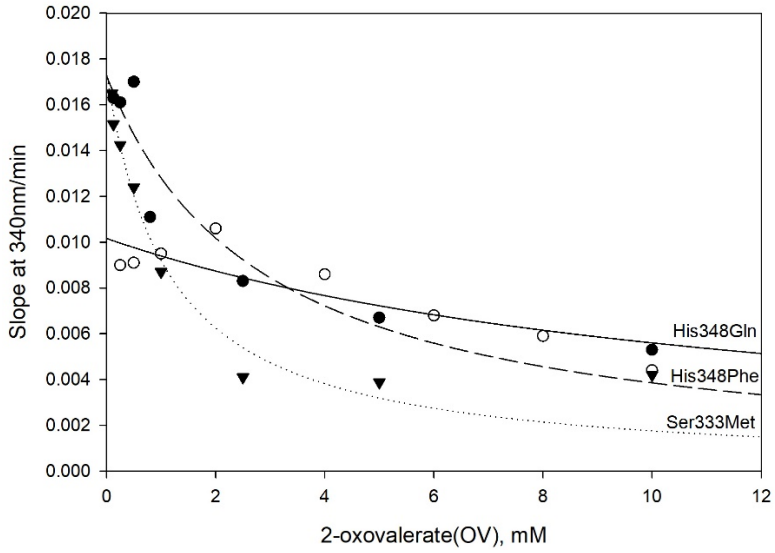

Figure 3.11 Substrate inhibition kinetics of the 2-oxovalerate dehydrogenase complexes consisting of E2o variants His348Phe, His348Gln and Ser333Met in overall activity with 2-oxovalerate.

3.3.3 E1o-His298Asp/E2-variants/E3 complexes active with 2-OHe

The engineered 2-oxo aliphatic acid dehydrogenase was evaluated to accept alternate functionalized aliphatic substrates. The kinetic parameters were determined for 2-OHe. This substrate is the next higher homolog of 2-OV, which contains a terminal alkene (Figure 3.1). The 2-OHe contains an alkene substituent that is useful for potential functionalization to increase subsequent product diversity. Similarly to 2-OV, no overall activity was detectable with wt-OGDHc and complex reconstituted with E1o-His298Asp/E2o/E3 and 2-OHe. The k_{cat}/K_m was 15.3, 1.98, 1.17, and 0.59 $mM^{-1} \cdot s^{-1}$ for Ser333Met, His348Phe, His348Tyr and His348Gln, respectively (Figures 3.6c, 3.7c, 3.8c, 3.9c). Ser333Met variant is the most active. This is expected because methionine provides a small and hydrophobic pocket. On the other hand, the Phe, Tyr, and Gln substitutions at position 348 may fulfill a space constraint. The complexes assembled as $[E1o\text{-}His298Asp/E2o\text{-}His348Gln/E3]_{2\text{-}OHe}$, $[E1o\text{-}His298Asp/E2o\text{-}His348Tyr/E3]_{2\text{-}OHe}$,

[E1o-His298Asp/E2o-His348Phe/E3]$_{2\text{-OHe}}$, and [E1o-His298Asp/E2o-Ser333Met/E3]$_{2\text{-OHe}}$ when compared to [E1o-His298Asp/E2o/E3]$_{2\text{-OG}}$, displayed overall activities of 3.4%, 4.54%, 5.2%, and 9.3%, respectively (Table 3.3).

3.3.4 The activity of reconstituted E1o-His298Asp/E2-variants/E3 active with 2-OG

The OGDHc variants acquired new substrate specificity for aliphatic substrates and it also retained activity towards 2-OG. The kinetic parameters were compared with wt-OGDHc with the variant complexes and 2-OG. The k_{cat}/K_m was 1.2-fold greater for wt-OGDHc compared to E1-His298Asp/E2o/E3. The variant's reduced catalytic efficiency is mainly due to the reduction of k_{cat} (Table 3.3). Next, E1-His298Asp/E3 reconstituted with E2o-His348Tyr, His348Phe, Ser333Met or His348Gln was considered and the k_{cat}/K_m was decreased by 2.5, 3.6, 4.1 and 5.9-fold relative to wt-OGDHc, respectively. The decrease was attributed to reduction of k_{cat}.

Next, the E1o-His298Asp and E3 was assembled with E2o-His348Phe, E2o-His348Gln, E2o-His348Tyr and E2o-Ser333Met. The overall activity was 11.3%, 16.1%, 10.6% and 13% compared to wt-OGDHc towards 2-OG (Table 3.3), respectively.

Volume calculations indicate that the pocket size does not change for His to Tyr or Phe substitutions at position 348 (Figures 3.4A, 3.4B, 3.4D). Histidine to tyrosine is a conservative substitution, and it is the most active variant towards 2-OG[133]. The tyrosine hydroxyl group can interact with the terminal carboxylate of 2-OG. The Phe residue could only fulfill a volume requirement. The Met or Gln substitutions lead to a smaller binding pocket, which may lead to unfavorable steric interaction with 2-OG. In addition, the hydrophobic side chain of Met leads to detrimental interactions with the carboxylate of 2-OG.

It is clear that the amino acid substitutions identified by our experiments could not be predicted. For example, Phe is one the most hydrophobic amino acids. However, 2-OG remains active with E2o His348Phe. In fact, the catalytic efficiency is only decreased by 3.6-fold [13,134].

3.3.5 E1o specific activity towards 2-OG, 2-OV, and 2-OHe

The E1o-specific activity ratio for wt-E1o$_{2\text{-OV}}$: wt-E1o$_{2\text{-OG}}$, wt-E1o$_{2\text{-OHe}}$: wt-E1o$_{2\text{-OG}}$, E1-His298Asp$_{2\text{-OV}}$; wt-E1o$_{2\text{-OG}}$, and E1-His298Asp$_{2\text{-OHe}}$: wt-E1o$_{2\text{-OG}}$ are 5.5, 2.0, 17.4, and 5.4%, respectively (Table 3.4). The E2o variants were assembled with E1o-His298Asp and E3 to form the engineered complexes. The overall activity (NADH) for this complex was determined with 2-OG, 2-OV and 2-OHe. First, the overall activity was determined with the natural substrate, 2-OG. The control complex formed by E1o-His298Asp/E2o/E3 has approximately 29.4% activity in comparison to wt-OGDHc with 2-OG.

Table 3.4 E1o-specific Activity and Kinetic Parameters for Various Substrates

Wild-type E1o-specific activity

Substrate	DCPIP activity ($\mu mol.min^{-1}.mg^{-1}$)	K_m (mM)	k_{cat} (s^{-1})	k_{cat}/K_m ($mM^{-1}s^{-1}$)
2-OG[a]	0.775 ± 0.04	0.006 ± 0.02	2.7	456.6
2-OV[b]	0.0429 ± 0.004	8.18 ± 0.63	0.152	0.0165
2-OHE[c]	0.0168 ± 0.0072	8.01 ± 1.9	0.0595	0.0074

E1o-specific activity for E1oH298D[d]

Substrate	DCPIP activity ($\mu mol.min^{-1}.mg^{-1}$)	K_m (mM)	k_{cat} (s^{-1})	k_{cat}/K_m ($mM^{-1}s^{-1}$)
2-OG[a]	0.206 ± 0.057	1.87 ± 0.81	0.73	0.39
2-OV[b]	0.135 ± 0.04	6.62 ± 0.93	0.48	0.0725
2-OHe[c]	0.042 ± 0.011	11.1 ± 1.3	0.148	0.0134

[a] 2-OG, 2-oxoglutaric acid; [b] 2-OV, 2-oxovaleric acid; [c] 2-OHe, 2-oxo-5-hexenoic acid
[d]E1oH298D parameters are determined for four different preparations of the pure enzyme and the average value of the parameters is shown.

3.3.6 Enzymatic synthesis of butyryl-CoA from 2-oxovalerate

The synthesis of the butyryl-CoA by E1oHis298Asp assembled with each of the E2o variants and E3 into the corresponding OGDHc was demonstrated and provides strong evidence that 2-oxovalerate could be a satisfactory substrate for butyryl-CoA synthesis by some E2o variants, particularly by the E2oHis348Gln variant. Hence, the method could be employed for bio-based production of butyryl-CoA for E2oHis348Gln and variants (Figures 3.12-3.17). Table 3.5 summarizes the MALDI TOF/TOF data for all analyzed E2o variants.

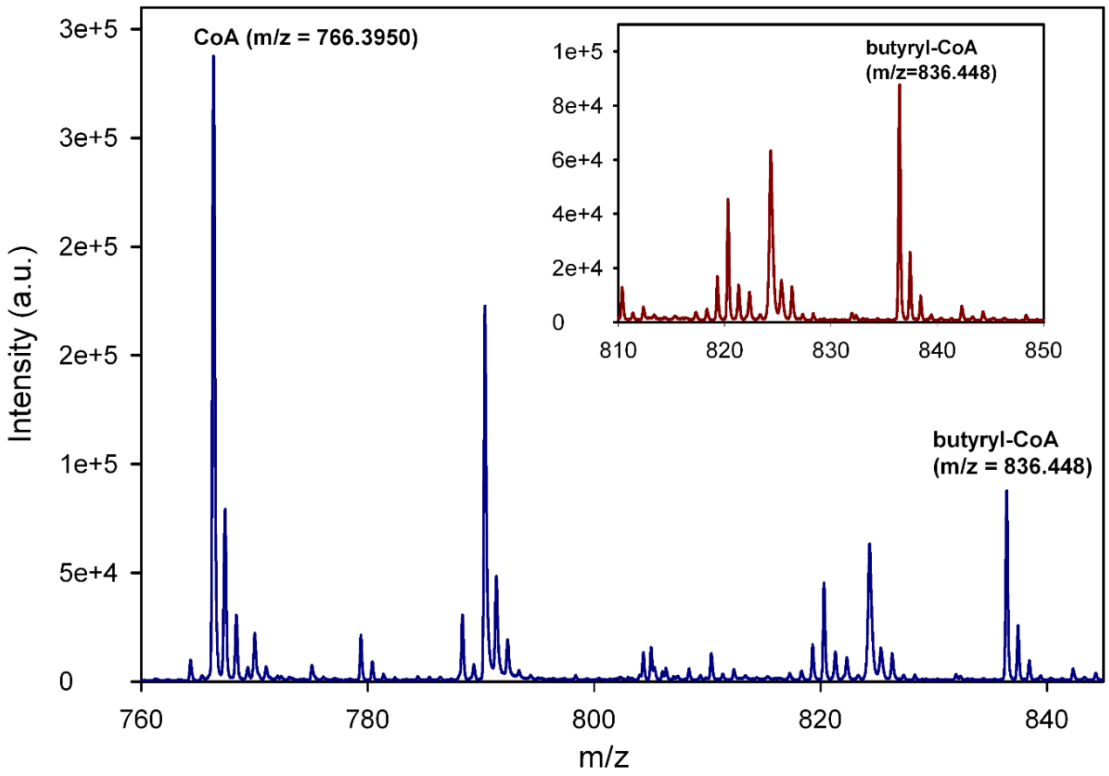

Figure 3.12 MALDI TOF/TOF detection of the butyryl-CoA formed in the enzymatic reaction from 2-oxovalerate and CoA by OGDHc assembled from E1oH298D/E2oH348Q/E3. Both, CoA (*m/z* = 766.395) and butyryl-CoA (m/z = 836.448) are present on the spectrum. Inset shows an enlarged region of the butyryl-CoA peak. For experimental conditions, see Materials and Methods section.

Table 3.5 Summary of the MALDI-TOF/TOF data for Butyryl-CoA Detection in the OGDHc Reaction

E2o variant assembled with E1o-H298D and E3[a]	**CoA substrate [b]**	**Butyryl-CoA synthesised**	**Butyryl-CoA / (CoA + butyryl-CoA) (the relative peak heights)**
His348Phe	m/z = 766.296	m/z = 836.342	0.019 (1.9%)
His348Tyr	m/z = 766.293	m/z = 836.334	0.044 (4.4%)
His348Gln	m/z = 766.395	m/z = 836.448	0.221 (22%)
Ser333Met	m/z = 766.403	m/z = 836.442	0.066 (6.6%)

[a] Butyryl-CoA synthesis was conducted for ~ 15 h at 30 °C. For His348Phe E2o, data are presented after one h reaction time since no butyryl-CoA was detected after 15 h of reaction. [b] The concentrations of CoA and 2-oxovalerate of 300 μM and 4 mM, respectively were used in the reaction mixture.

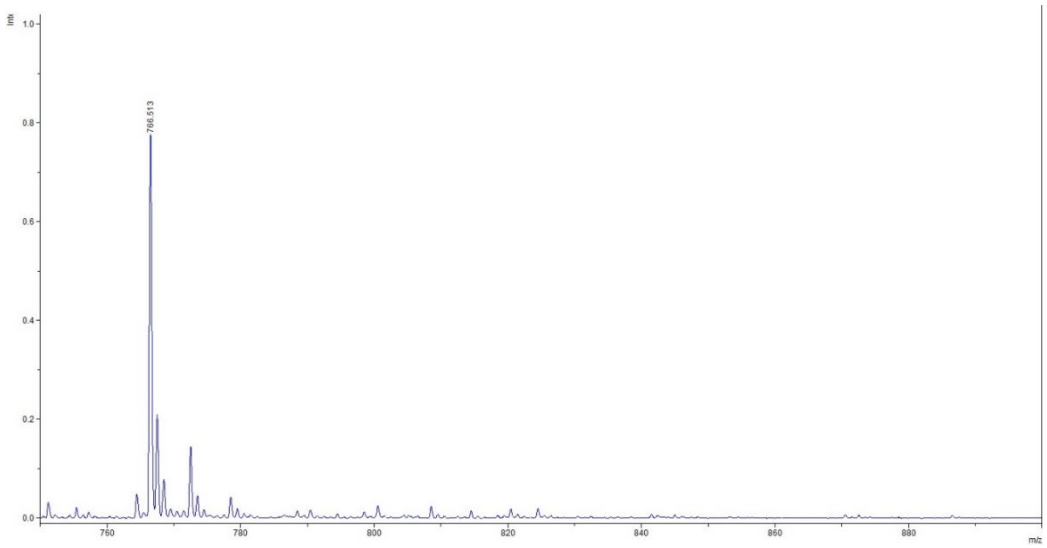

Figure 3.13 MALDI TOF/TOF spectrum of the CoA standard (m/z = 766.513).

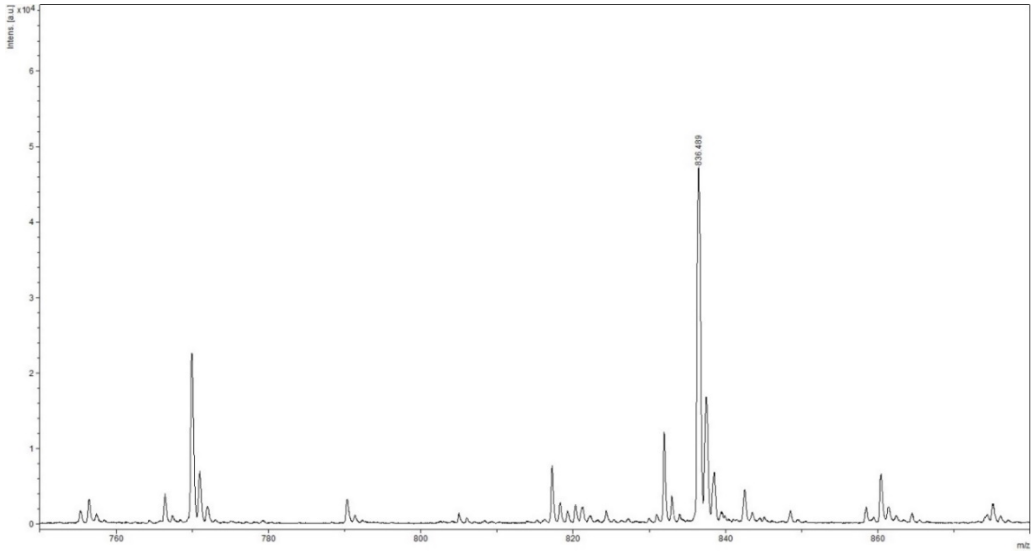

Figure 3.14 MALDI TOF/TOF spectrum of the butyryl-CoA standard (m/z = 836.489).

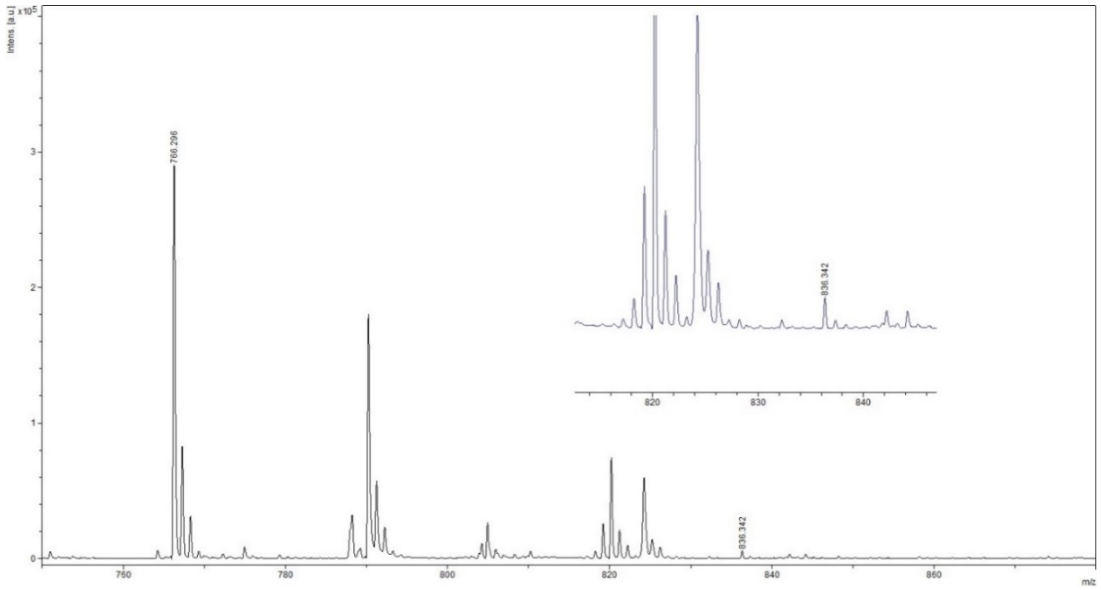

Figure 3.15 MALDI TOF/TOF detection of the butyryl-CoA formed in the enzymatic reaction from 2-oxovalerate and CoA by OGDHc assembled from E1o-His298Asp, E2o-His348Phe and E3. Both, CoA (*m/z* = 766.296) and butyryl-CoA (m/z = 836.342) are present on the spectrum. Inset shows an enlarged region of the butyryl-CoA peak.

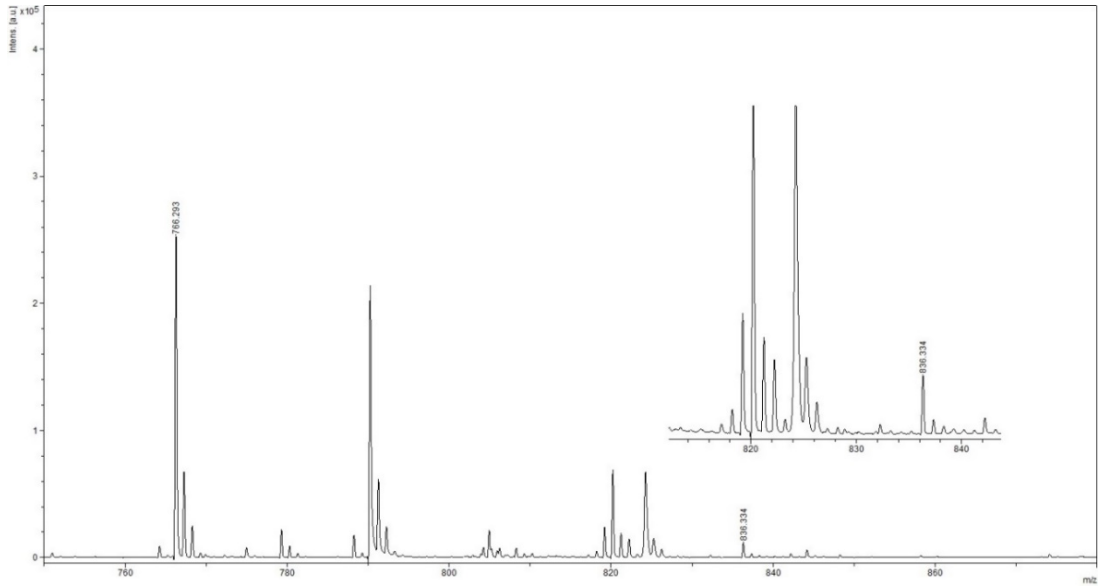

Figure 3.16 MALDI TOF/TOF detection of the butyryl-CoA formed in the enzymatic reaction from 2-oxovalerate and CoA by OGDHc assembled from E1o-His298Asp, E2o-His348Tyr and E3. Both, CoA (*m/z* = 766.293) and butyryl-CoA (m/z = 836.334) are present on the spectrum. Inset shows an enlarged region of the butyryl-CoA peak.

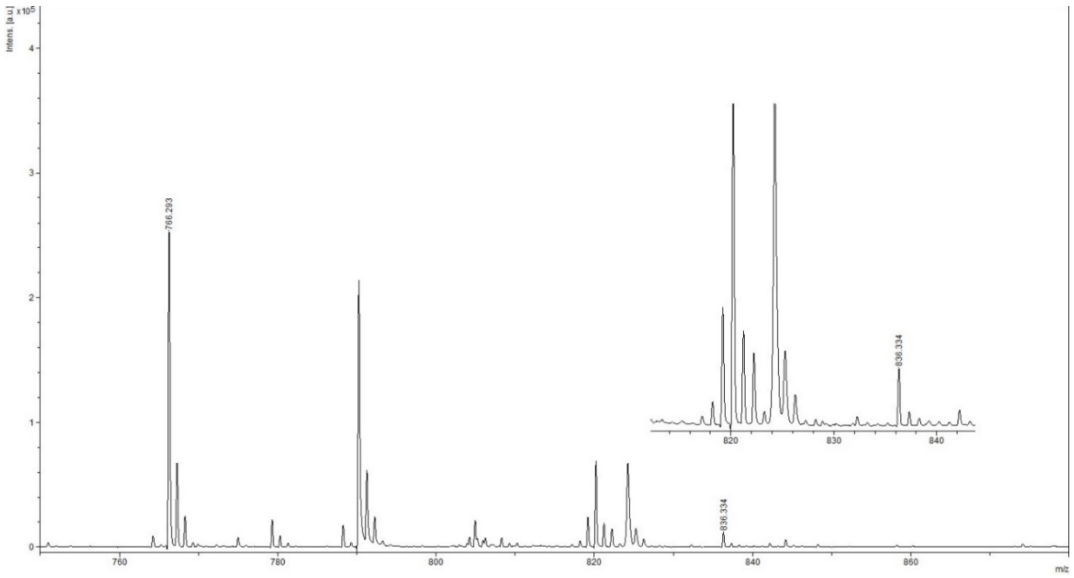

Figure 3.17 MALDI TOF/TOF detection of the butyryl-CoA formed in the enzymatic reaction from 2-oxovalerate and CoA by OGDHc assembled from E1o-His298Asp, E2o-Ser333Met and E3. Both, CoA (*m/z* = 766.403) and butyryl-CoA (m/z = 836.442) are present on the spectrum. Inset shows an enlarged region of the butyryl-CoA peak.

3.4 Conclusion

The OGDHc is an example of an enzyme in a highly conserved pathway across all kingdoms. In this study, it was evolved from a 2-oxo acid dehydrogenase to a 2-oxo aliphatic acid dehydrogenase. This was accomplished by engineering two consecutive components of the multienzyme complex. The promiscuous variant components were able to catalyze the reaction with both natural and unnatural substrates. In short, a generalist could be converted to a new specialist through a negative selection. For example, variants could be screened that are not active toward natural substrate while retaining activity for the non-cognate substrate. Similar to natural evolution, the new pathway could be engineered to suit particular user-defined goals. For example, orthogonal pathways can be engineered from existing pathways. These designed routes can run in parallel to the existing pathways and can be used for chemical and synthetic biology [135].

APPENDIX A

CARBOLIGATION WITH THIAMIN DIPHOSPHATE DEPENDENT ENZYMES

A.1 Introduction

Carboligation is defined as formation of novel C-C bonds [136]. A common reaction characteristic of ThDP dependent enzymes (glyoxylate carboligase, 1-deoxy-D-xylulose-5-phosphate synthase (DXPS), benzaldehyde lyase etc…) involves formation of novel C-C bonds or carboligation [137–141]. Previously, the synthetic program using the carboligation reactions was initiated by Jordan group with various active site modifications in both yeast pyruvate decarboxylase (yPDC) from *Sachharomyces cerevisae* and E1p from pyruvate dehydrogenase complex of *Escherichia coli* [142–144].

The E1o subunit of OGDHc is known for its decarboxylase activity as the natural reaction. The function of OGDHc starts with the decarboxylation of 2-OG by E1o to form the ThDP adduct of succinic semialdehyde (enamine) intermediate (Figure A.1, step 1) [145]. This intermediate is a substrate for the E2oLDo. The succinyl group is transferred from the E1o active site to LDo followed by the succinyl transferase action at the CDo. However, in absence of E2 or E3 subunits, the catalytic potential of the central enamine intermediate has been exploited for the purpose of carboligation. Thus, with the addition of appropriate acceptors, E1o is able to catalyze the formation of δ-hydroxy-γ-keto acids [145]. These are important intermediates for organic synthesis. For some enzymes, carboligation is a natural course of the pathway, while for all 2-oxoacid decarboxylases, it is a side reaction [142,143,146,147]. ThDP dependent enzymes (E1p, benzoylformate decarboxylase, etc.), have been demonstrated for carboligation potential

as industrial biocatalysts. This is due to for their innate promiscuity towards non-natural substrates and perform carboligation [148]. [44,117,149,150].

The mechanism of carboligation by E1o is similar to that of the ThDP dependent enzymes. In the first step, C2-ThDP bound intermediate is formed by nucleophilic addition of the ThDP-ylide to the carbonyl carbon of a donor substrate (Figure A.1). Next, this step is followed by the decarboxylation reaction, which results in the formation of an activated carbonyl compound bound to C2 α-ThDP (C2 α-carbanion/enamine) (Figure A.1). This reaction is common to ThDP dependent class of enzymes.

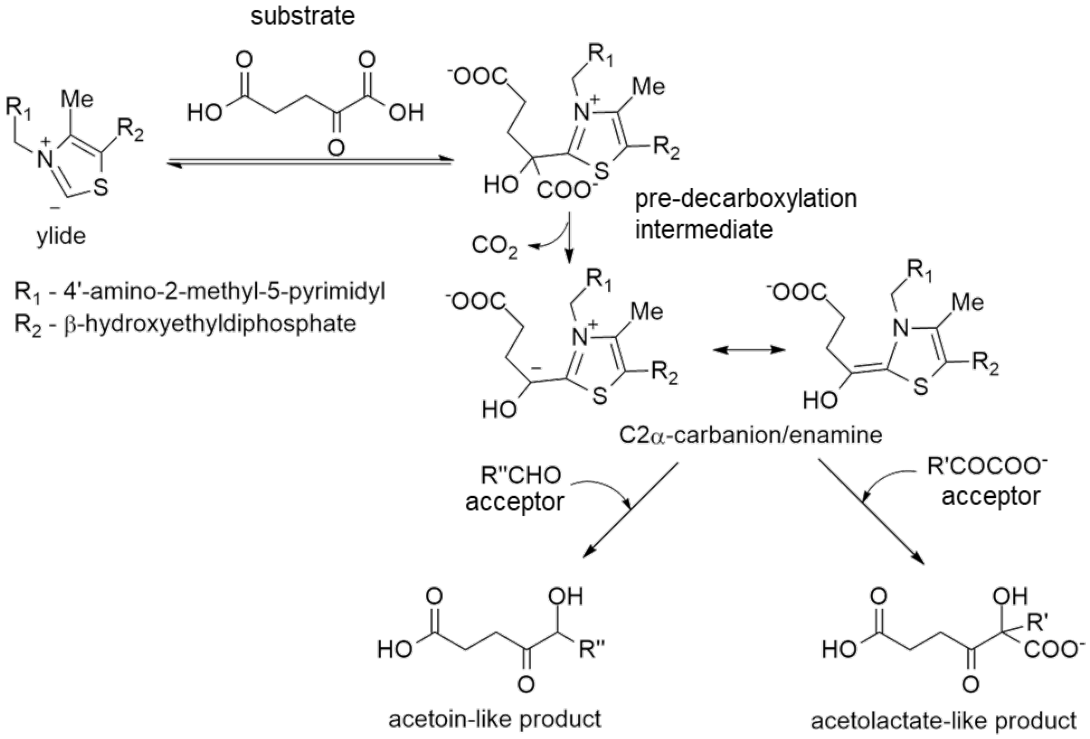

Figure A.1 E1o catalyzed reaction mechanism of carboligation reaction.

The ThDP acts as an electron sink and the reactivity of the carbonyl carbon atom adjacent to C2 α -ThDP undergoes an 'Umpolung' reaction and this alters the reactivity of the bound carbonyl carbon from an electrophile to a nucleophile. Also, an enamine-

carbanion, has the properties of an activated aldehyde. Therefore, addition of an acceptor molecule aldehyde (methyl glyoxal), ketone (ethyl glyoxalate) or keto-acid (2-OV, 2-OG) (Figure A.2) results in formation of chiral 2-hydroxy ketones (acetoin-like) or hydroxy-ketoacids (acetolactate-like) [145,151,152].

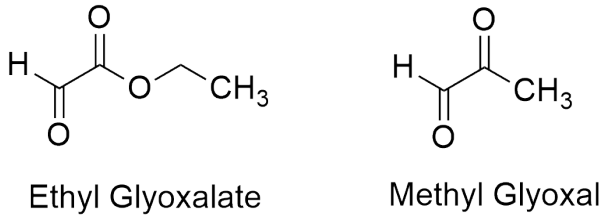

Figure A.2 Examples acceptor substrates: Ethyl glyoxalate and methyl glyoxal.

This property has been used for chiral synthesis over the years [137,151,153]. E1o component has been studied for the purpose as well [91,92,147]. E1o has been previously proved to have a broad substrate range, making it an excellent candidate for protein engineering [12,13]. Carboligation studies have also been reported by our group with the E1o component using a 2-keto acid (2-OG, 2-OV and 2-oxo-isovaleric acid) as a substrates with various acceptor aldehydes (ethyl glyoxalate and methyl glyoxal) [147].

Thiamin dependent decarboxylases have been engineered to produce enantioselective carboligase products from amino acid analogs [142,144]. These molecules are potential lead molecules in drug development pipeline for some of the well-known drugs such as: the tranquilizer and smoking cessation drug bupropion [154], the anti-allergic drug cytoxazon [155], and the multidrug-pump inhibitor 5-methoxyhydnocarpin [156]. Carboligase products are also precursors for Alzheimers drugs [142,144].

The objective of this study is to explore the carboligation properties of the E1o component of the *E.coli* 2-oxoglutarate dehydrogenase multienzyme complex (OGDHc) and its variant His298Asp [147]. In addition, MenD was evaluated for carboligation (*vide infra)*. A combination of different substrates and acceptor compounds were used to demonstrate the ability of the enzymes to catalyze carboligation. Studies on several aliphatic and aromatic substrate-acceptor combination have also been reported for carboligation reactions catalyzed by E1o [145,157]. The products were characterized by CD spectroscopy and proton NMR.

MenD (2-succinyl-5-enolpyruvyl-6-hydroxy-3-cyclohexadiene-1-carboxylate synthase; EC 2.5.1.64 or 2.2.1.9), is involved in the second step of menaquinone biosynthesis. MenD catalyzes carboligase reactions as E1o. It catalyzes a ThDP and Mg^{+2}-dependent 1,4-addition of 2-OG to isochorismate to form SEPHCHC and CO_2 (Figure A.3) [158–160]. MenD is the only enzyme known to catalyze the addition of a ThDP intermediate to the β-carbon of a second substrate [145,161]. This reaction is similar to the Stetter reaction, which is a 1,4-addition, or conjugate addition, of an aldehyde to a β-unsaturated compound. A functionally active MenD was expressed and purified and tested of carboligation reactions.

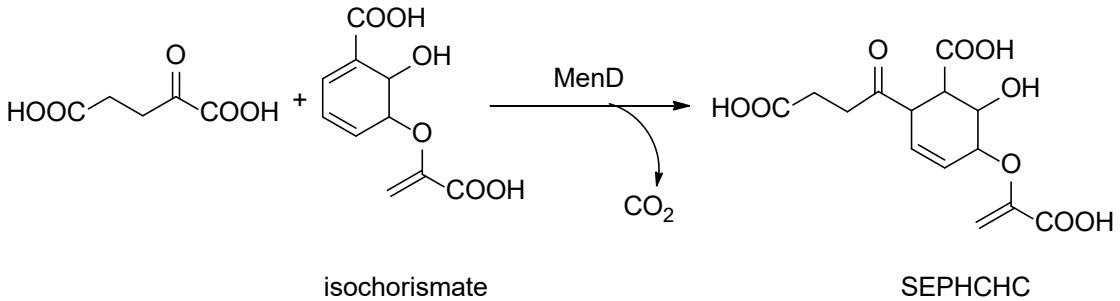

Figure A.3 Reaction catalyzed by MenD.

This work reinforces the versatility of E1o as a valuable chiral synthetic tool. This is supported by the fact that the enzyme accepts 2-oxoglutaric acid (2-OG), 2-oxoadipic acid (2-OA), 2-oxo-hexanoic acid (2-OH) and 2-oxo-5-hexenoic (2-OHe) acid as substrates. Glyoxalate, propanal and butyraldehyde are the acceptor compounds (Figure A.4).

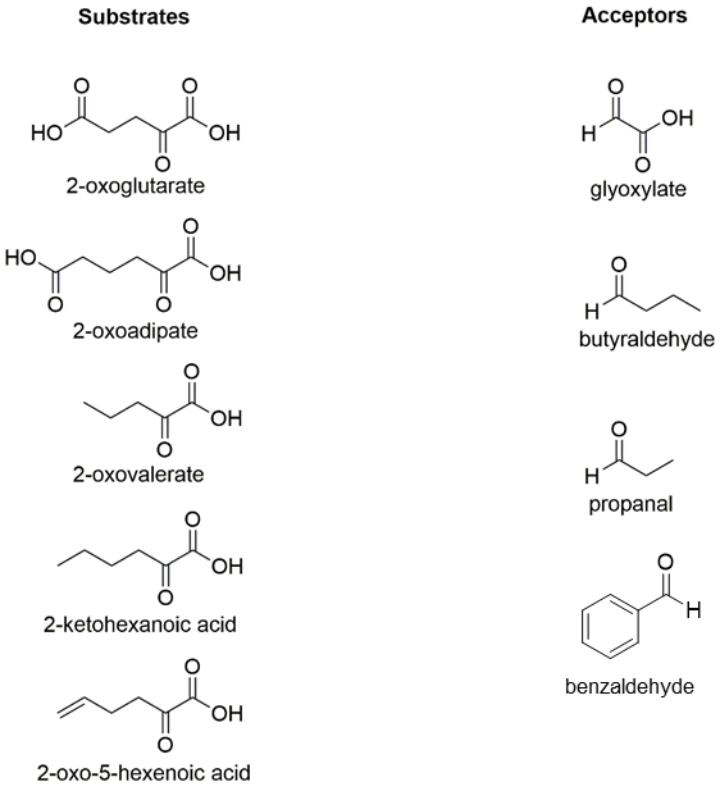

Figure A.4 Substrates and acceptors for carboligase reaction for E1o and MenD.

A.2 Materials and methods

A.2.1 Materials

Ni-NTA agarose used for protein purification was purchased from GE Healthcare Life Sciences. Thiamin diphosphate (ThDP), dithiothreitol (DTT), isopropyl-β-D-thiogalactopyranoside (IPTG), NAD^+, coenzyme A (CoA), Micrococcal Nuclease, and

DNase I, Lyophilized were purchased from Affymetrix USB. *E. coli* strain JW0715 containing the plasmid pCA24N encoding the OGDHc-E1 (E1o) component [ASKA clone (-)] was obtained from National Bio Resource Project (NIG, Japan). Sodium pyruvate, 2,6-dichlorophenolindophenol (DCPIP), 2-oxoglutarate (2-OG), 2-oxovalerate (2-OV), 2-oxoadipate (2-OA), and glyoxylic acid were purchased from Sigma Aldrich. Butyraldehyde and propanal were purchased from Acros Organics (part of Thermo Fisher Scientific). 2-Ketohexanoic acid (2-OH) was purchased from Santa Cruz Biotechnology. 4-Pentenal was purchased from Thermo Fisher Scientific Chemicals.

A.2.2 Expression and purification of wild type E1o human, MenD, wild type E1o *E.coli* and its variants

Wild type E1o was obtained from *E. coli* strain JW0715 harboring the plasmid pCA24N encoding the OGDHc-E1 (E1o) component. An *E. coli* AG1 frozen stock harboring the E1o plasmid was streaked on LB agar plates containing chloramphenicol (100 μg/mL) and incubated at 37 °C overnight. A single colony was used to inoculate 5 tubes with 10 ml LB containing chloramphenicol (100 μg/mL).

The overnight culture was used to inoculate 4L of LB medium containing chloramphenicol (30 μg/mL), 1.0 mM thiamin hydrochloride, and 2.0 mM $MgCl_2$. Cells were grown at 37 °C, 250 rpm till to OD_{600} reached 0.60-0.70, then 0.50 mM IPTG was added and cells were grown overnight at 27 °C with shaking. The cells were collected at 4400 g at 4 °C and washed with 20 mM KH_2PO_4 (pH 7.0) containing 0.15 M NaCl. Cell pellets were stored at -20 °C until purification.

Cell Disruption and Purification.

All subsequent steps were carried out at 4 °C. The cells were resuspended in 40-50 ml sonication buffer: 20 mM KH_2PO_4 (pH 7.4) containing 0.3 M NaCl, 5.0 mM $MgCl_2$, 2.0 mM ThDP, 1.0 mM benzamidine hydrochloride, 25 mM imidazole, and 1.0 mM PMSF (1.0 mM). Lysozyme was added to a final concentration of 0.60 mg/ml, and cells were incubated for 20 min on ice. Nuclease and DNase were added at 1,000 units each and cells were incubated for 20 min on ice. The cells were sonicated for 10 min (20 s pulsar "on" and 20 s pulsar "off") using the Sonic Dismembrator Model 550 (Fisher Scientific). The lysate was centrifuged at 30,000 g at 4 °C for 30 min.

His_6-tag wild type E1o or E1o variant were purified by using a His6-tag a Ni Sepharose 6 Fast Flow Column (GE Healthcare). The column was equilibrated with 150 ml of sonication buffer and 50 ml of cell lysate was applied on the column. The column was then washed with 10 column volume (CV) of binding buffer containing 20 mM KH_2PO_4 (pH 7.5), 0.3 M KCl, 5 mM $MgCl_2$, 2 mM ThDP and 25 mM imidazole followed by 10 CV of washing buffer containing 20 mM KH_2PO_4 (pH 7.5), 0.3 M KCl, 5 mM $MgCl_2$, 2 mM ThDP and 50 mM imidazole. The bound proteins were eluted using elution buffer containing 20 mM KH_2PO_4 (pH 7.5), 0.3 M KCl, 5 mM $MgCl_2$, 2 mM ThDP and 200 mM imidazole. Fractions with enzyme were combined, dialyzed against 20 mM KH_2PO_4 (pH 7.5), 0.30 M KCl, 2.0 mM $MgCl_2$, 0.5 mM ThDP and 1.0 mM benzamidine hydrochloride. Next, the protein was precipitated by PEG-8000 (50% w/v) adding 0 – 16% PEG dropwise (~4 ml per 25 ml protein) on ice with stirring for 10-15 minutes. The protein was collected by centrifugation at 15,000 rpm for 20 minutes at 4 ^oC. The resulting protein pellet was dissolved in ~0.5 ml of 50 mM KH_2PO_4 (pH 7.5) containing 0.4 M ammonium chloride, 1.0 mM MgCl2, 0.2 mM ThDP, and 1.0 mM

benzamidine hydrochloride. The purity was confirmed by SDS-PAGE. Wild type E1o and E1o variants were stored at -80 °C.

A.2.3 CD Spectroscopy for Product Accumulation

CD spectra were recorded on a Chirascan CD Spectrometer (Applied Photophysics, Leatherhead, U.K.) in 2.4 ml volume with 1 cm path length cell at 30 ºC in the near-UV (270 – 400 nm) wavelength region. E1oec (1.0 mg/ml) in 50 mM KH2PO4 (pH 7.5) containing 0.15M NaCl, 0.1 mM ThDP, and 0.5 mM MgCl2 was incubated with 5.0 mM 2-OA in the presence of the acceptor 15 mM glyoxylic acid and CD spectra was acquired at various times to detect product accumulation. E1oh (1.0 mg/ml, 4.4 μM) in 50 mM KH2PO4 (pH 7.5) containing 0.15M NaCl, 0.2 mM ThDP, and 1.0 mM MgCl2 was incubated with 2.0 mM 2-OG in the presence of the acceptor 1.0 mM glyoxylic acid and CD spectra was acquired at various times to detect product accumulation.

A.2.4 Steady State Kinetics of E1oec activity by CD spectroscopy

Time dependent product formation was monitored continuously at 278 nm in the kinetics mode by CD. A typical reaction mixture in a 2.4 ml cuvette contained 50 mM KH2PO4 (pH 7.5), 0.15 M NaCl, 0.2 mM ThDP, and 1.0 mM MgCl2, and varying concentrations of glyoxylic acid and fixed concentration of 2-OG or varying concentrations of 2-OA and fixed concentration of glyoxylic acid. The reaction was started by the addition of 20 μg of E1oec and was monitored for 500 s at 30 ºC. A similar reaction mixture was used with varying concentrations of 2-OG and fixed concentration of glyoxylic acid with E1oh. The reaction was started with 10 μg E1oh and was monitored for 500 s at 37 ºC. Steady

state velocities calculated from the linear region of the progress curves were fit to a hyperbolic Michaelis-Menten plot (Equation A.1).

A.2.5 E1oec specific activity assay with DCPIP

The E1-specific activity of wild type E1o and its variant His298Asp were measured by monitoring the reduction of DCPIP at 600 nm using a Varian DMS 300 spectrophotometer. The assay medium (1 ml) contained in 50 mM KH_2PO_4 (pH 7.5), 0.5 mM $MgCl_2$, 0.2 mM ThDP, 0.1 mM DCPIP and 2.0 mM 2-OG or 20.0 mM 2-OV at 30 °C. The reaction was initiated by adding the enzyme (20 µg). One unit of activity is defined as the amount of DCPIP reduced (µmol/min/mg of E1o). For K_m measurement, similar conditions were used in the presence of substrates [2-OH (2.0 – 20 mM) or 2-oxo-5-hexenoic acid (2.0 – 20 mM)]. The observed slope was plotted against [substrate] and the resulting progress curves were fit to a hyperbolic Michaelis-Menten plot and K_m values were calculated by using Equation A.1.

$$v = (V_m * x^n) / (x^n + K_m^n) \quad (A.1)$$

Where V_m is the maximum slope observed, x is the ligand concentration, n is the Hill coefficient ($K_m = S_{0.5}$ if $n \neq 1$) and K_m is the Michaelis constant for the varied substrate.

A.2.6 Carboligation reaction on an analytical scale

20 mM butyraldehyde and 30 mM 2-oxoglutarate were incubated with 0.7 mg/ml E1oec in 1.2 mL of reaction buffer (50 mM KH_2PO_4 (pH 7.5) supplemented with 0.2 M NH_4Cl, 0.5 mM ThDP, 2.0 mM $MgCl_2$ and 5% DMSO). The reaction mixture was incubated for 20-24 hours at room temperature and 400 rpm using an orbital shaking platform on a

magnetic stirrer. After reaction was completed, circular dichroism (CD) spectroscopy was performed at 270-450 nm range for product detection. For NMR analysis, the complete reaction mixture was extracted as follows: (1) 25 µl of 50% formic acid to bring the pH down to ~3, (2) spin the sample down at 3,000 rpm for 5 minutes to pellet any protein precipitation and transfer to new tube, (3) add 3 x 300 µl $CDCl_3$ (plus 18 mg Na_2SO_4 if strong emulsion forms) and spin down sample at 3,000 rpm for 3 minutes. To the remaining water layer, CD spectroscopy was again performed to determine amount of product extracted.

E1o catalyzed reaction conditions: The reactions were performed in 50 mM KH_2PO_4, 0.1 mM ThDP, 2 mM $MgCl_2$, pH (8.0) at 30 ºC and 300 rpm using a Thermomixer (Eppendorf). The final concentration of E1o was set to 700 µg/mL.

MenD-catalyzed reaction conditions: The reactions were performed in phosphate buffer (50 mM potassium phosphate, 0.1 mM ThDP, 2 mM MgCl2·6H2O, pH (8.0) at 30 ºC and 300 rpm using a Thermomixer (Eppendorf). The final concentration of MenD was set to 500 µg/mL.

A.2.7 Expression and purification of MenD

The cells for MenD were grown similarly to E1o with slight modifications. *E. coli* AG1 cells harboring the MenD plasmid were streaked onto Luria agar plates containing chloramphenicol (30 µg/mL) and incubated overnight at 37 ˚C. A single colony was picked and incubated in 20 mL of LB media containing chloramphenicol (30 µg/mL) and allowed to grow overnight at 37 ˚C with shaking. This was diluted 10X into an 800 mL LB media kept at 37 °C with constant shaking, containing chloramphenicol (30 µg/mL), thiamin hydrochloride (1.0 mM), and $MgCl_2$ (1.0 mM). The cultures were induced with

IPTG (0.5 mM) when the culture attained an OD_{600} between 0.5 - 0.8. After induction the cultures were allowed to grow overnight with constant shaking at temperature reduced to 25 ˚C. The cells were later centrifuged and collected at 4,400 g, 4 ˚C, washed with KH_2PO_4 (50 mM, pH 7.5) and KCl (0.15 M). The supernatant was discarded and the pellets stored at -20 ˚C prior to sonication. The cells were resuspended in the sonication buffer containing KH_2PO_4 (50 mM, pH 7.5), KCl (0.3 M), ThDP (0.5 mM), $MgCl_2$ (2.0 mM), benzamidine hydrochloride (1.0 mM) and PMSF (1.0 mM in methanol) with lysozyme (0.6 mg/mL). The sonication and treatment with streptomycin sulfate (0.5% w/v) was carried out similarly to E1o (2.3.1). The supernatant collected at the end was applied to a Ni-Sepharose 6 fast column equilibrated with sonication buffer without lysozyme and PMSF. The loaded protein was subsequently washed with increasing concentrations of imidazole (30 - 50 mM) containing, KH_2PO_4 (50 mM, pH 7.5), KCl (0.3 M). ThDP (0.5 mM), $MgCl_2$ (2.0 mM), benzamidine hydrocloride (1.0 mM) and eluted using buffer containing imidazole (150 mM). Fraction from the elution were collected and dialyzed against a dialysis buffer similarly to (2.3.1) with modified KH_2PO_4 (50 mM) concentration. The protein was filtered using ultrafiltration with a cutoff of 30 kDa.

A.3 Results and Discussion

The studies reported here are an expansion of the previously reported studies done by the Jordan group adding to the repertory of E1o in chiral synthesis. In addition to the use of 2-oxoacids as substrates, structurally similar carboxylic acids were also tested (Figure A.4). First, kinetic studies were conducted to verify whether or not the substrates from Figure A.4 are accepted by E1o. Upon verification that they were in fact accepted

substrates, overnight carboligation reaction products (Figure A.5) were detected using CD spectroscopy and ^{1}H NMR. CD spectroscopy provides valuable information regarding stereochemistry of the resulting carboligation products. Specifically, the (*R*) enantiomer displays a negative CD peak while the (*S*) enantiomer a positive one all around 278-285 nm similar to the CD spectrum of acetoin enantiomers.

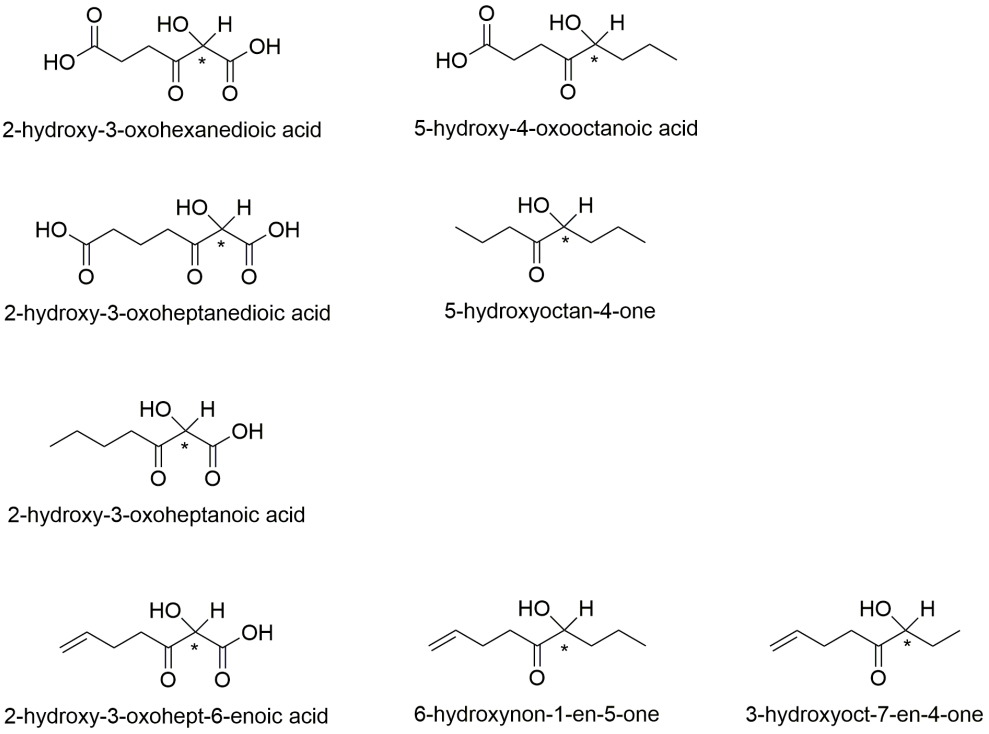

Figure A.5 Structure and nomenclature of the chiral products produced from the E1o and variants catalyzed reaction by using variety of acceptors and substrates.

A.3.1 Steady-state kinetics of E1oec by CD spectroscopy or E1o specific activity assay with DCPIP

First, kinetic studies were conducted to verify if the following substrates are accepted by E1oec in addition to gathering kinetic data for the acceptor, glyoxylate. Through the use of either CD spectroscopy, for product accumulation studies or kinetic mode studies, or

the E1o specific activity assay with DCPIP, various kinetic parameters were obtained (Table A.1).

Table A.1 E1o Specific Activity and Kinetic Parameters for Various Substrates and Acceptors

		Kinetic Parameters		
Substrate or Acceptor	DCPIP Activity (μmol $min^{-1}\cdot mg^{-1}$)	k_{cat} (s^{-1})	K_m (mM)	k_{cat}/K_m (s^{-1}/mM^{-1})
2-oxoglutarate	0.775 $\pm$ 0.04	2.15 $\pm$ 0.10	0.006 $\pm$ 0.02	456.6
Glyoxylate	n/a[b]		5.71 $\pm$ 0.64	
2-oxovalerate[a]	0.135 $\pm$ 0.04	0.48 $\pm$ 0.06	6.62 $\pm$ 0.93	0.0725
2-oxoadipate	n/a[b]		12.3 $\pm$ 1.8	
2-ketohexanoic acid	0.020	0.110	4.32 $\pm$ 0.50	0.0225
2-oxo-5-hexenoic acid	0.0168 $\pm$ .007	0.146	8.01 $\pm$ 1.9	0.0183

[a] DCPIP assay conducted with E1oec H298D
[b] n/a, not applicable.

Beginning with the E1oec natural substrate, 2-oxoglutarate, and glyoxylate as the acceptor, the K_m value was determined for glyoxylate using a fixed concentration of 2-oxoglutarate (Figure A.6). The kinetic mode on the CD spectroscopy was used to monitor product formation at 278 nm, with a negative slope indicating the accumulation of a (-) peak. As shown previously, the negative peak at 278 nm indicated the formation of the (*R*)-enantiomer [162].

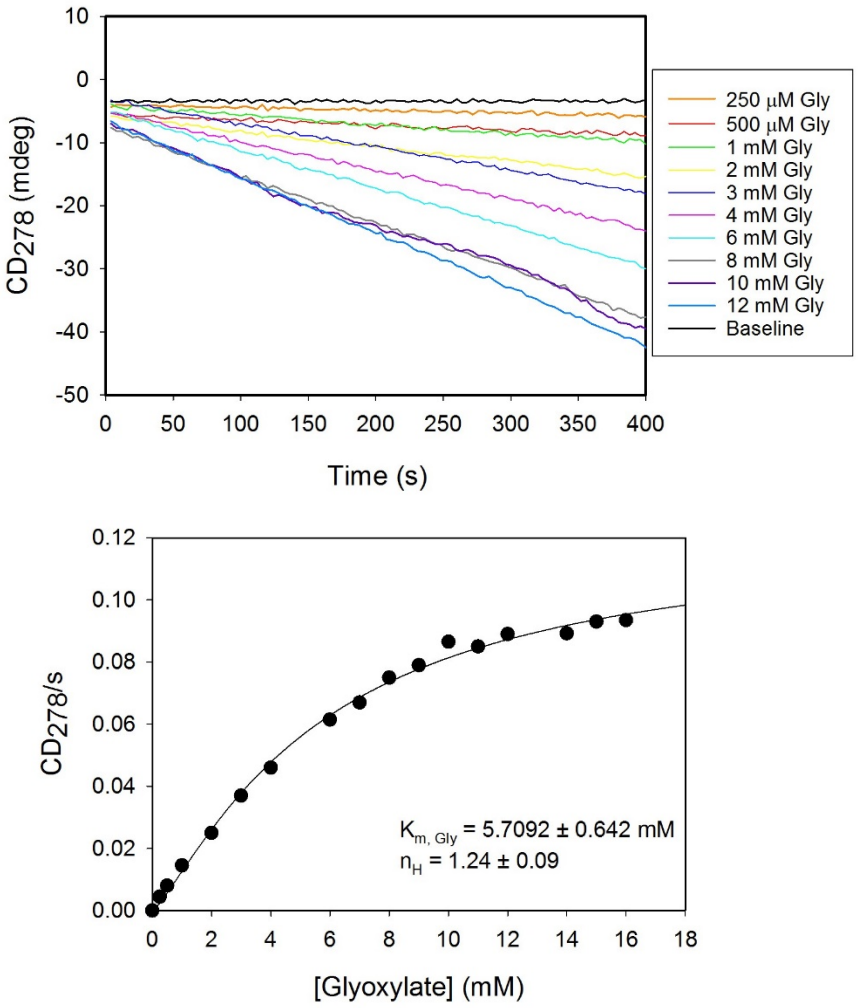

Figure A.6 Steady-state kinetics for E1oec with 2-OG and glyoxylate using kinetic mode on CD spectroscopy (top) and resulting Michaelis-Menten plot (bottom).

Similar experiments were conducted with the substrate 2-oxoadipate, which demonstrated for the first time that E1oec does in fact accept 2-oxoadipate as a substrate. First, a wavelength scan was conducted using CD spectroscopy were the carboligation product peak at (+) 278 nm accumulated over time (Figure A.7, top). The positive peak does indicate that the resulting carboligation product is the (*S*)-enantiomer. Upon confirmation that E1oec does in fact accept 2-oxoadipate as a substrate, steady state kinetic data was collected using CD spectroscopy (Figure A.7, middle and bottom).

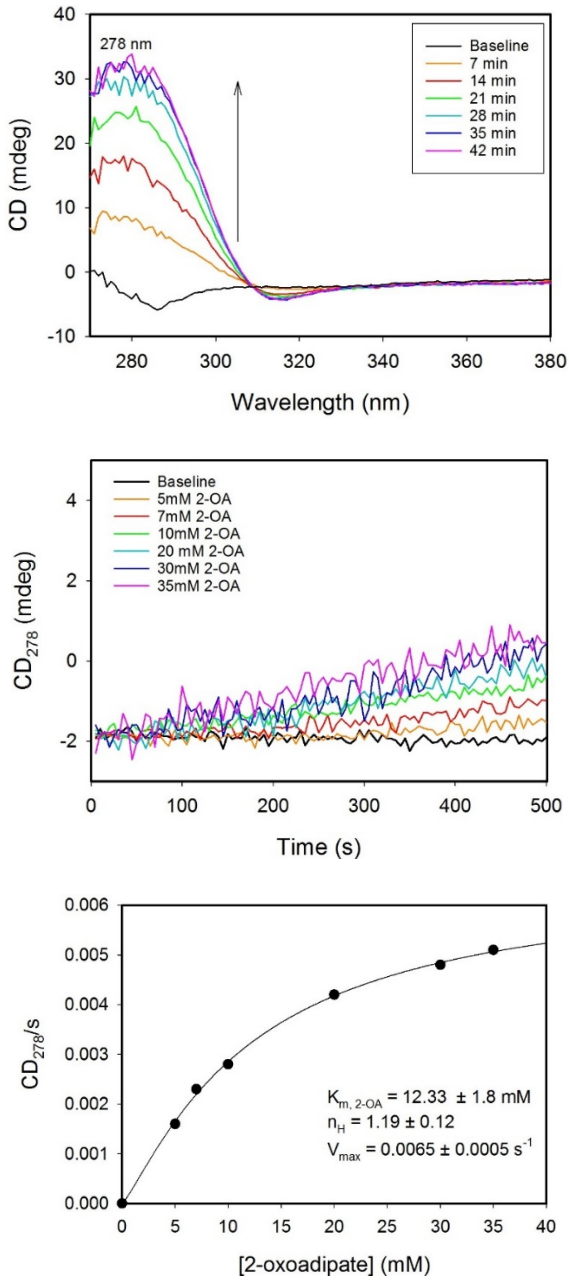

Figure A.7 Product detection and kinetics for E1oec with 2-OA and glyoxylate.
(Top) Near-UV CD wavelength scan acquired at the indicated times to detect accumulation of (S)-chiral carboligation product produced by E1oec (1.0 mg/ml) from 2-oxoadipate (5 mM) and glyoxylate (15 mM) at 30 °C in 50 mM KH_2PO_4 (pH 7.5) containing 0.15 M NaCl, 1.0 $MgCl_2$ and 0.1 mM ThDP. (Middle) Steady-state progress curves of the reaction with E1oec (80 μg) at the indicated concentrations of 2-oxoadipate (2-OA) in the presence of 30 mM glyoxylate in 50 mM KH_2PO_4 (pH 7.5) containing 0.15 M NaCl, 1.0 $MgCl_2$ and 0.1 mM ThDP. (Bottom) Dependence of the ellipticity at 278 nm on the concentration of 2-oxoadipate. The data was fit using the hill equation.

In the case of the carboxylic acid substrates, the E1o specific activity assay with DCPIP was used where DCPIP acts as the acceptor similar to the carboligation reactions. The two substrates tested were 2-oxo-hexanoic acid (Figure A.8), containing a saturated side chain, and 2-oxo-5-hexenoic acid (Figure A.9), containing a terminal alkene functional group. Both carboxylic acids tested were shown to be accepted by E1oec as substrates demonstrating once again the versatility of E1o for carboligation reactions.

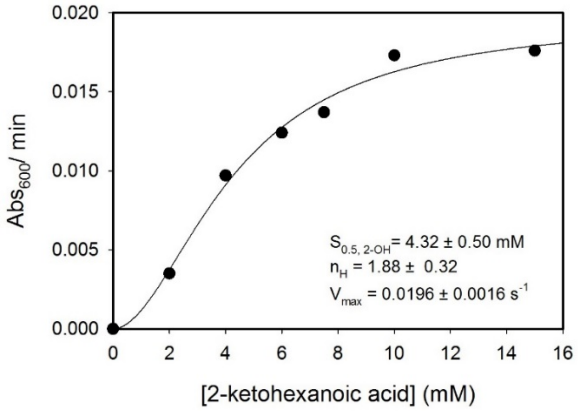

Figure A.8 E1oec kinetic parameters with 2-ketohexanoic acid from DCPIP activity assay.

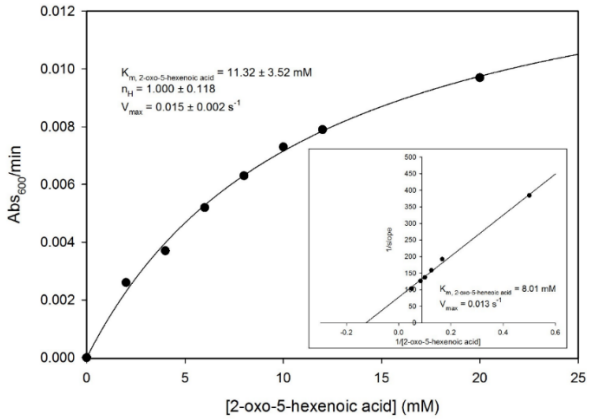

Figure A.9 E1oec kinetic parameters with 2-oxo-5-hexenoic acid from DCPIP activity assay.

4.3.2 Carboligation reaction on an analytical scale with E1oec or E1o-His298Asp

Once the 2-oxoacid and carboxylic acid substrates were confirmed to be accepted as substrates by E1o, glyoxylate and the straight chain aldehydes were introduced as acceptors to test E1o-catalyzed chiral carboligation reactions. Similar to the analytical scale production and work up implemented by Muller *et al*. with some modifications.

First, the 2-oxoacids, 2-OG and 2-OV, were tested with the straight chain acceptor, butyraldehyde (Figures A.10 and A.11). As determined previously, the E1oec variant, His298Asp, was shown to accept 2-oxovalerate as a substrate and therefore was used in these studies. In both cases, the (*R*)-enantiomer was produced as apparent by the negative CD peak at 279 nm with 2-OG (Figure A.10) and 2-OV (Figure A.11). Next, the chiral carboligation product was confirmed through the use of CD spectroscopy as well as NMR spectroscopy. First, carboligation product peak was detected by CD spectroscopy followed by pH adjustment to ~3, conditions under which product extraction into chloroform could be performed. The ^{1}H NMR spectrum of the resulting extracted product was then recorded. As all the carboligation products have in common the CH-OH functional group, they all exhibit a ^{1}H NMR resonance with a proton chemical shift near 4-5 ppm (Figure A.5).

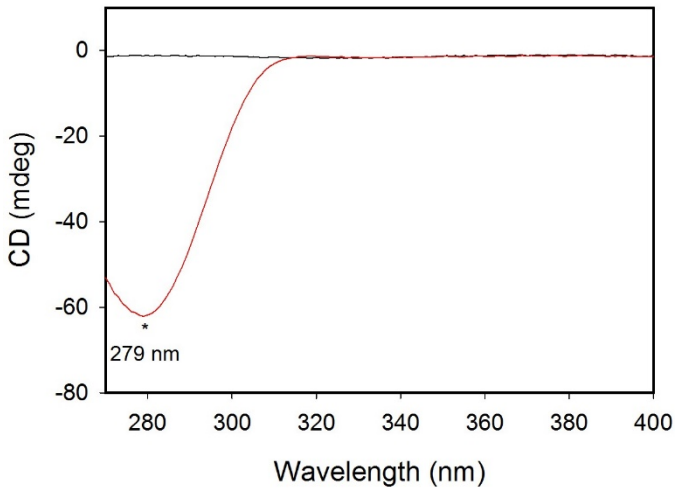

Figure A.10 E1oec catalyzed carboligation reaction with 2-oxoglutarate and butyraldehyde. A 1 mm path length cuvette was used, therefore actual ellipticity is 10x of that shown.

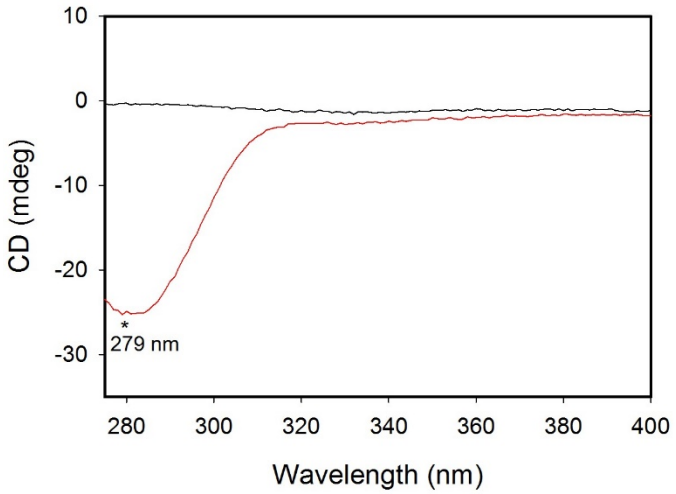

Figure A.11 E1oec H298D catalyzed carboligation reaction with 2-oxovalerate and butyraldehyde. A 1 mm path length cuvette was used, therefore actual ellipticity is 10x of that shown.

In the case of 2-oxoglutarate and butyraldehyde, the 1H NMR spectrum was obtained to verify the carboligation product (5-hydroxy-4-oxo-octanoic acid) formed (Figure A.12). The unique proton chemical shift for the CH-OH functional group at ~4.4 ppm (H_c) and ~2.7 ppm (OH) is seen on the NMR spectrum in addition to the other protons.

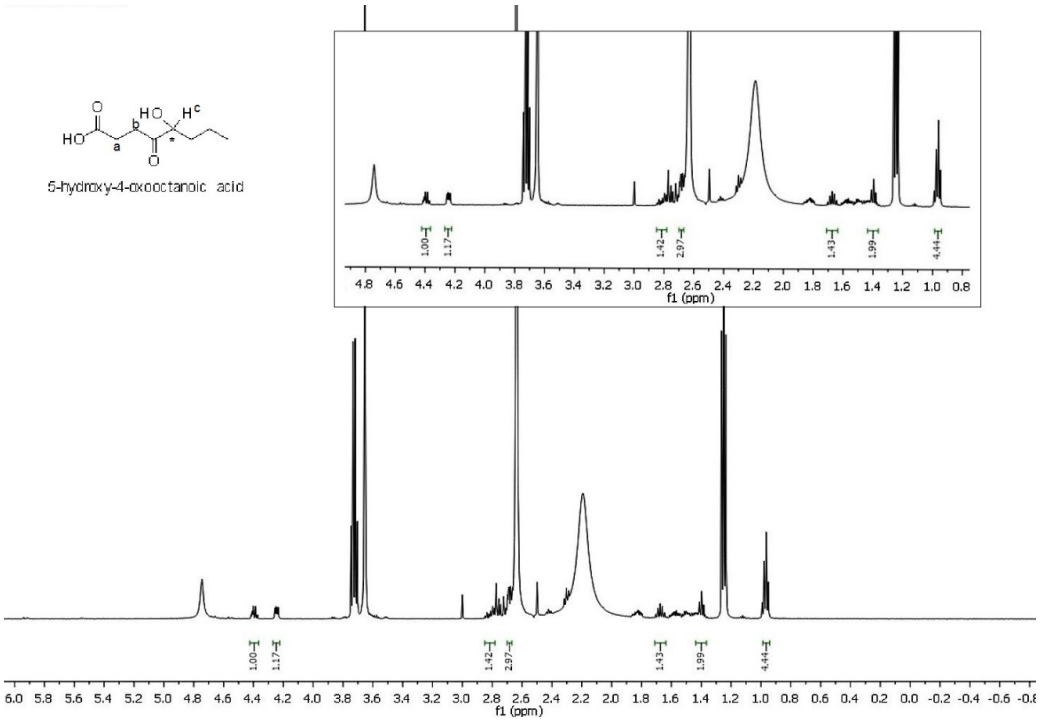

Figure A.12 ^{1}H NMR spectrum of E1o-ec catalyzed carboligation product of 2-oxoglutarate with butyraldehyde. The large peaks correspond to water (in $CDCl_3$) near ~2.0 ppm and DMSO-d6 near ~2.6 ppm.

Next, the carboxylic acids, 2-ketohexanoic acid and 2-oxo-5-hexenoic acid, were tested with various acceptors. The substrate 2-ketohexanoic acid was tested with glyoxylate, and in this case the (*S*)-enantiomer was formed verified by the (+) CD peak at ~290 nm (Figure A.13).

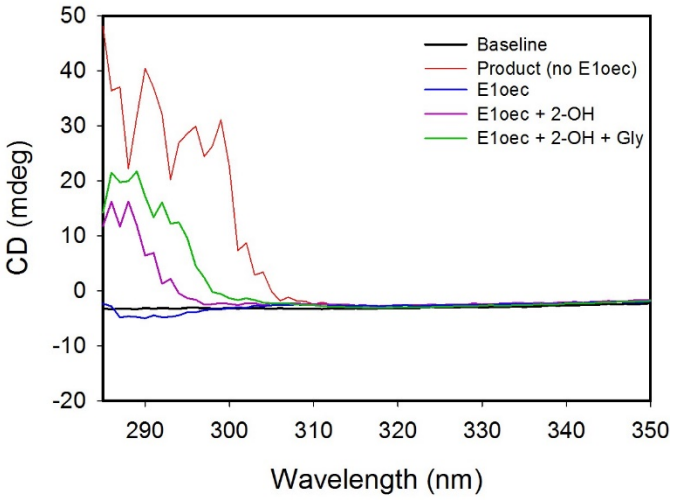

Figure A.13 E1oec catalyzed carboligation reaction with 2-OH & glyoxylate**.**

Of all the substrates tested, 2-oxo-5-hexenoic acid was of most interest due to the introduction of the terminal alkene functional group. The resulting carboligation product with glyoxylate, butyraldehyde, and propanal were confirmed by CD spectroscopy (Figure A.14). Remarkably, the carboligation product with glyoxylate produced the (S)-enantiomer as shown by the positive peak at ~280 nm (Figure A.12, top), while both butyraldehyde and propanal produced the (R)-enantiomer with a negative peak at 282 nm (Figure A.12, middle and bottom).

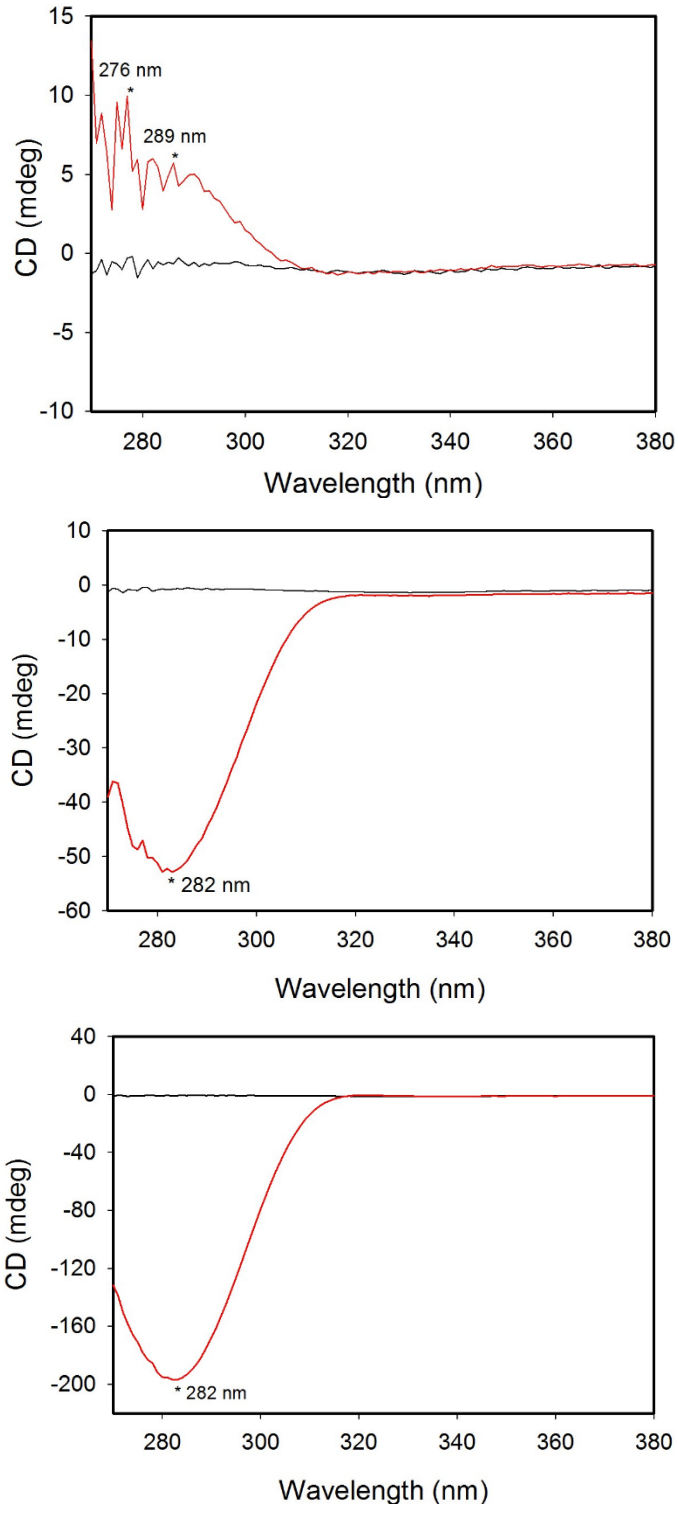

Figure A.14 CD spectroscopy of E1oec catalyzed carboligation reaction with 2-oxo-5-hexenoic acid and various acceptors. (Top) with glyoxylate, (Middle) with butyraldehyde, and (Bottom) with propanal.

4.3.3 Carboligation reaction on an analytical scale with human E1o

In addition to the above work with E1oec, similar initial studies were conducted using human E1o. For the first time, human E1o was used to catalyze carboligation reactions and therefore the natural substrate, 2-oxoglutarate, as well as the substrate 2-oxoadipate were tested with the acceptor glyoxylate. First, the carboligation product produced by 2-oxoglutarate and glyoxylate was verified by CD spectroscopy. Similar to the E1oec results, human E1o produced the (R)-enantiomer as indicated by the (-) 279 nm peak (Figure A.15).

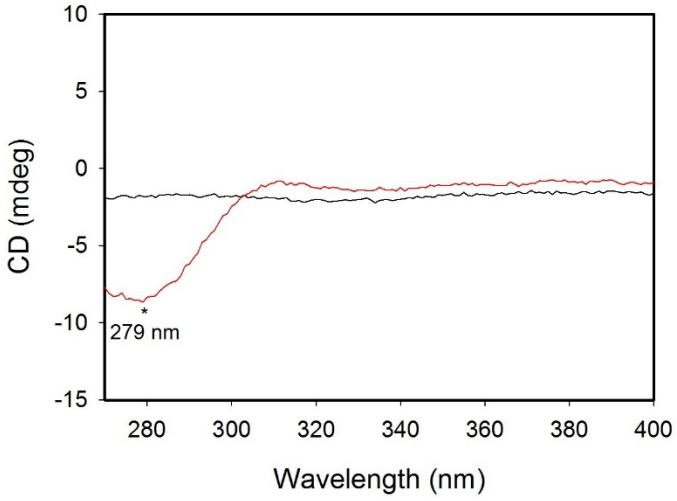

Figure A.15 Human E1o catalyzed carboligation reaction with 2-oxoglutarate and glyoxylate. A 1 mm path length cuvette was used, therefore actual ellipticity is 10x of that shown.

Next, the carboligation product, 2-hydroxy-3-oxohexanedioic acid, was confirmed by 1H NMR spectroscopy (Figure A.16). Not only is the CH-OH functional group clearly visible (~4.4 ppm for -CH and ~2.75 ppm for -OH), but the other proton peaks at ~2.7 and 2.5 ppm are also visible. For the first time, the carboligation reaction was successfully carried out by E1o-h.

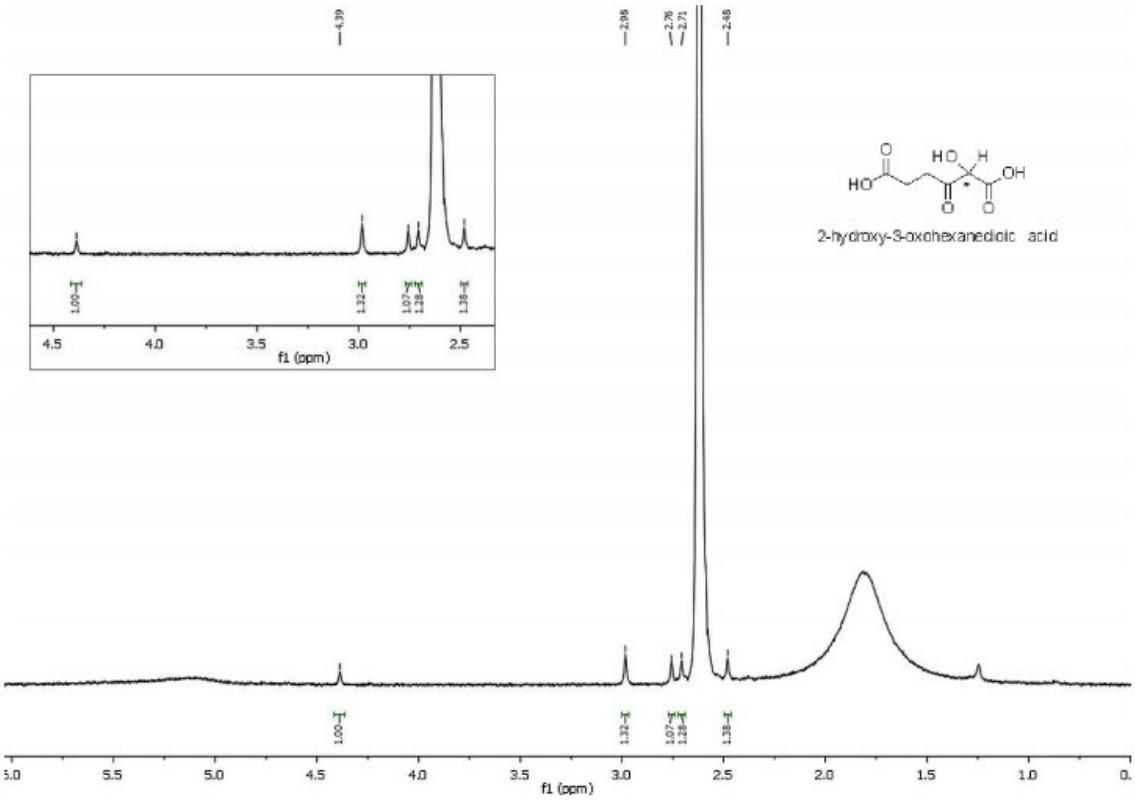

Figure A.16 ^{1}H NMR spectrum of E1o-h catalyzed carboligation product of 2-oxoglutarate with glyoxylate. The large peaks correspond to water (in $CDCl_3$) near ~1.7 ppm and DMSO-d_6 near ~2.6 ppm.

Next, the substrate 2-oxoadipate was used with the acceptor glyoxylate, and in fact human E1o can catalyze the formation of the carboligation product (Figure A.17). The most obvious difference is that the product formed is the (S)-enantiomer proving that a one-carbon difference changes the orientation of the resulting carboligation product. The NMR spectra of the product has also been shown in Figure A.18.

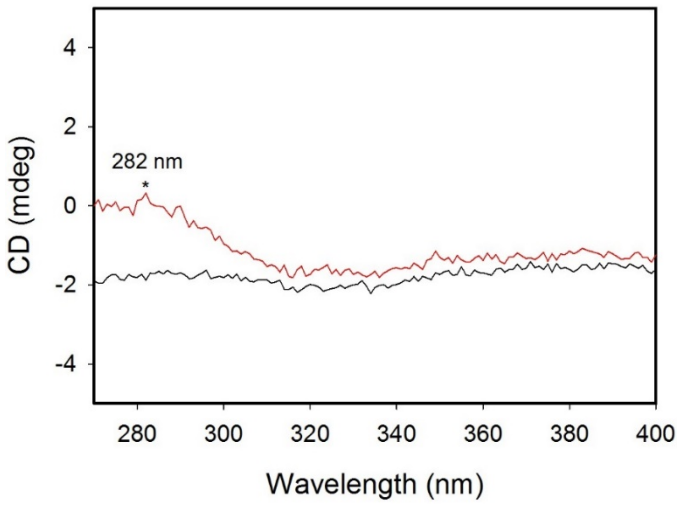

Figure A.17 Human E1o catalyzed carboligation reaction with 2-oxoadipate and glyoxylate. A 1 mm path length cuvette was used, therefore actual ellipticity is 10x of that shown.

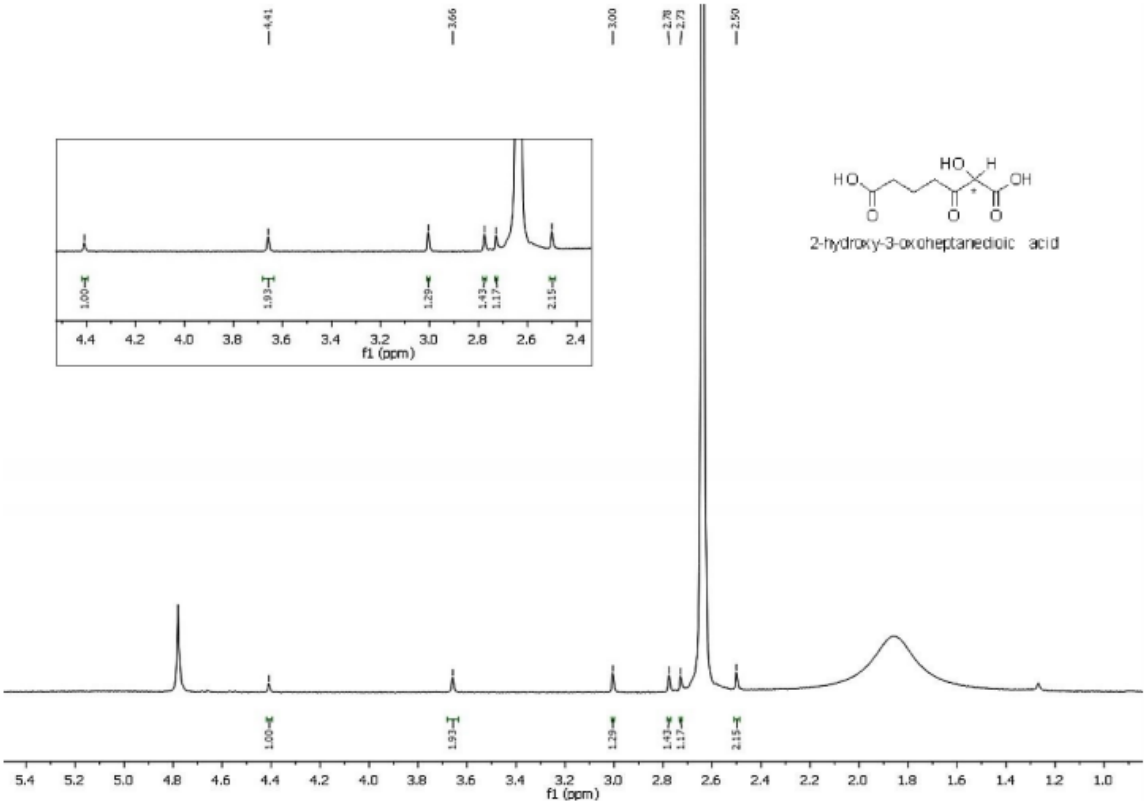

Figure A.18 ^{1}H NMR spectrum of E1o-h catalyzed carboligation product of 2-oxoadipate with glyoxylate. The large peaks correspond to water (in $CDCl_3$) near ~1.8 ppm and DMSO-d6 near ~2.6 ppm.

4.3.4 Comparative carboligation reactions of E1o and MenD

The carboligation reactions were carried out and the presence of a chiral product in excess was confirmed using CD spectroscopy. The results are summarized in (Table A.2).

Table A.2 CD Spectra Data for E1o and MenD

Enzyme	Substrate	Acceptor	CD_{278} (mdeg)
E1o (700 μg)	2-oxoglutarate[a]	Propanal[b]	-54
		Benzaldehyde[b]	-16
	2-oxoglutarate[c]	Propanal[b]	-19
		Benzaldehyde[d]	-9
MenD (500 μg)	2-oxoglutarate[a]	Benzaldehyde[b]	Nd
	2-oxo-5-hexenoic acid[a]	Propanal	Nd
	2-oxo-5-hexenoic acid[a]	Benzaldehyde	Nd

([a] 30 mM substrate, [b,d] 20 mM acceptor and [c] 10 mM substrate) Nd: not detected

The CD was able to detect significant amount of enantiomer at 278 nm. For reaction between propanal as acceptor and 2-oxoglutarate as substrate with E1o, the majority of the product obtained was in the (R)-configuration (Figure A.19). The same was observed for reactions with MenD. When reactions between benzaldehyde as acceptor and 2-oxoglutarate as substrate were catalyzed using MenD, almost all of the product obtained was in its (R)-configuration (Figure A.20). For MenD, the best results were obtained when the substrate concentration was kept close to the enzymes K_m value, above its K_m the enzyme suffered saturation inhibition and decreased activity. E1o also gave similar reactions between benzaldehyde and 2-oxoglutarate. But, the amount of substrate used did not saturate E1o unlike with MenD. (K_m value for 2-oxoglutarate for

E1o: 0.1 mM; and MenD: 1.5 mM, from the literature [17,46]. For the reactions of 2-oxo-5-hexenoic acid with MenD, there was no product detected in CD for reaction with propanal or benzaldehyde. This adds to the fact that the residues that perform the ThDP-dependent decarboxylase activity are conserved in the family and mutations induced at the conserved domain and/or the hydrophobic chains supporting the active-site pocket can alter its substrate spectrum and reactivity (Figures A.17, A.18).

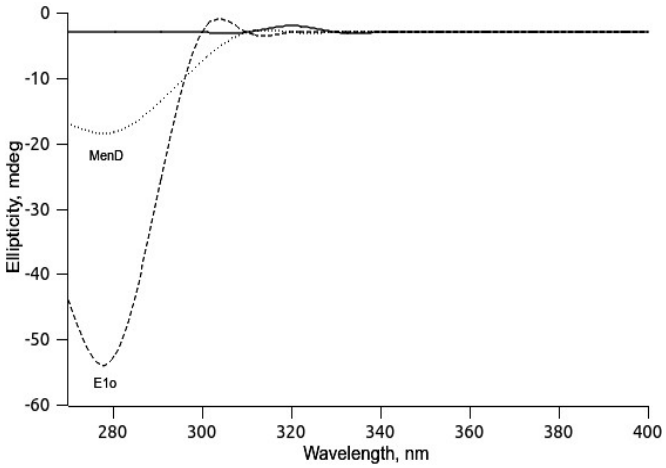

Figure A.19 CD spectra of 2-oxoglutarate and propanal.

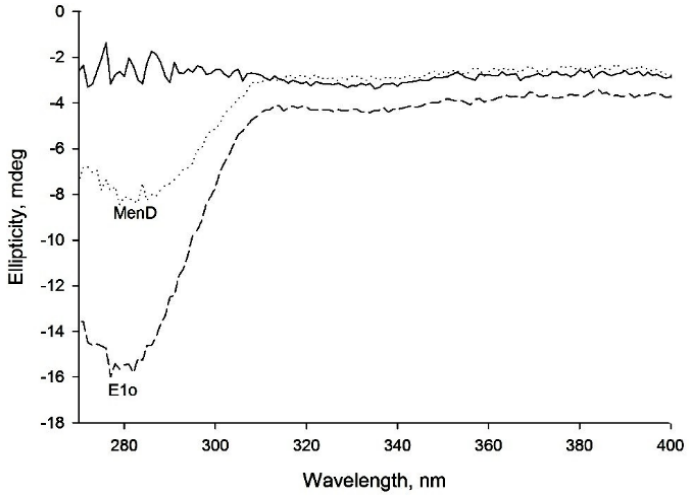

Figure A.20 CD spectra of 2-oxoglutarate and benzaldehyde.

APPENDIX B

SEQUENCING RESULTS

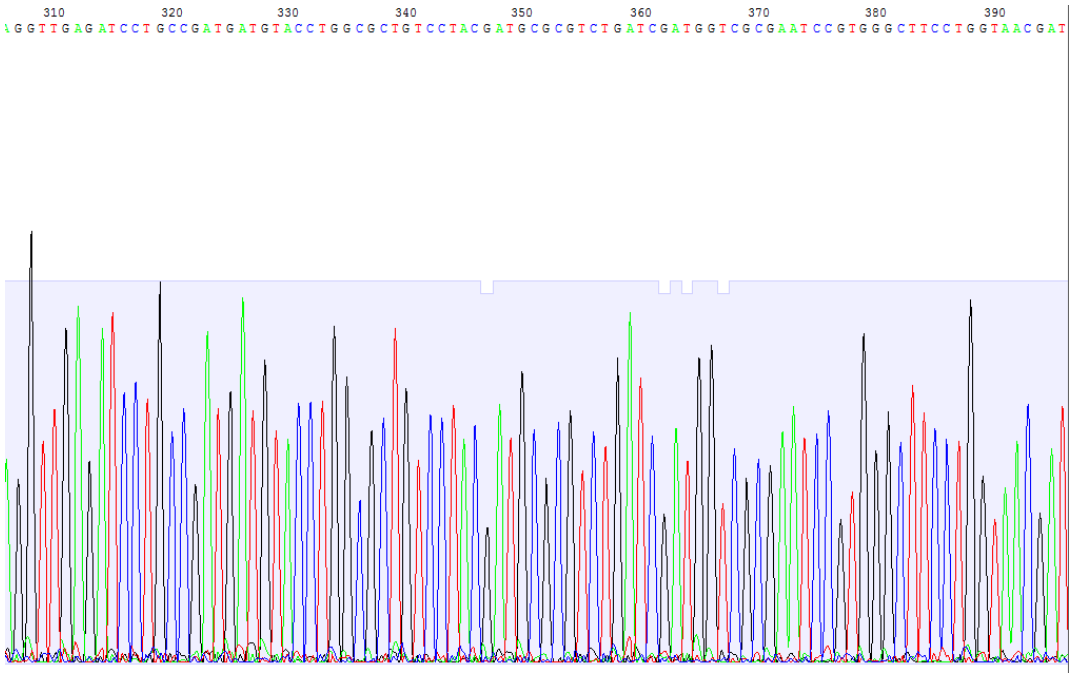

Figure B.1 DNA sequencing results with primer E2o-His375Ala.

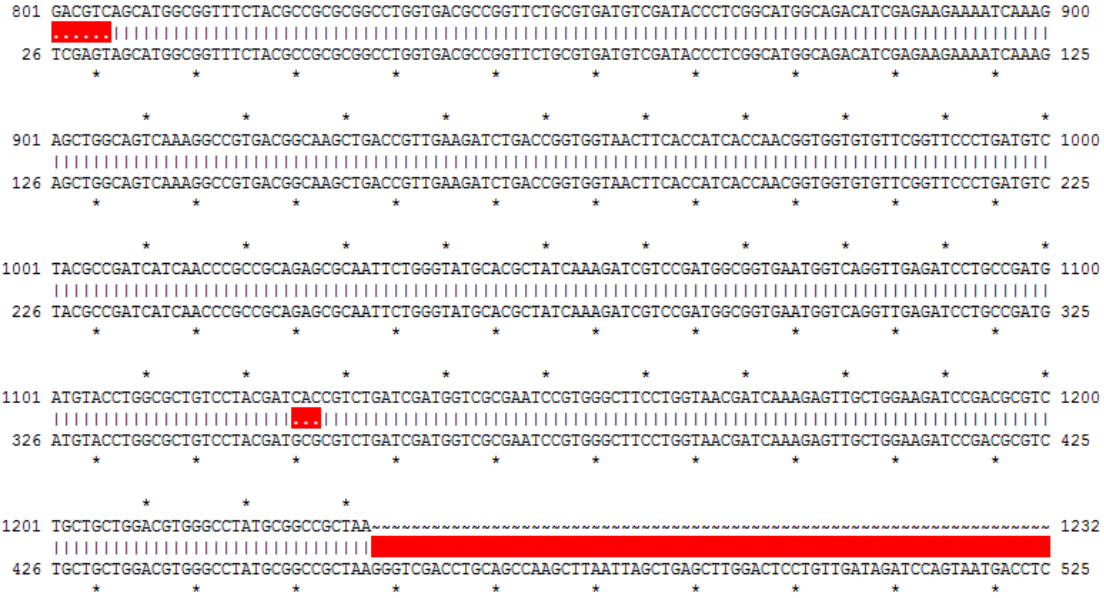

Figure B.2 DNA sequencing alignment of wt-E2o and E2o-His375Ala confirming mutation.

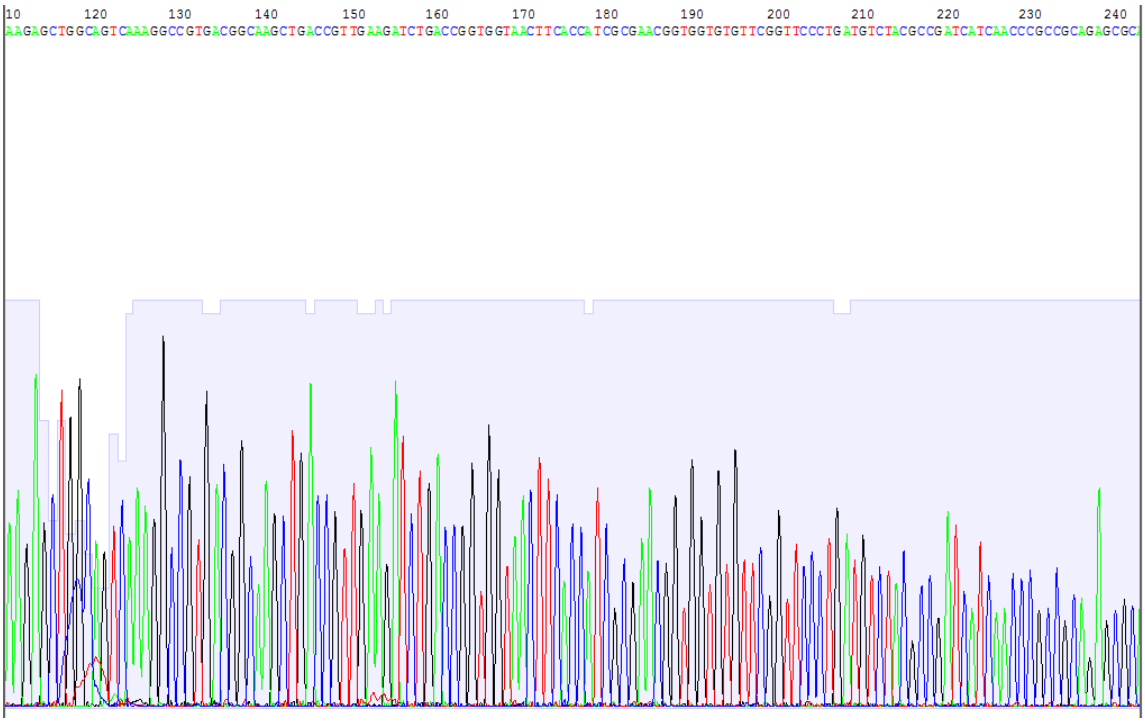

Figure B.3 DNA sequencing results with primer E2o-Thr323Ala.

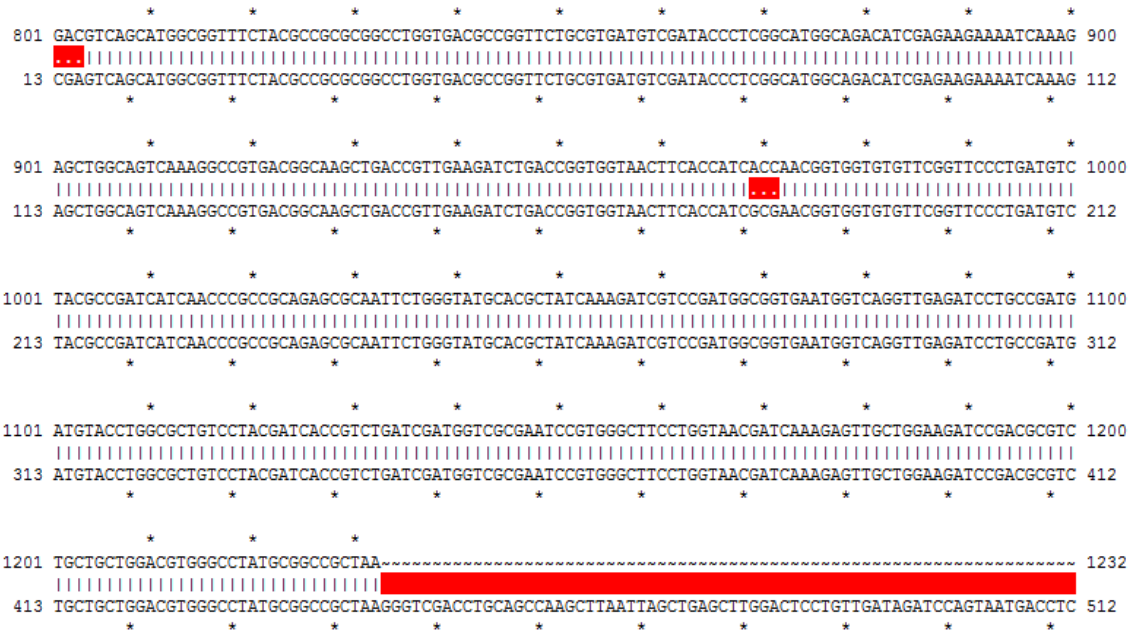

Figure B.4 DNA sequencing alignment of wt-E2o and E2o-Thr323Ala confirming mutation.

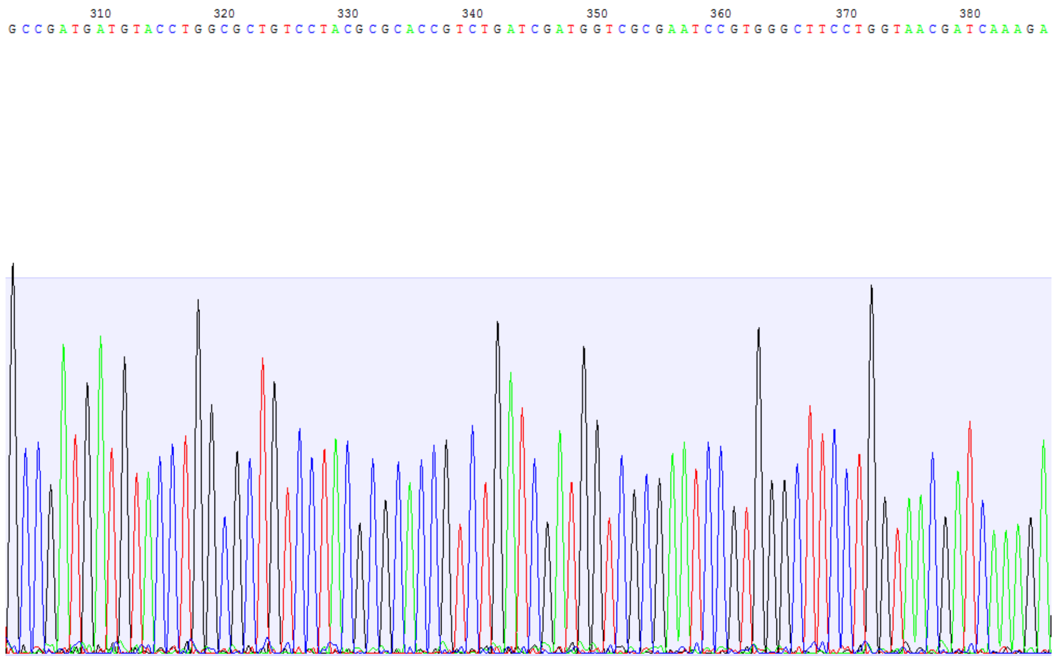

Figure B.5 DNA sequencing results with primer E2o-Asp374Ala.

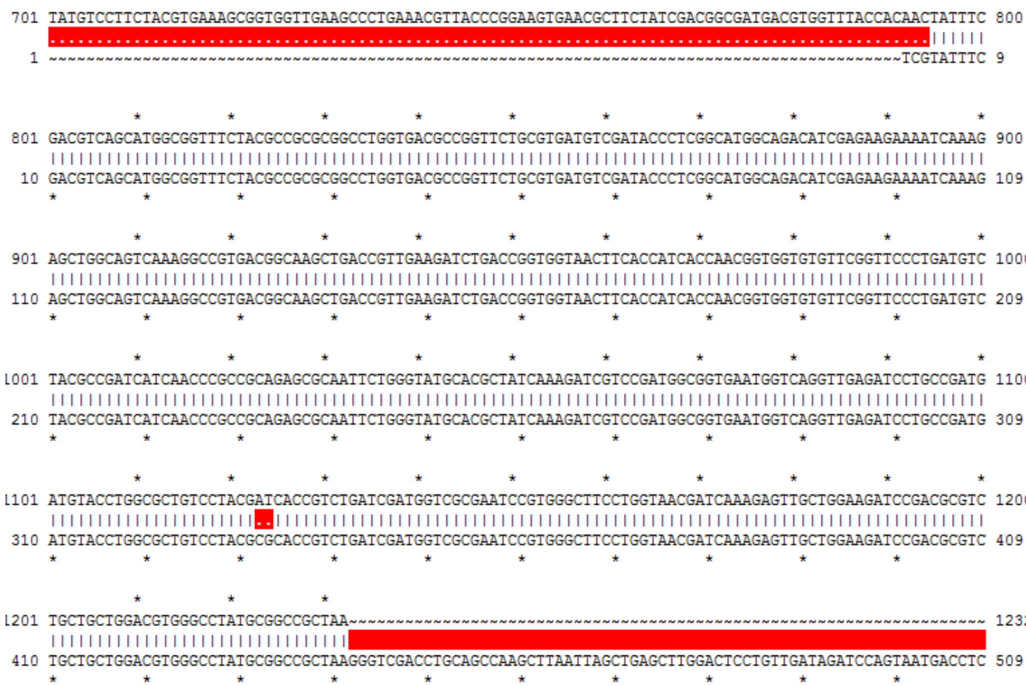

Figure B.6 DNA sequencing alignment of wt-E2o and E2o-Asp374Ala confirming mutation.

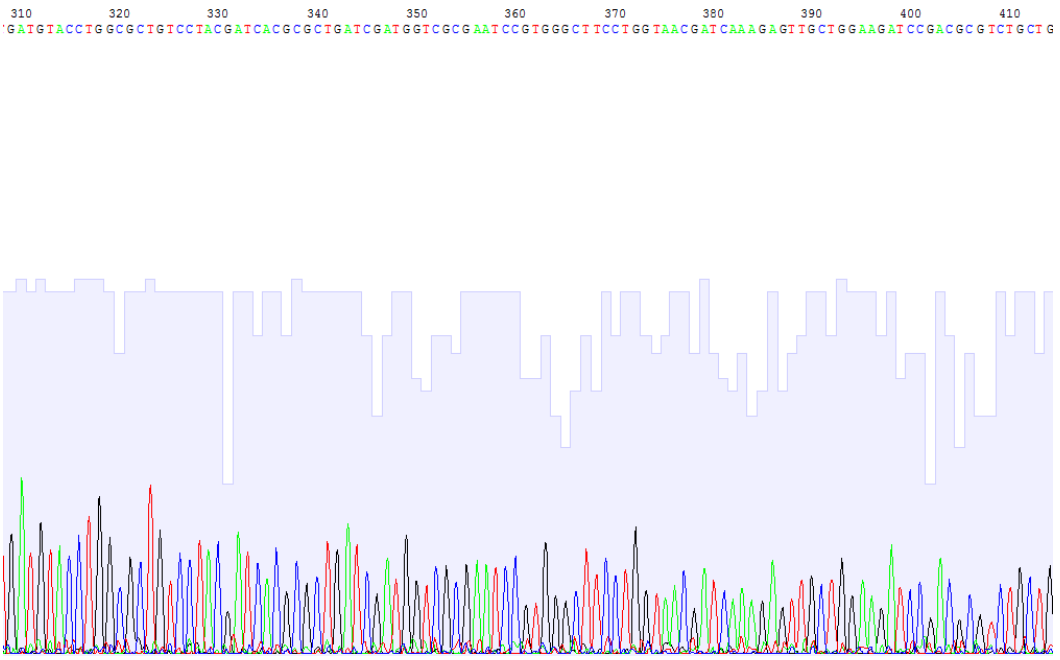

Figure B.7 DNA sequencing results with primer E2o-Arg376Ala.

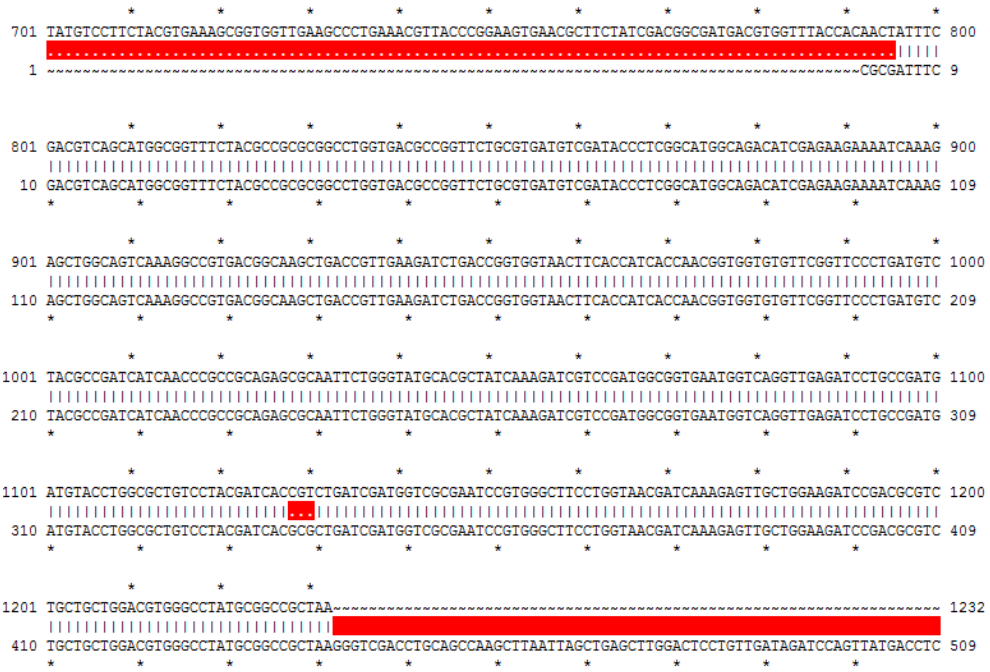

Figure B.8 DNA sequencing alignment of wt-E2o and E2o-Arg376Ala confirming mutation.

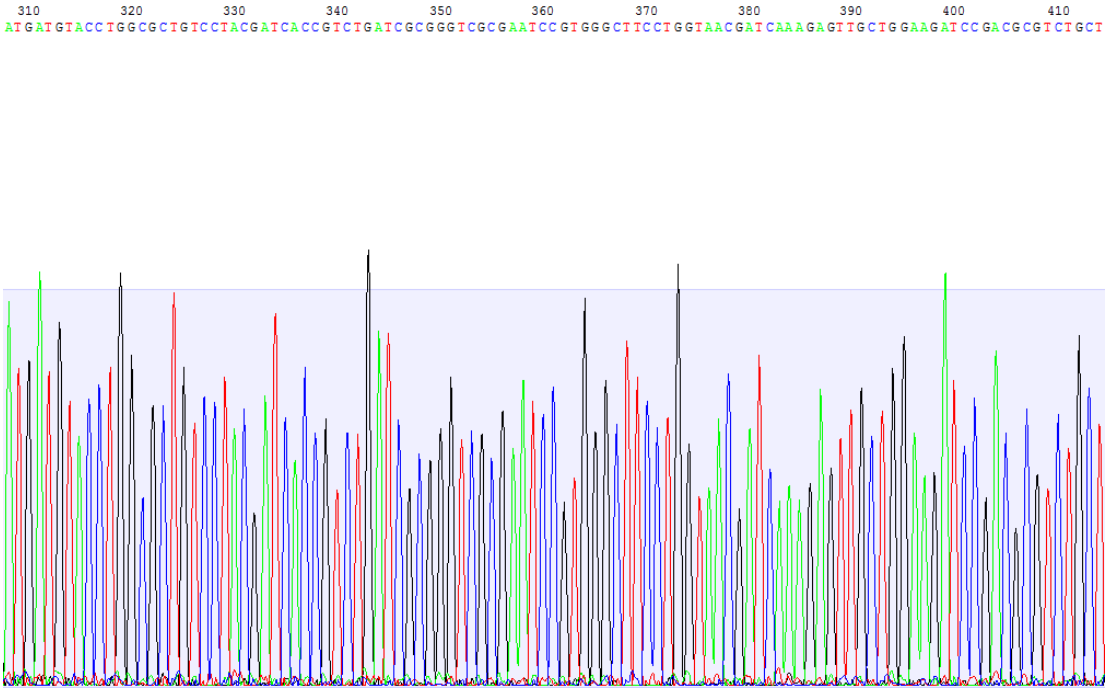

Figure B.9 DNA sequencing results with primer E2o-Arg379Ala.

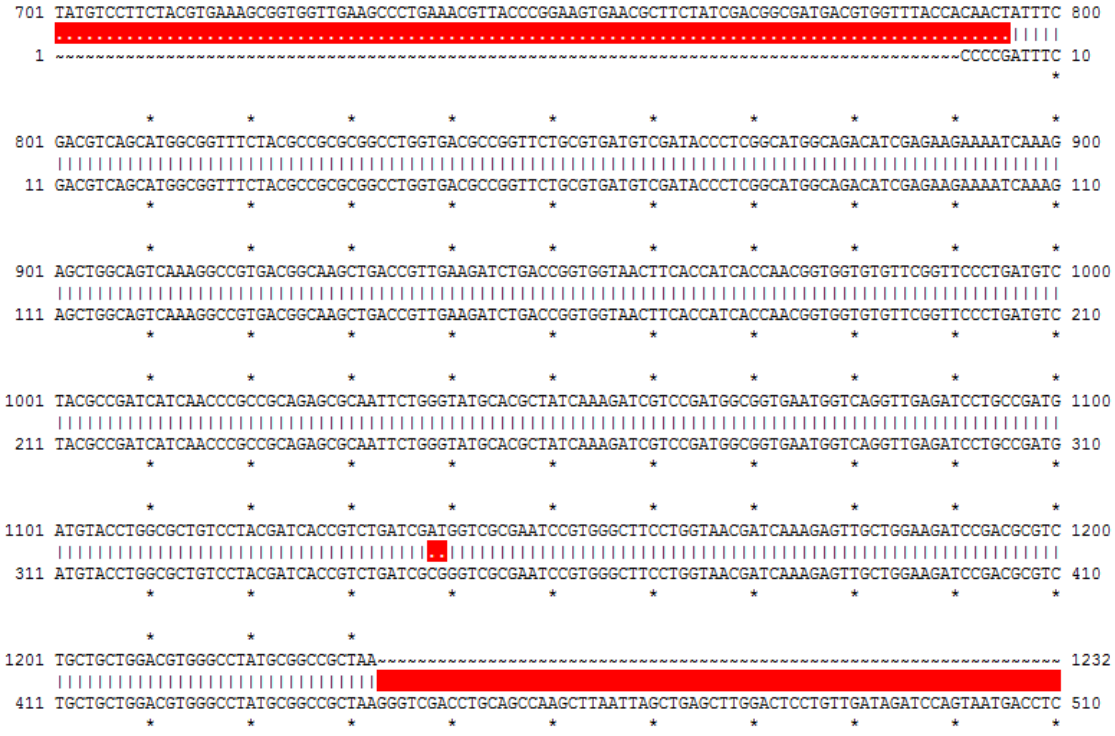

Figure B.10 DNA sequencing alignment of wt-E2o and E2o-Arg376Ala confirming mutation.

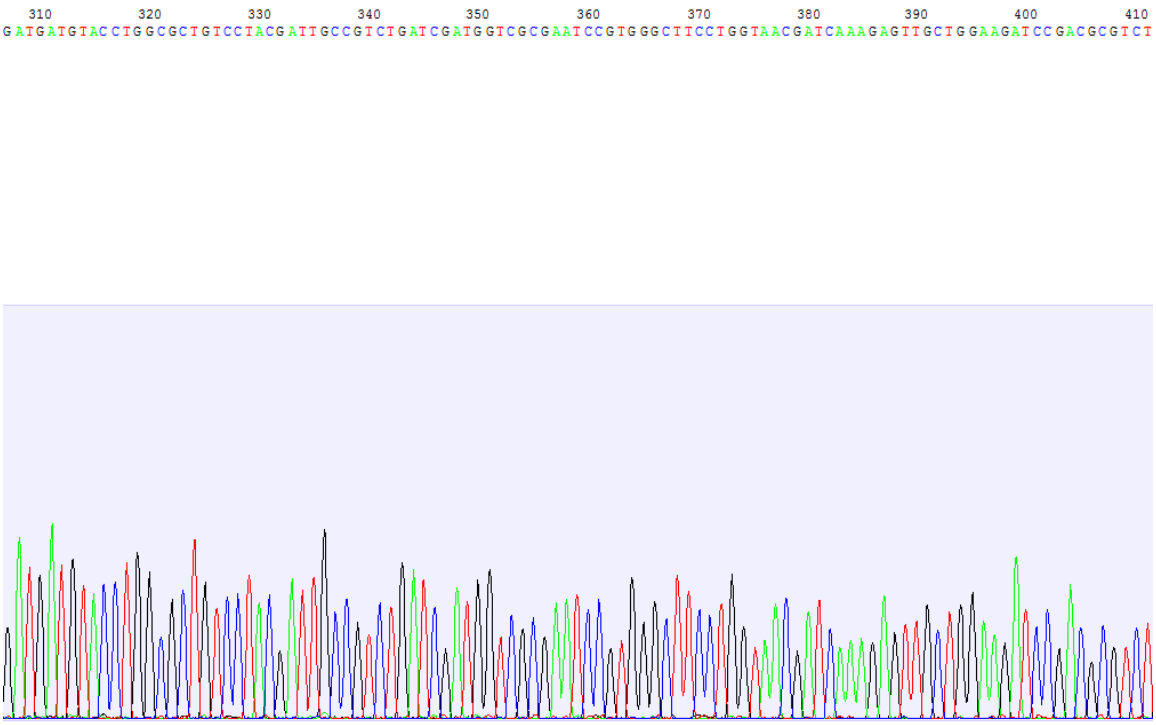

Figure B.11 DNA sequencing results with primer E2o-His375Cys.

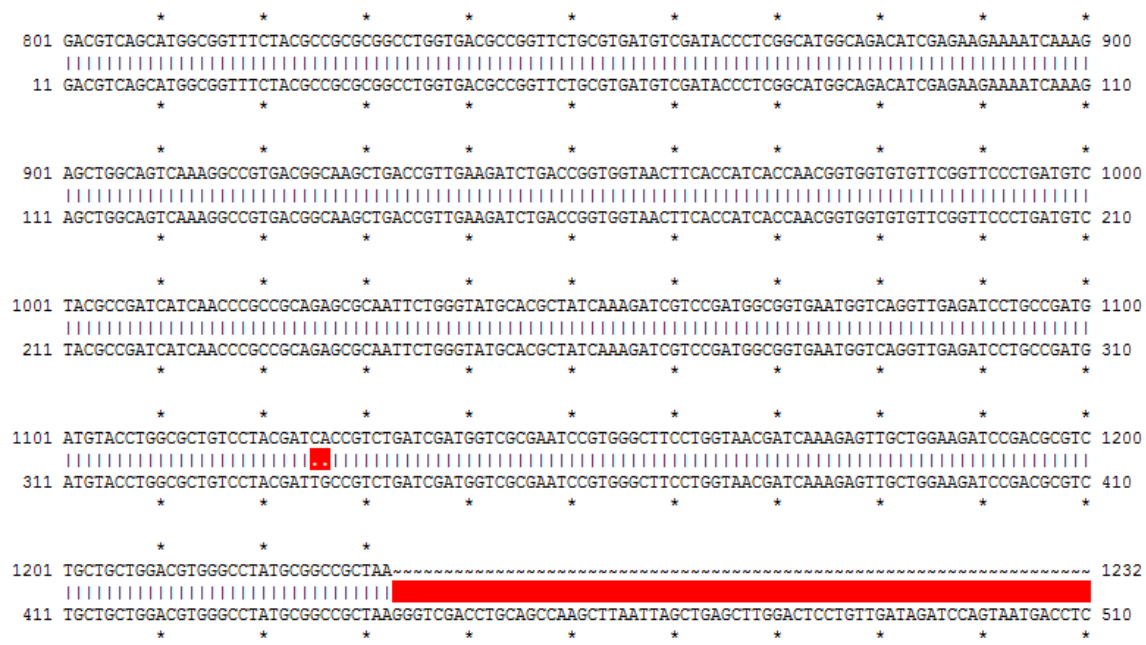

Figure B.12 DNA sequencing alignment of wt-E2o and E2o- His375Cys confirming mutation.

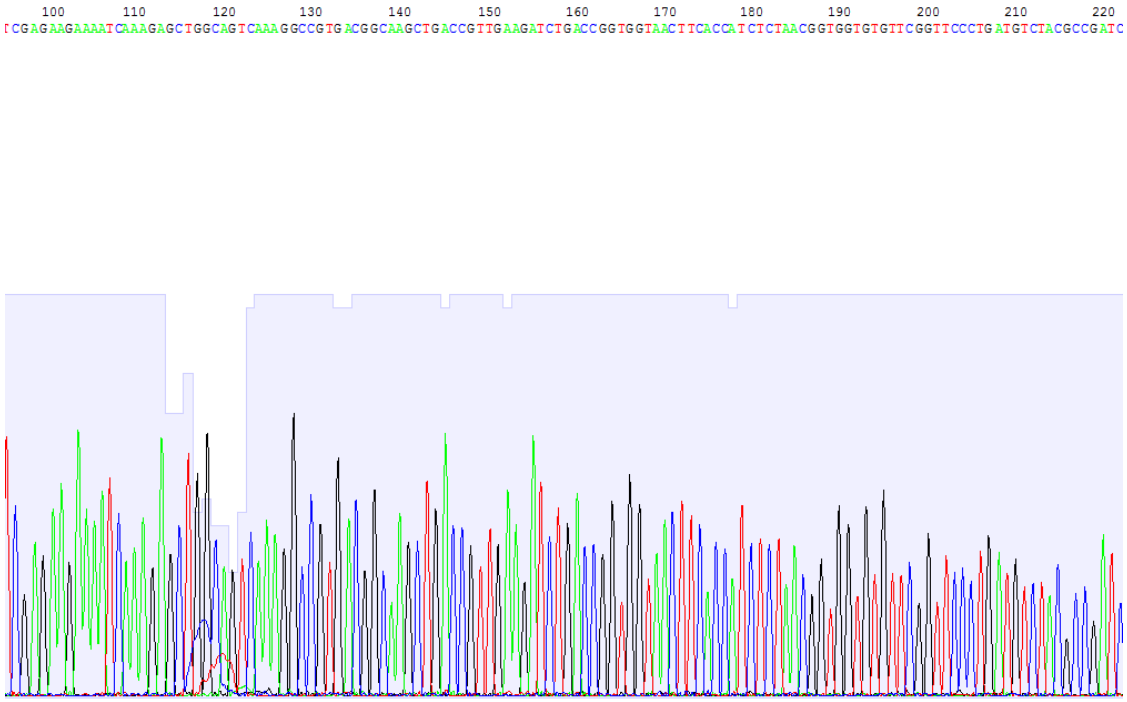

Figure B.13 DNA sequencing results with primer E2o-Thr323Ser.

Figure B.14 DNA sequencing alignment of wt-E2o and E2o-Thr323Ser confirming mutation.

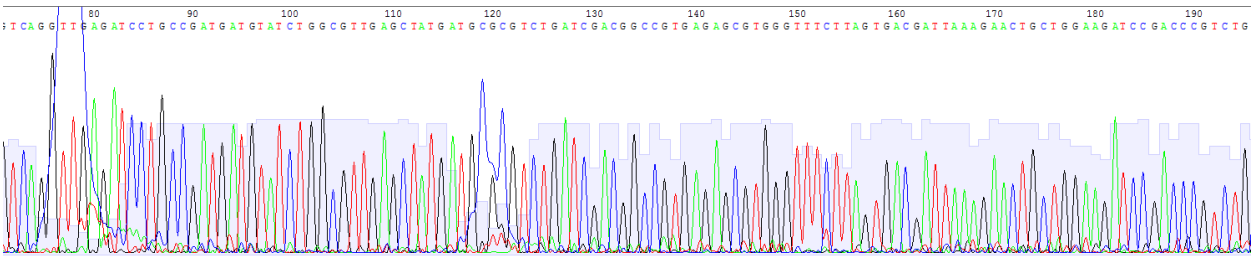

Figure B.15 DNA sequencing results with primer E2oCD-His375Ala.

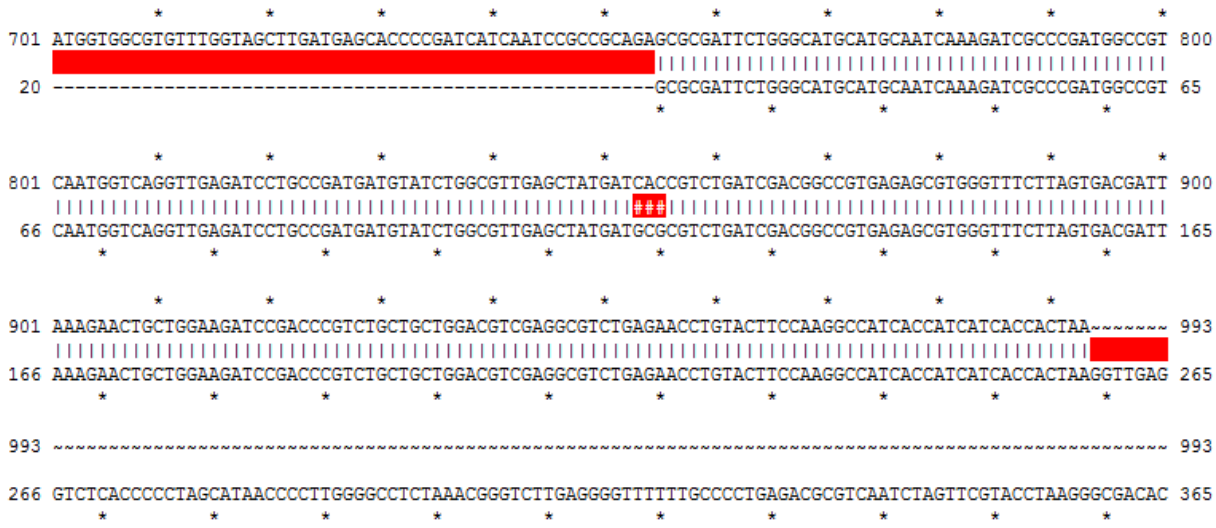

Figure B.16 DNA sequencing alignment of wt-E2o and E2oCD-His375Ala confirming mutation.

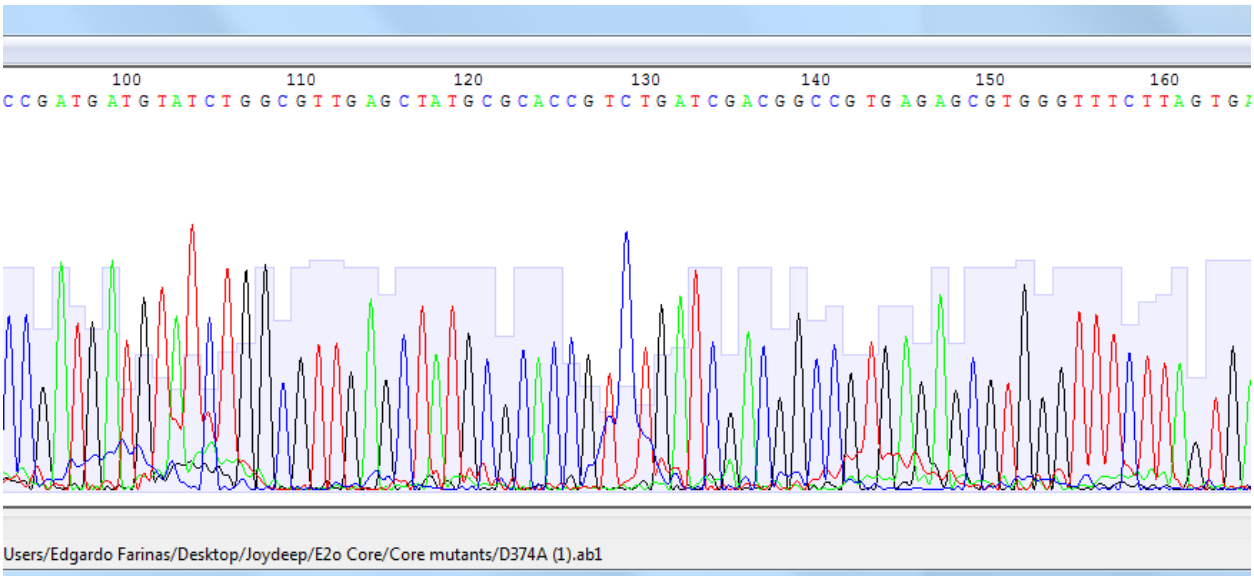

Figure B.17 DNA sequencing results with primer E2oCD-Asp374Ala.

```
          *         *         *         *         *         *         *         *         *         *
701 ATGGTGGCGTGTTTGGTAGCTTGATGAGCACCCCGATCATCAATCCGCCGCAGAGCGCGATTCTGGGCATGCATGCAATCAAAGATCGCCCGATGGCCGT 800
    ||||||||||||||||||||||||||||||||||||||||||||||||||||||||||||||||||||||||||||||||||||||||||||||||||||
 26 ----------------------------------------------------------CGCGATTCTGGGCATGCATGCAATCAAAGATCGCCCGATGGCCGT 70
                                                              *         *         *         *         *

          *         *         *         *         *         *         *         *         *         *
801 CAATGGTCAGGTTGAGATCCTGCCGATGATGTATCTGGCGTTGAGCTATGATCACCGTCTGATCGACGGCCGTGAGAGCGTGGGTTTCTTAGTGACGATT 900
    ||||||||||||||||||||||||||||||||||||||||||||||||||||##||||||||||||||||||||||||||||||||||||||||||||||
 71 CAATGGTCAGGTTGAGATCCTGCCGATGATGTATCTGGCGTTGAGCTATGCGCACCGTCTGATCGACGGCCGTGAGAGCGTGGGTTTCTTAGTGACGATT 170
          *         *         *         *         *         *         *         *         *         *

          *         *         *         *         *         *         *         *         *
901 AAAGAACTGCTGGAAGATCCGACCCGTCTGCTGCTGGACGTCGAGGCGTCTGAGAACCTGTACTTCCAAGGCCATCACCATCATCACCACTAA~~~~~~~ 993
    |||||||||||||||||||||||||||||||||||||||||||||||||||||||||||||||||||||||||||||||||||||||||||||||||||||
171 AAAGAACTGCTGGAAGATCCGACCCGTCTGCTGCTGGACGTCGAGGCGTCTGAGAACCTGTACTTCCAAGGCCATCACCATCATCACCACTAAGGTTGAG 270
          *         *         *         *         *         *         *         *         *         *
```

Figure B.18 DNA sequencing alignment of wt-E2o and E2oCD-Asp374Ala confirming mutation.

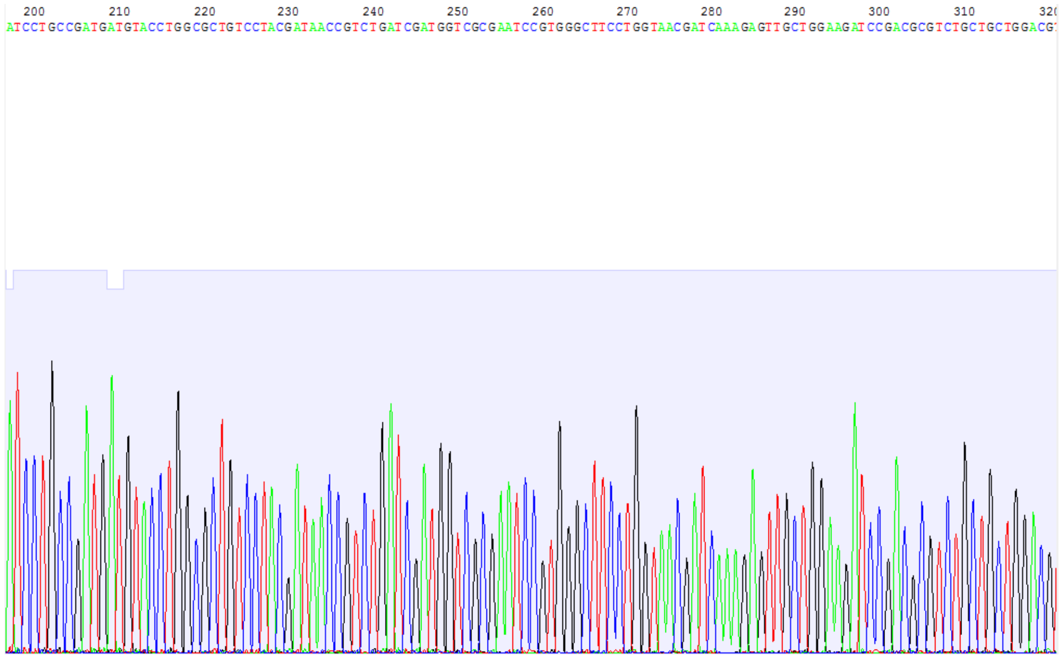

Figure B.19 DNA sequencing results with primer E2o-His375Asn.

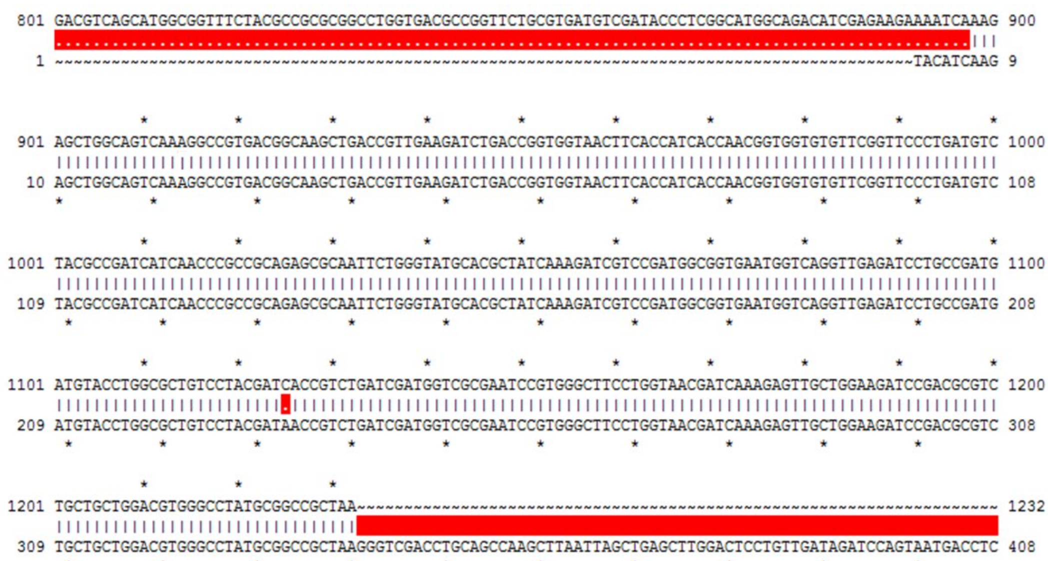

Figure B.20 DNA sequencing alignment of wt-E2o and E2o-His375Asn confirming mutation.

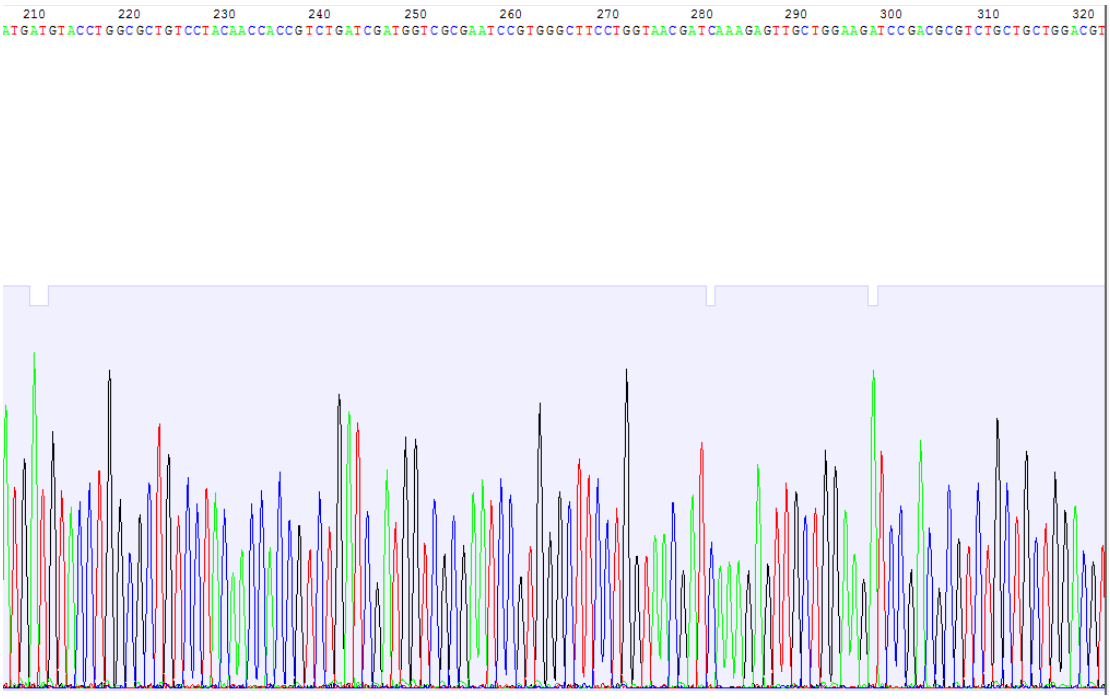

Figure B.21 DNA sequencing results with primer E2o-Asp374Asn.

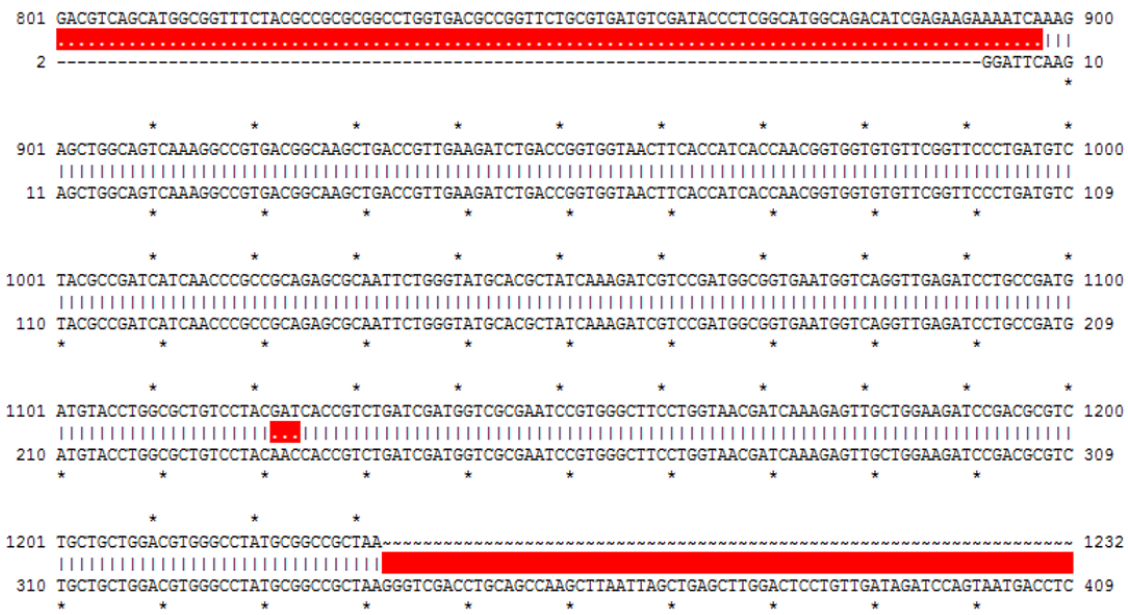

Figure B.22 DNA sequencing alignment of wt-E2o and E2o-Asp374Asn confirming mutation.

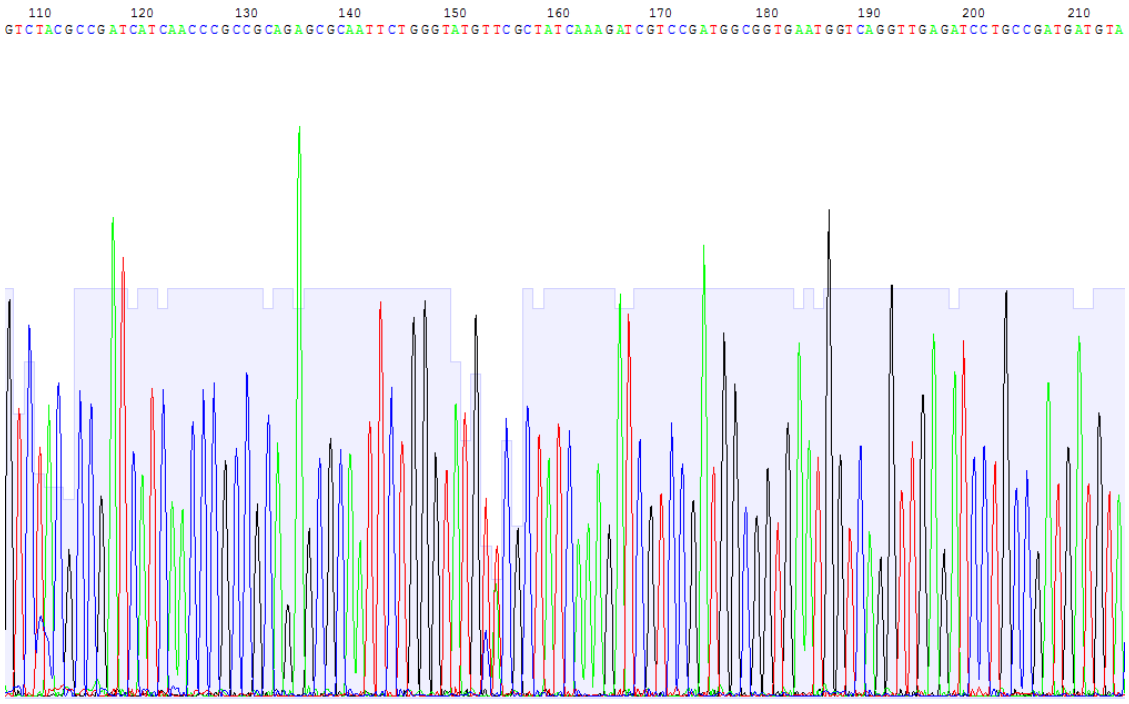

Figure B.23 DNA sequencing results for E2o-His348Phe.

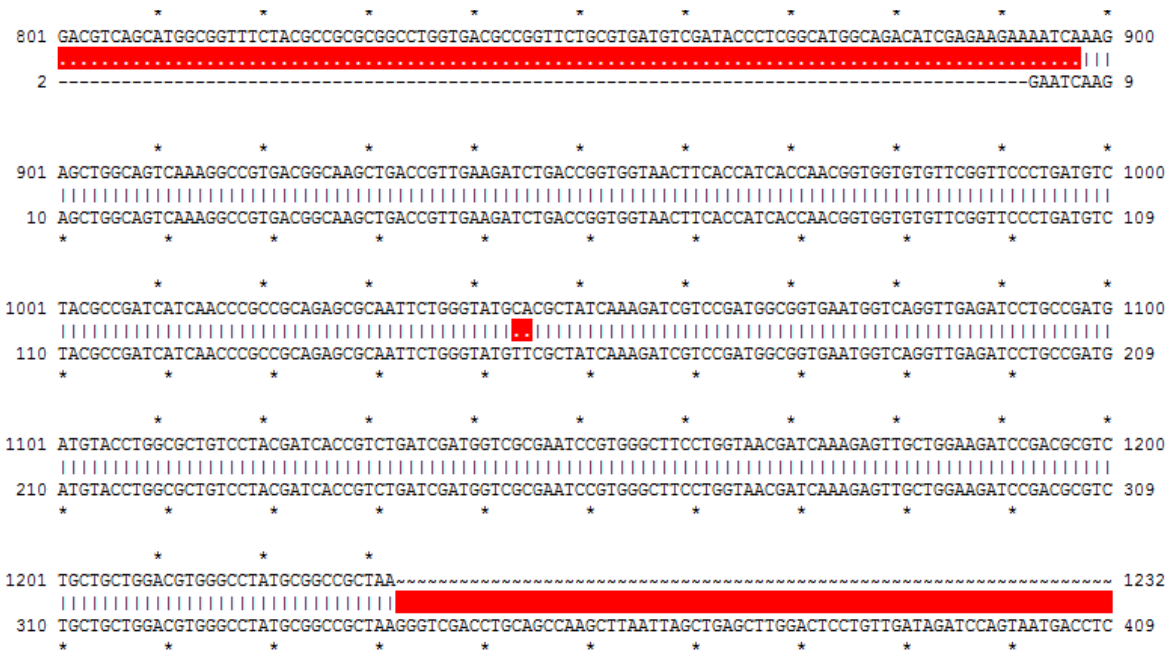

Figure B.24 DNA sequencing alignment of wt-E2o and E2o-His348Phe confirming mutation.

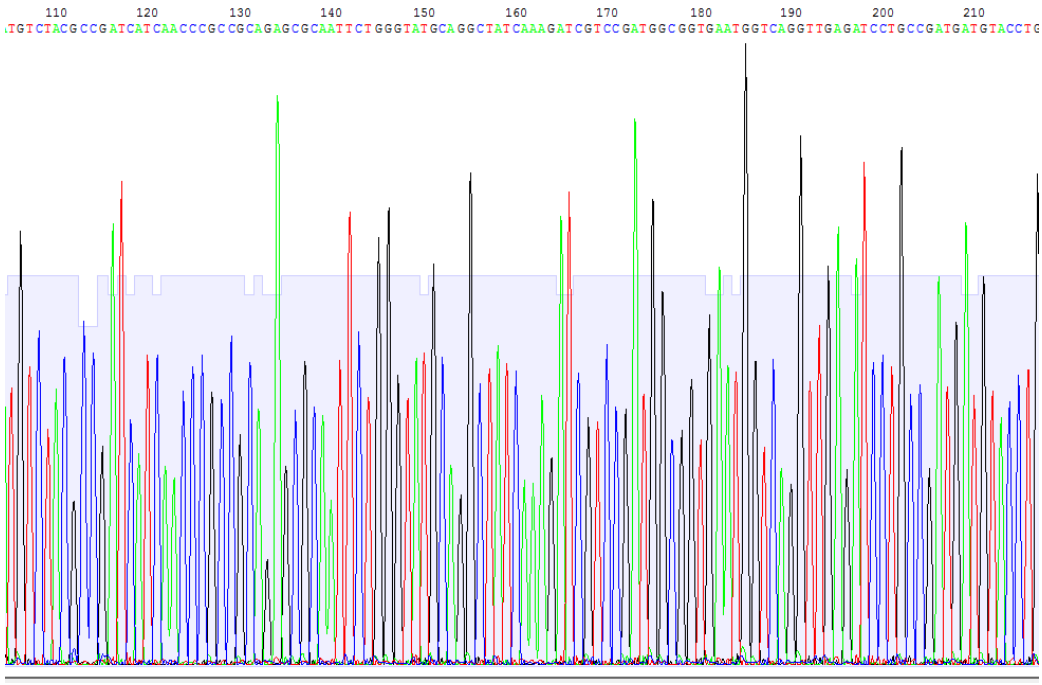

Figure B.25 DNA sequencing results for E2o-His348Gln.

Figure B.26 DNA sequencing alignment of wt-E2o and E2o-His348Gln confirming mutation.

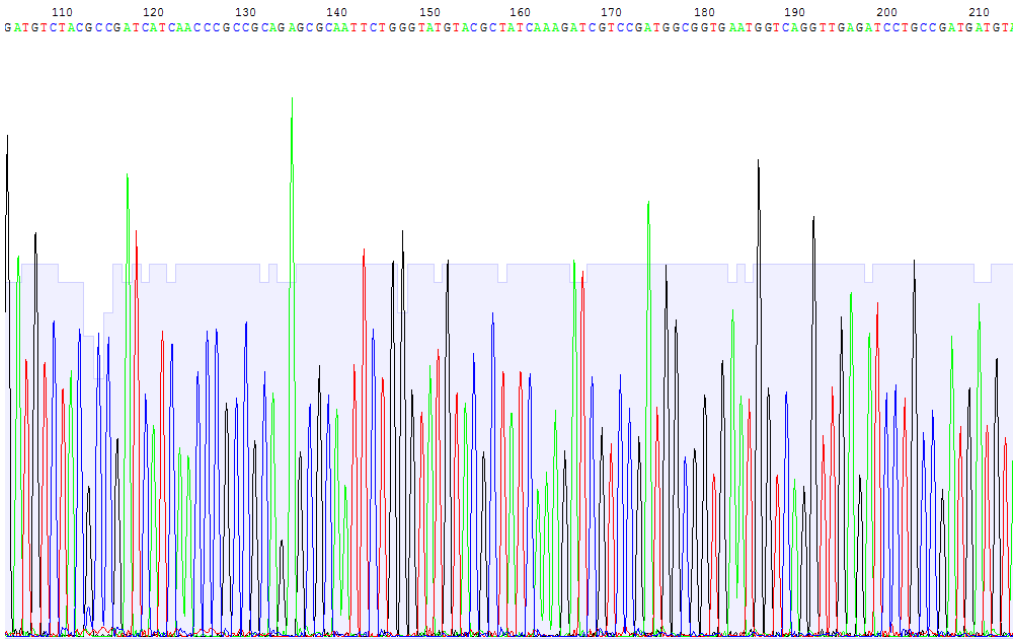

Figure B.27 DNA sequencing results for E2o-His348Gln.

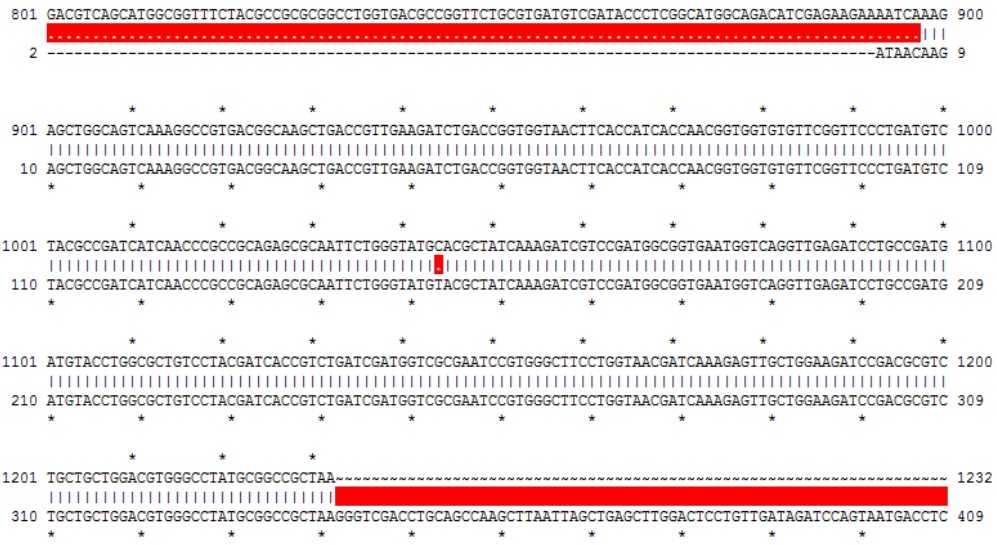

Figure B.28 DNA sequencing alignment of wt-E2o and E2o-His348Tyr confirming mutation.

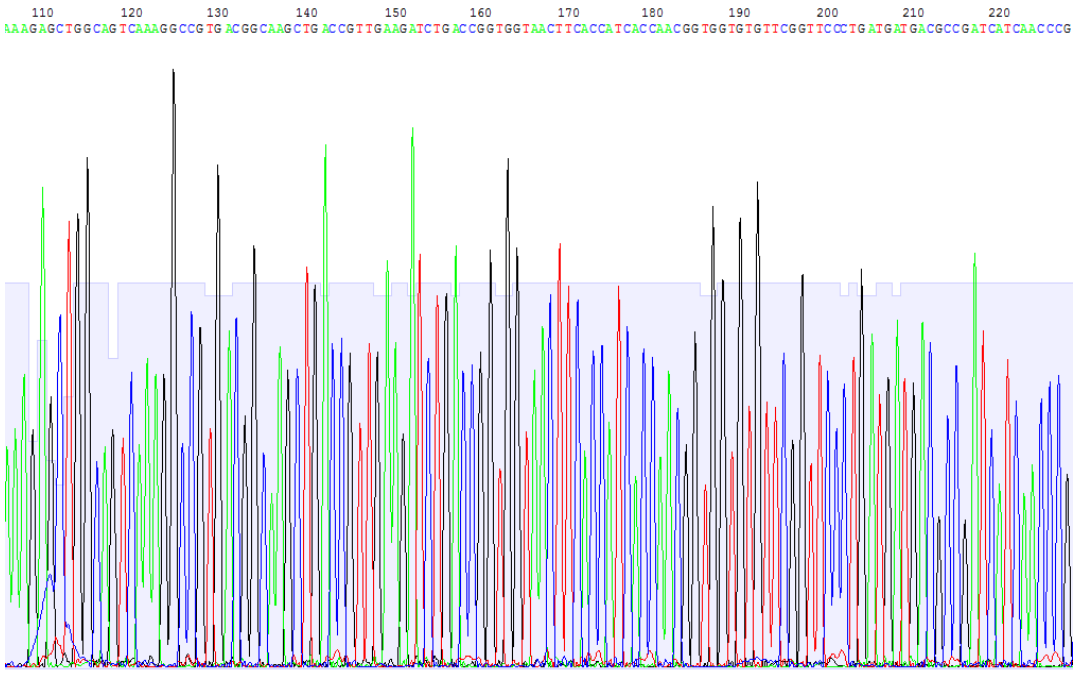

Figure B.29 DNA sequencing results for E2o-His348Gln.

Figure B.30 DNA sequencing alignment of wt-E2o and E2o-Ser333Met confirming mutation.

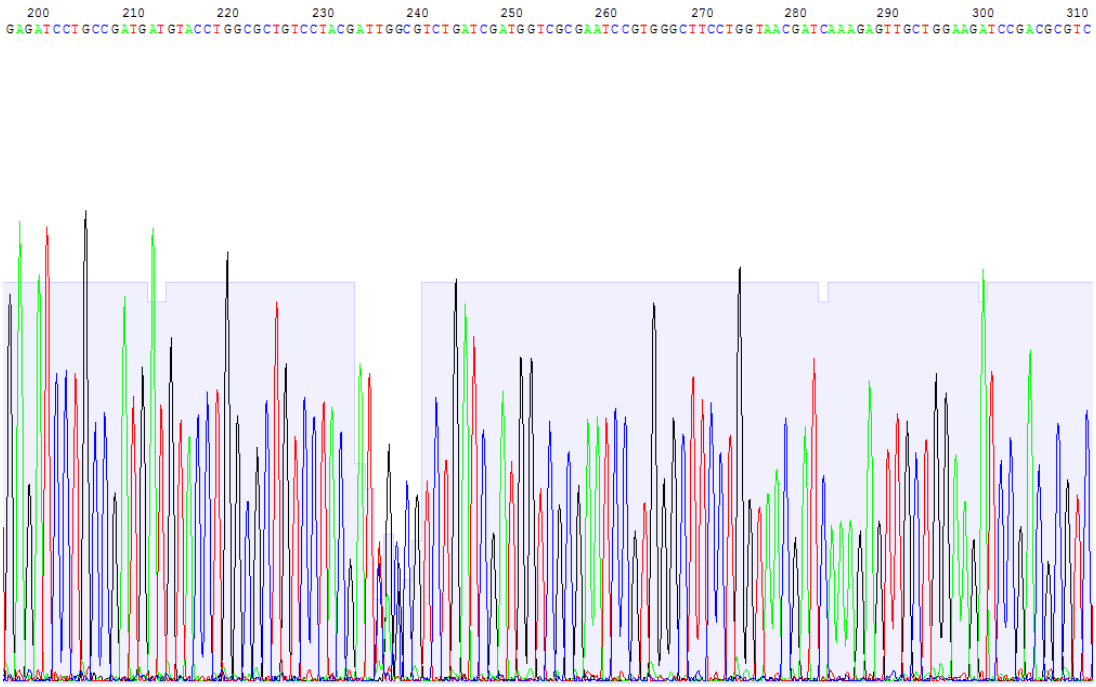

Figure B.31 DNA sequencing results for E2o-His375Trp.

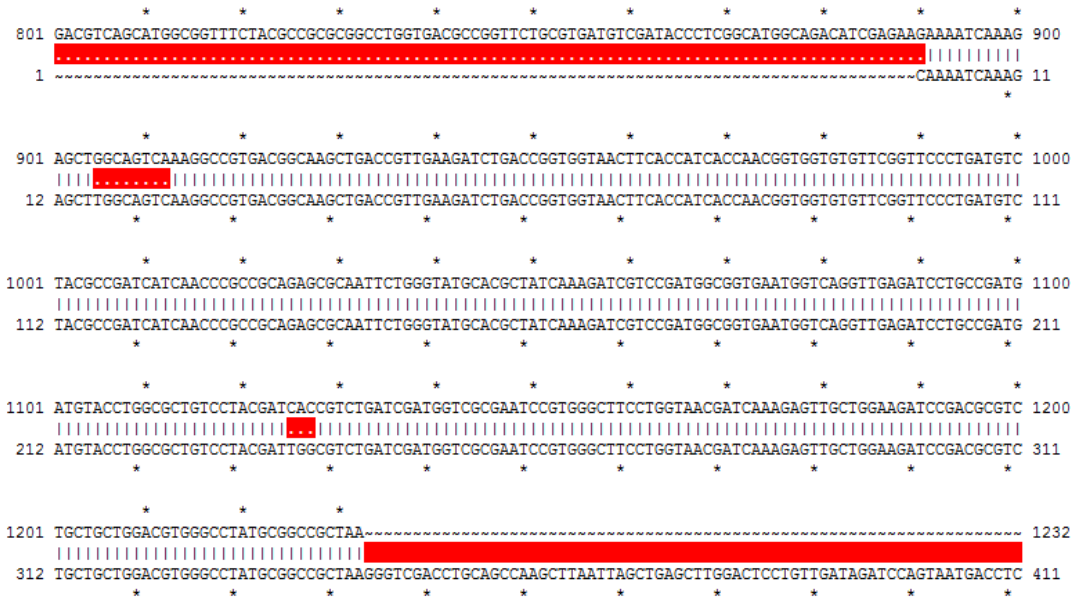

Figure B.32 DNA sequencing alignment of wt-E2o and E2o-His375Trp confirming mutation.

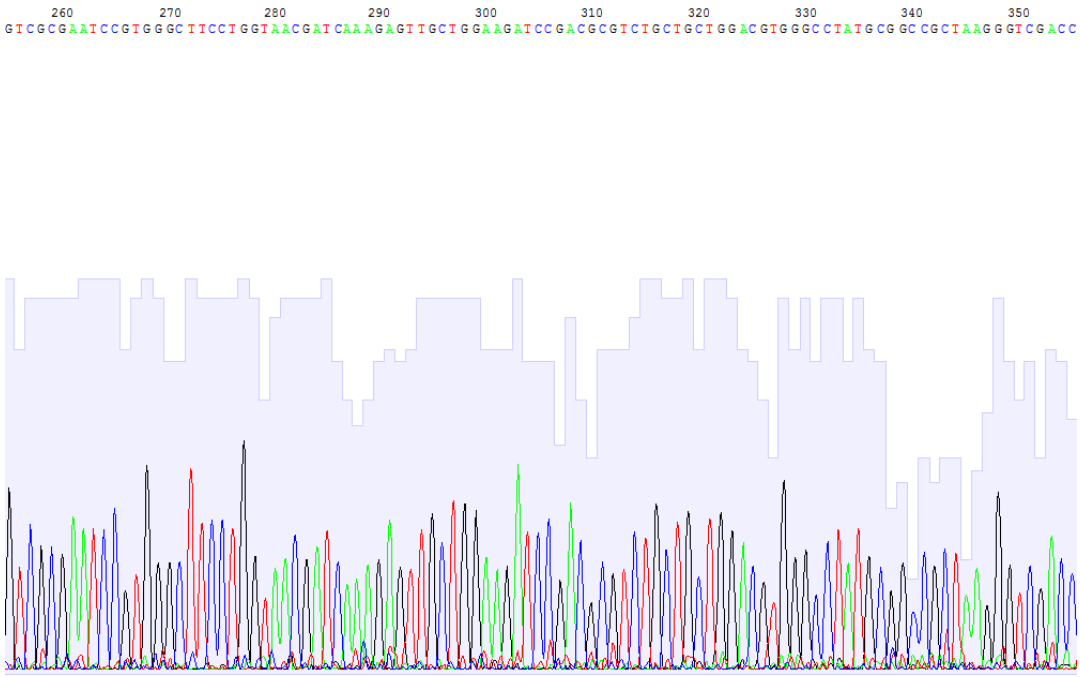

Figure B.33 DNA sequencing for E2o-His375Gly.

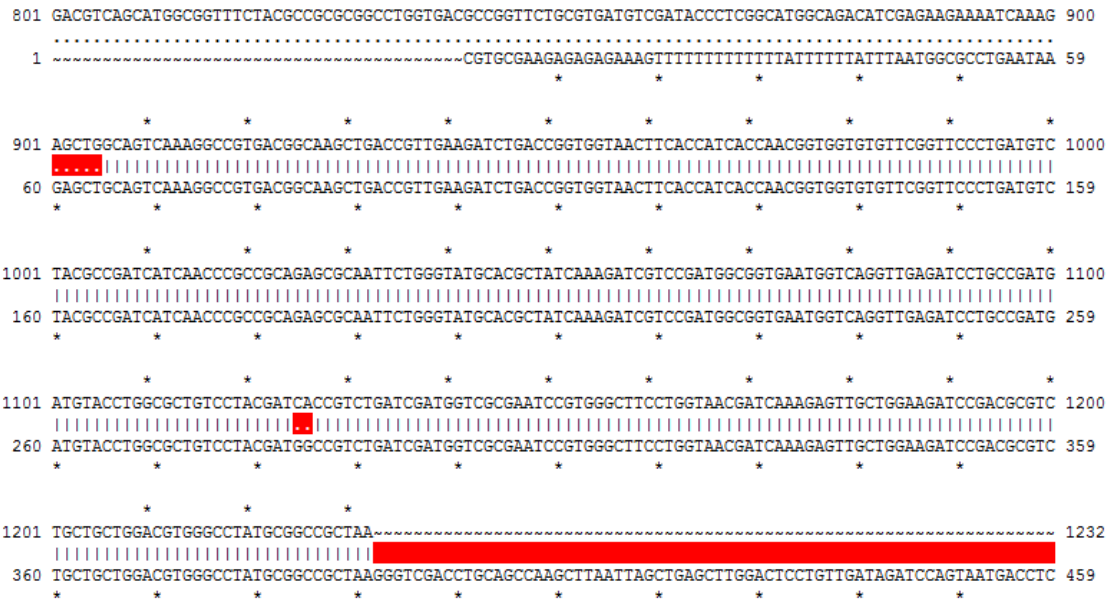

Figure B.34 DNA sequencing alignment of wt-E2o and E2o-His375Gly confirming mutation.

REFERENCES

1 Garrett RH & Grisham CM (2008) *Biochemistry (4th Ed.)*.

2 Hansford RG (1980) Control of Mitochondrial Substrate Oxidation. *Curr. Top. Bioenerg.* **10**, 217–278.

3 Tretter L & Adam-Vizi V (2005) Alpha-ketoglutarate dehydrogenase: a target and generator of oxidative stress. *Phil. Trans. R. Soc. B* **360**, 2335–2345.

4 Tretter L & Adam-Vizi V (2000) Inhibition of Krebs Cycle Enzymes by Hydrogen Peroxide: A Key Role of α-Ketoglutarate Dehydrogenase in Limiting NADH Production under Oxidative Stress. *J. Neurosci.* **20**, 8972–8979.

5 Perham RN (1991) Domains, Motifs, and Linkers in 2-Oxo Acid Dehydrogenase Multienzyme Complexes: A Paradigm in the Design of a Multifunctional Protein. *Biochemistry* **30**, 8501–8512.

6 Bunik V, Westphal AH & de Kok A (2000) Kinetic properties of the 2-oxoglutarate dehydrogenase complex from Azotobacter vinelandii. *Eur. J. Biochem.* **267**, 3583–3591.

7 Pettit FH, Hamilton L, Munk P, Namihira G, Eley MH, Willms CR & Reed LJ (1973) α-Keto Acid Dehydrogenase Complexes XIX. Subunit structure of the Escherichia coli α-ketoglutarate dehydrogenase complex. *J. Biol. Chem.* **248**, 5282–5890.

8 Koike K, Suematsu T & Ehara M (2000) Cloning, overexpression and mutagenesis of cDNA encoding dihydrolipoamide succinyltransferase component of the porcine 2-oxoglutarate dehydrogenase complex. *Eur. J. Biochem.* **267**, 3005–3016.

9 Mattevi A, Obmolova G, Kalk KH, Teplyakov A & Hoi WGJ (1993) Crystallographic Analysis of Substrate Binding and Catalysis in dihydrolipoyl transacetylase (E2p). *Biochemistry* **32**, 3887–3901.

10 Bénit P, Letouzé E, Rak M, Aubry L, Burnichon N, Favier J, Gimenez-Roqueplo AP & Rustin P (2014) Unsuspected task for an old team: Succinate, fumarate and other Krebs cycle acids in metabolic remodeling. *Biochim. Biophys. Acta - Bioenerg.* **1837**, 1330–1337.

11 Perham RN (2000) Swinging Arms and Swinging Domains in Multifunctional Enzymes: Catalytic Machines for Multistep Reactions. *Annu. Rev. Biochem.* **69**, 961–1004.

12 Frank RAW, Price AJ, Northrop FD, Perham RN & Luisi BF (2007) Crystal Structure of the E1 Component of the Escherichia coli 2-Oxoglutarate Dehydrogenase Multienzyme Complex. *J. Mol. Biol.* **368**, 639–651.

13 Shim DJ, Nemeria NS, Balakrishnan A, Patel H, Song J, Wang J, Jordan F & Farinas ET (2011) Assignment of function to histidines 260 and 298 by engineering the E1 component of the Escherichia coli 2-oxoglutarate dehydrogenase complex; Substitutions that lead to acceptance of substrates lacking the 5-carboxyl group. *Biochemistry* **50**, 7705–7709.

14 Khaĭlova LS, Bernkhardt R & Khiubner G (1977) [Study of the kinetic mechanism of the pyruvate-2,6-dichlorophenolindophenol reductase activity of muscle pyruvate dehydrogenase]. *Biokhimiia* **42**, 113–7.

15 Reed LJ & Hackert ML (1990) Structure-function relationships in dihydrolipoamide acyltransferases. *J. Biol. Chem.* **265**, 8971–4.

16 Knapp JE, Mitchell DT, Yazdi MA, Ernst SR, Reed LJ & Hackert ML (1998) Crystal structure of the truncated cubic core component of the Escherichia coli 2-oxoglutarate dehydrogenase multienzyme complex. *J. Mol. Biol.* **280**, 655–668.

17 Knapp JE, Carroll D, Lawson JE, Ernst SR, Reed LJ & Hackert ML (2000) Expression , purification , and structural analysis of the trimeric form of the catalytic domain of the Escherichia coli dihydrolipoamide succinyltransferase. *Protein Sci.* **9**, 37–48.

18 Chandrasekhar K, Wang J, Arjunan P, Sax M, Park YH, Nemeria NS, Kumaran S, Song J, Jordan F & Furey W (2013) Insight to the interaction of the dihydrolipoamide acetyltransferase (E2) core with the peripheral components in the Escherichia coli pyruvate dehydrogenase complex via multifaceted structural approaches. *J. Biol. Chem.* **288**, 15402–15417.

19 Wang J, Nemeria NS, Chandrasekhar K, Kumaran S, Arjunan P, Reynolds S, Calero G, Brukh R, Kakalis L, Furey W & Jordan F (2014) Structure and function of the catalytic domain of the dihydrolipoyl acetyltransferase component in Escherichia coli pyruvate dehydrogenase complex. *J. Biol. Chem.* **289**, 15215–15230.

20 Choi J-M, Han S-S & Kim H-S (2015) Industrial applications of enzyme biocatalysis: Current status and future aspects. *Biotechnol. Adv.* **33**, 1443–1454.

21 Fernandes P (2010) Enzymes in food processing: a condensed overview on strategies for better biocatalysts. *Enzyme Res.* **2010**, 862537.

22 Alfa MJ & Jackson M (2001) A new hydrogen peroxide–based medical-device detergent with germicidal properties: Comparison with enzymatic cleaners. *Am. J. Infect. Control* **29**, 168–177.

23 Badgujar KC, Pai PA & Bhanage BM (2016) Enhanced biocatalytic activity of immobilized Pseudomonas cepacia lipase under sonicated condition. *Bioprocess Biosyst. Eng.* **39**, 211–221.

24 Kumar D, . S, Thakur N, Verma R & Bhalla TC (2009) Microbial Proteases and Application as Laundry Detergent Additive. *Res. J. Microbiol.* **3**, 661–672.

25 Guan L-J, Ohtsuka J, Okai M, Miyakawa T, Mase T, Zhi Y, Hou F, Ito N, Iwasaki A, Yasohara Y & Tanokura M (2015) A new target region for changing the substrate specificity of amine transaminases. *Sci. Rep.* **5**, 10753.

26 Cobb RE, Chao R & Zhao H (2013) Directed Evolution: Past, Present and Future. *AIChE J.* **59**, 1432–1440.

27 Desai AA (2011) Sitagliptin Manufacture: A Compelling Tale of Green Chemistry, Process Intensification, and Industrial Asymmetric Catalysis. *Angew. Chemie Int. Ed.* **50**, 1974–1976.

28 Savile CK, Janey JM, Mundorff EC, Moore JC, Tam S, Jarvis WR, Colbeck JC, Krebber A, Fleitz FJ, Brands J, Devine PN, Huisman GW & Hughes GJ (2010) Biocatalytic asymmetric synthesis of chiral amines from ketones applied to sitagliptin manufacture. *Science* **329**, 305–9.

29 Chapman J, Ismail A & Dinu C (2018) Industrial Applications of Enzymes: Recent Advances, Techniques, and Outlooks. *Catalysts* **8**, 238.

30 Starai VJ & Escalante-Semerena JC (2004) Acetyl-coenzyme A synthetase (AMP forming). *Cell. Mol. Life Sci.* **61**, 2020–2030.

31 Strauss E (2010) Coenzyme A Biosynthesis and Enzymology. *Compr. Nat. Prod. II*, 351–410.

32 Gopinath P, Vidyarini RS & Chandrasekaran S (2009) Synthesis of Thioesters from Carboxylic Acids via Acyloxyphosphonium Intermediates with Benzyltriethylammonium Tetrathiomolybdate as the Sulfur Transfer Reagent. *J. Org. Chem.* **74**, 6291–6294.

33 Ficht S, Payne RJ, Guy RT & Wong C-H (2008) Solid-Phase Synthesis of Peptide and Glycopeptide Thioesters through Side-Chain-Anchoring Strategies. *Chem. - A Eur. J.* **14**, 3620–3629.

34 Dawson PE, Muir TW, Clark-Lewis I & Kent SB (1994) Synthesis of proteins by native chemical ligation. *Science* **266**, 776–9.

35 Dawson PE & Kent SBH (2000) Synthesis of Native Proteins by Chemical Ligation. *Annu. Rev. Biochem.* **69**, 923–960.

36 Mukaiyama T, Araki M & Takei H (1973) Reaction of S-(2-pyridyl) thioates with Grignard reagents. Convenient method for the preparation of ketones. *J. Am. Chem. Soc.* **95**, 4763–4765.

37 Anderson RJ, Henrick CA & Rosenblum LD (1974) General ketone synthesis. Reaction of organocopper reagents with S-alkyl and S-aryl thioesters. *J. Am. Chem. Soc.* **96**, 3654–3655.

38 Fowelin C, Schüpbach B & Terfort A (2007) Aromatic Thioesters as Protecting Groups for Thiols Against 1,2-Didehydrobenzenes. *European J. Org. Chem.* **2007**, 1013–1017.

39 Janette M. Villalobos, Jiri Srogl A & Liebeskind LS (2007) A New Paradigm for Carbon−Carbon Bond Formation: Aerobic, Copper-Templated Cross-Coupling. *J Am Chem Soc* **129**, 15734–15735.

40 Mercer AC & Burkart MD (2007) The ubiquitous carrier protein—a window to metabolite biosynthesis. *Nat. Prod. Rep.* **24**, 750.

41 Kazemi M & Shiri L (2015) Thioesters synthesis: Recent adventures in the esterification of thiols. *J. Sulfur Chem.* **36**, 613–623.

42 Tracewell CA & Arnold FH (2009) Directed enzyme evolution: climbing fitness peaks one amino acid at a time. *Curr. Opin. Chem. Biol.* **13**, 3–9.

43 Hammer SC, Knight AM & Arnold FH (2017) Design and evolution of enzymes for non-natural chemistry. *Curr. Opin. Green Sustain. Chem.* **7**, 23–30.

44 Kazlauskas RJ (2005) Enhancing catalytic promiscuity for biocatalysis. *Curr. Opin. Chem. Biol.* **9**, 195–201.

45 Nigel S, Berry A & Perham R (1990) [1990] Redesing of the coenzyme specificity of a dehygrogenase by protein engineering. *Nature* **343**, 38–43.

46 Carter P, Nilsson B, Burnier JP, Burdick D & Wells JA (1989) Engineering subtilisin BPN′ for site-specific proteolysis. *Proteins Struct. Funct. Genet.* **6**, 240–248.

47 Wells JA, Powers DB, Bott RR, Graycar TP & Estell DA (1987) Designing substrate specificity by protein engineering of electrostatic interactions. *Proc. Natl. Acad. Sci.* **84**, 1219–1223.

48 Dalby PA (2003) Optimising enzyme function by directed evolution. *Curr. Opin. Struct. Biol.* **13**, 500–5.

49 Park S, Morley KL, Horsman GP, Holmquist M, Hult K & Kazlauskas RJ (2005) Focusing Mutations into the P. fluorescens Esterase Binding Site Increases Enantioselectivity More Effectively than Distant Mutations. *Chem. Biol.* **12**, 45–54.

50 Strausberg SL, Ruan B, Fisher KE, Alexander PA & Bryan PN (2005) Directed Coevolution of Stability and Catalytic Activity in Calcium-free Subtilisin. *Biochemistry* **44**, 3272–3279.

51 Morley KL & Kazlauskas RJ (2005) Improving enzyme properties: when are closer mutations better? *Trends Biotechnol.* **23**, 231–237.

52 Chica RA, Doucet N & Pelletier JN (2005) Semi-rational approaches to engineering enzyme activity: Combining the benefits of directed evolution and rational design. *Curr. Opin. Biotechnol.* **16**, 378–384.

53 Glieder A, Farinas ET & Arnold FH (2002) Laboratory evolution of a soluble, self-sufficient, highly active alkane hydroxylase. *Nat. Biotechnol.* **20**, 1135–1139.

54 Gupta N & Farinas ET (2009) Narrowing laccase substrate specificity using active site saturation mutagenesis. *Comb. Chem. High Throughput Screen.* **12**, 269–74.

55 Gupta N & Farinas ET (2010) Directed evolution of CotA laccase for increased substrate specificity using Bacillus subtilis spores. *Protein Eng. Des. Sel.* **23**, 679–682.

56 Chen K & Arnold FH (1993) Tuning the activity of an enzyme for unusual environments: sequential random mutagenesis of subtilisin E for catalysis in dimethylformamide. *Proc. Natl. Acad. Sci.* **90**, 5618–5622.

57 Arnold FH (1993) Protein engineering for unusual environments. *Curr. Opin. Biotechnol.* **4**, 450–455.

58 You L & Arnold FH (1996) Directed evolution of subtilisin E in *Bacillus subtilis* to enhance total activity in aqueous dimethylformamide. *Protein Eng. Des. Sel.* **9**, 719–719.

59 Kan SBJ, Lewis RD, Chen K & Arnold FH (2016) Directed evolution of cytochrome c for carbon-silicon bond formation: Bringing silicon to life. *Science* **354**, 1048–1051.

60 Chockalingam K, Chen Z, Katzenellenbogen JA & Zhao H (2005) Directed evolution of specific receptor-ligand pairs for use in the creation of gene switches. *Proc. Natl. Acad. Sci.* **102**, 5691–5696.

61 Gershwin ME, Bowtell DDL, Tempst P, Erdjument-Bromage H, Habelhah H, Laine A & Ronai Z (2004) Regulation of 2-Oxoglutarate (α-Ketoglutarate) Dehydrogenase Stability by the RING Finger Ubiquitin Ligase Siah. *J. Biol. Chem.* **279**, 53782–53788.

62 Perham RN (1991) Domains, motifs, and linkers in 2-oxo acid dehydrogenase multienzyme complexes: a paradigm in the design of a multifunctional protein. *Biochemistry* **30**, 8501–8512.

63 Bleile DM, Munk P, Oliver RM & Reed LJ (1979) Subunit structure of dihydrolipoyl transacetylase component of pyruvate dehydrogenase complex from Escherichia coli. *Biochemistry* **76**, 4385–4389.

64 Cronan JE (2016) Assembly of Lipoic Acid on Its Cognate Enzymes: an Extraordinary and Essential Biosynthetic Pathway. *Microbiol. Mol. Biol. Rev.* **80**, 429–450.

65 Spalding MD & Prigge ST (2010) Lipoic Acid Metabolism in Microbial Pathogens. *Microbiol. Mol. Biol. Rev.* **74**, 200–228.

66 Ricaud PM, Howard MJ, Roberts EL, Broadhurst RW & Perham RN (1996) Three-dimensional structure of the lipoyl domain from the dihydrolipoyl succinyltransferase component of the 2-oxoglutarate dehydrogenase multienzyme complex of Escherichia coli. *J. Mol. Biol.* **264**, 179–190.

67 Stepp LR, Bleile DM, McRorie DK, Pettit FH & Reed LJ (1981) Use of Trypsin and Lipoamidase To Study the Role of Lipoic Acid Moieties in the Pyruvate and α-Ketoglutarate Dehydrogenase Complexes of Escherichia coli. *Biochemistry* **20**, 4555–4560.

68 Derosier DJ, Oliver RM & Reed LJ (1971) Crystallization and preliminary structural analysis of dihydrolipoyl transsuccinylase, the core of the 2-oxoglutarate dehydrogenase complex. *Proc. Natl. Acad. Sci. U. S. A.* **68**, 1135–7.

69 Shaw W V & Leslie AGW (1991) Chloramphenicol Acetyltransferase. *Annu. Rev. Biophys. Biophys. Chem.* **20**, 363–386.

70 Yu X, Hiromasa Y, Tsen H, Stoops JK, Roche TE & Zhou ZH (2008) Structures of the Human Pyruvate Dehydrogenase Complex Cores: A Highly Conserved Catalytic Center with Flexible N-Terminal Domains. *Structure* **16**, 104–114.

71 Guest JR (1987) Functional implications of structural homologies between chloramphenicol acetyltransferase and dihydrolipoamide acetyltransferase. *FEMS Microbiol. Lett.* **44**, 417–422.

72 Shaw W V. (1983) Chloramphenicol Acetyltransferase: Enzymology and Molecular Biology. *Crit. Rev. Biochem.* **14**, 1–46.

73 Leslie AGW, Moody PCE & Shaw W V. (1986) Structure of Chloramphenicol Acetyltransferase at 1.75- angstrom Resolution. *Proc. Natl. Acad. Sci. U. S. A.* **85**, 4133–4137.

74 Shaw W V & Leslie AGW (1991) Chloramphenicol Acetyl Transferase. *Ann. Rev. Biophys.* **20**, 363–86.

75 Lewendon A, Murray IA, Shaw W V., Gibbs MR & Leslie AGW (1994) Replacement of catalytic histidine-195 of chloramphenicol acetyltransferase: Evidence for a general base role for glutamate. *Biochemistry* **33**, 1944–1950.

76 Kleanthous C, Cullis PM & Shaw W V. (1985) 3-(Bromoacetyl)chloramphenicol, an active site-directed inhibitor for chloramphenicol acetyltransferase. *Biochemistry* **24**, 5307–5313.

77 Quinlan CL, Goncalves RLS, Hey-Mogensen M, Yadava N, Bunik VI & Brand MD (2014) The 2-Oxoacid Dehydrogenase Complexes in Mitochondria Can Produce Superoxide/Hydrogen Peroxide at Much Higher Rates Than Complex I. *J. Biol. Chem.* **289**, 8312–8325.

78 Brand MD (2016) Mitochondrial generation of superoxide and hydrogen peroxide as the source of mitochondrial redox signaling. *Free Radic. Biol. Med.* **100**, 14–31.

79 Nemeria NS, Ambrus A, Patel H, Gerfen G, Adam-Vizi V, Tretter L, Zhou J, Wang J & Jordan F (2014) Human 2-oxoglutarate dehydrogenase complex E1 component forms a thiamin-derived radical by aerobic oxidation of the enamine intermediate. *J. Biol. Chem.* **289**, 29859–29873.

80 Nemeria NS, Gerfen G, Guevara E, Nareddy PR, Szostak M & Jordan F (2017) The human Krebs cycle 2-oxoglutarate dehydrogenase complex creates an additional source of superoxide/hydrogen peroxide from 2-oxoadipate as alternative substrate. *Free Radic. Biol. Med.* **108**, 644–654.

81 Gibson GE, Xu H, Chen H-L, Chen W, Denton TT & Zhang S (2015) Alpha-ketoglutarate dehydrogenase complex-dependent succinylation of proteins in neurons and neuronal cell lines. *J. Neurochem.* **134**, 86–96.

82 Wang Y, Guo YR, Liu K, Yin Z, Liu R, Xia Y, Tan L, Yang P, Lee J-H, Li X, Hawke D, Zheng Y, Qian X, Lyu J, He J, Xing D, Tao YJ & Lu Z (2017) KAT2A coupled with the α-KGDH complex acts as a histone H3 succinyltransferase. *Nature* **552**, 273.

83 Sabari BR, Zhang D, David Allis C & Zhao Y (2017) Metabolic regulation of gene expression through histone acylations. *Nat Rev Mol Cell Biol.* **18**, 90–101.

84 Nemeria NS, Gerfen G, Nareddy PR, Yang L, Zhang X, Szostak M & Jordan F (2018) The mitochondrial 2-oxoadipate and 2-oxoglutarate dehydrogenase complexes share their E2 and E3 components for their function and both generate reactive oxygen species. *Free Radic. Biol. Med.* **115**, 136–145.

85 Tan M, Peng C, Anderson KA, Chhoy P, Xie Z, Dai L, Park J, Chen Y, Huang H, Zhang Y, Ro J, Wagner GR, Green MF, Madsen AS, Schmiesing J, Peterson BS, Xu G, Ilkayeva OR, Muehlbauer MJ, Braulke T, Mühlhausen C, Backos DS, Olsen CA, McGuire PJ, Pletcher SD, Lombard DB, Hirschey MD & Zhao Y (2014) Lysine Glutarylation Is a Protein Posttranslational Modification Regulated by SIRT5. *Cell Metab.* **19**, 605–617.

86 Mattevi A, Obmolova G, Kalk KH, Westphal AH, de Kok A & Hol WGJ (1993) Refined Crystal Structure of the Catalytic Domain of Dihydrolipoyl Transacetylase (E2p) from Azotobacter vinelandii at 2·6 Å Resolution. *J. Mol. Biol.* **230**, 1183–1199.

87 Kato M, Wynn RM, Chuang JL, Brautigam CA, Custorio M & Chuang DT (2006) A synchronized substrate-gating mechanism revealed by cubic-core structure of the bovine branched-chain a-ketoacid dehydrogenase complex. *Eur. Mol. Biol. Organ.* **25**, 5983–5994.

88 Izard T, Aevarsson A, Allen MD, Westphal AH, Perham RN, de Kok A & Hol WG (1999) Principles of quasi-equivalence and Euclidean geometry govern the assembly of cubic and dodecahedral cores of pyruvate dehydrogenase complexes. *Proc. Natl. Acad. Sci. U. S. A.* **96**, 1240–5.

89 Russell GC, Machado RS & Guest JR (1992) Overproduction of the pyruvate dehydrogenase multienzyme complex of Escherichia coli and site-directed substitutions in the E1p and E2p subunits. *Biochem. J.* **287 (Pt 2)**, 611–9.

90 Chakraborty J, Nemeria NS, Farinas E & Jordan F (2018) Catalysis of transthiolacylation in the active centers of dihydrolipoamide acyltransacetylase components of 2-oxo acid dehydrogenase complexes. *FEBS Open Bio* **8**, 880–896.

91 Balakrishnan A, Nemeria NS, Chakraborty S, Kakalis L & Jordan F (2012) Determination of Pre-Steady-State Rate Constants on the Escherichia coli Pyruvate Dehydrogenase Complex Reveals That Loop Movement Controls the Rate-Limiting Step. *J. Am. Chem. Soc.* **134**, 18644–18655.

92 Baykal A, Chakraborty S, Dodoo A & Jordan F (2006) Synthesis with good enantiomeric excess of both enantiomers of alpha-ketols and acetolactates by two thiamin diphosphate-dependent decarboxylases. *Bioorg. Chem.* **34**, 380–93.

93 Song J, Park Y-H, Nemeria NS, Kale S, Kakalis L & Jordan F (2010) Nuclear Magnetic Resonance Evidence for the Role of the Flexible Regions of the E1 Component of the Pyruvate Dehydrogenase Complex from Gram-negative Bacteria. *J. Biol. Chem.* **285**, 4680–4694.

94 Frey PA, Flournoy DS, Gruys K & Yang YS (1989) Intermediates in reductive transacetylation catalyzed by pyruvate dehydrogenase complex. *Ann. N. Y. Acad. Sci.* **573**, 21–35.

95 Dafydd Jones D & Perham RN (2008) The role of loop and β-turn residues as structural and functional determinants for the lipoyl domain from the Escherichia coli 2-oxoglutarate dehydrogenase complex. *Biochem. J* **409**, 357–366.

96 Jones DD, Stott KM, Reche PA & Perham RN (2001) Recognition of the lipoyl domain is the ultimate determinant of substrate channelling in the pyruvate dehydrogenase multienzyme complex. *J. Mol. Biol.* **305**, 49–60.

97 Fries M, Stott KM, Reynolds S & Perham RN (2007) Distinct Modes of Recognition of the Lipoyl Domain as Substrate by the E1 and E3 Components of the Pyruvate Dehydrogenase Multienzyme Complex. *J. Mol. Biol.* **366**, 132–139.

98 Jung SY, Li Y, Wang Y, Chen Y, Zhao Y & Qin J (2008) Complications in the assignment of 14 and 28 Da mass shift detected by mass spectrometry as in vivo methylation from endogenous proteins. *Anal. Chem.* **80**, 1721–9.

99 Mattevi A, Obmolova G, Kalk KH, Teplyakov A & Hol WG (1993) Crystallographic analysis of substrate binding and catalysis in dihydrolipoyl transacetylase (E2p). *Biochemistry* **32**, 3887–3901.

100 Song J & Jordan F (2012) Interchain Acetyl Transfer in the E2 Component of Bacterial Pyruvate Dehydrogenase Suggests a Model with Different Roles for Each Chain in a Trimer of the Homooligomeric Component. *Biochemistry* **51**, 2795–2803.

101 Hupe DJ & Jencks WP (1977) Nonlinear Structure-Reactivity Correlations. Acyl Transfer between Sulfur and Oxygen Nucleophiles. *J. Am. Chem. Soc.* **99**, 451–464.

102 Muir TW, Sondhi D & Cole PA (1998) Expressed protein ligation: a general method for protein engineering. *Proc. Natl. Acad. Sci. U. S. A.* **95**, 6705–10.

103 Robbins T, Liu Y-C, Cane DE & Khosla C (2016) Structure and mechanism of assembly line polyketide synthases. *Curr. Opin. Struct. Biol.* **41**, 10–18.

104 Carter P & Wells JA (1988) Dissecting the catalytic triad of a serine protease. *Nature* **332**, 564–568.

105 Bryan P, Pantoliano MW, Quill SG, Hsiao HY & Poulos T (1986) Site-directed mutagenesis and the role of the oxyanion hole in subtilisin. *Proc. Natl. Acad. Sci. U. S. A.* **83**, 3743–3745.

106 Chang TK, Chiang Y, Guo HX, Kresge AJ, Mathew L, Powell MF & Wells JA (1996) Solvent isotope effects in H2O-D2O mixtures (proton inventories) on serine-protease-catalyzed hydrolysis reactions. Influence of oxyanion hole interactions and medium effects. *J. Am. Chem. Soc.* **118**, 8802–8807.

107 Andrews FH & McLeish MJ (2013) Using site-saturation mutagenesis to explore mechanism and substrate specificity in thiamin diphosphate-dependent enzymes. *FEBS J.* **280**, 6395–6411.

108 Reetz MT, Zonta A, Schimossek K, Jaeger K-E & Liebeton K (1997) Creation of Enantioselective Biocatalysts for Organic Chemistry by In Vitro Evolution. *Angew. Chemie Int. Ed. English* **36**, 2830–2832.

109 Reetz MT (2001) Combinatorial and Evolution-Based Methods in the Creation of Enantioselective Catalysts. *Angew. Chemie (International ed.)* **40**, 284–310.

110 Reetz MT, Kahakeaw D & Sanchis J (2009) Shedding light on the efficacy of laboratory evolution based on iterative saturation mutagenesis. *Mol. BioSyst.* **5**, 115–122.

111 Reetz MT (2004) Controlling the enantioselectivity of enzymes by directed evolution: practical and theoretical ramifications. *Proc. Natl. Acad. Sci. U. S. A.* **101**, 5716–22.

112 Hammer SC, Knight AM & Arnold FH (2017) Design and evolution of enzymes for non-natural chemistry. *Curr. Opin. Green Sustain. Chem.* **7**, 23–30.

113 Tucker JL & Faul MM (2016) Industrial research: Drug companies must adopt green chemistry. *Nature* **534**, 27–29.

114 Lieber DJ, Catlett J, Madayiputhiya N, Nandakumar R, Lopez MM, Metcalf WW & Buan NR (2014) A multienzyme complex channels substrates and electrons through acetyl-coA and methane biosynthesis pathways in Methanosarcina. *PLoS One* **9**, 1–8.

115 Agapakis CM, Boyle PM & Silver PA (2012) Natural strategies for the spatial optimization of metabolism in synthetic biology. *Nat. Chem. Biol.* **8**, 527–535.

116 Jensen RA (1976) Enzyme recruitment in evolution of new function. *Annu.Rev.Microbiol.* **30**, 409–425.

117 Khersonsky O & Tawfik DS (2010) Enzyme Promiscuity: A Mechanistic and Evolutionary Perspective. *Annu. Rev. Biochem.* **79**, 471–505.

118 Newton MS, Arcus VL, Gerth ML & Patrick WM (2018) Enzyme evolution: innovation is easy, optimization is complicated. *Curr. Opin. Struct. Biol.* **48**, 110–116.

119 Renata H, Wang ZJ & Arnold FH (2015) Expanding the enzyme universe: Accessing non-natural reactions by mechanism-guided directed evolution. *Angew. Chemie - Int. Ed.* **54**, 3351–3367.

120 Yin Y-C, Yu H-L, Luan Z-J, Li R-J, Ouyang P-F, Liu J & Xu J-H (2014) Unusually Broad Substrate Profile of Self-Sufficient Cytochrome P450 Monooxygenase CYP116B4 from *Labrenzia aggregata*. *ChemBioChem* **15**, 2443–2449.

121 Arnold FH (2015) The nature of chemical innovation: new enzymes by evolution. *Q. Rev. Biophys.* **48**, 404–410.

122 Coelho PS, Brustad EM, Kannan A & Arnold FH (2013) Olefin Cyclopropanation via Carbene Transfer Catalyzed by Engineered Cytochrome P450 Enzymes. *Science* **339**, 307–310.

123 Chandru K, Gilbert A, Butch C, Aono M & Cleaves HJ (2016) The abiotic chemistry of thiolated acetate derivatives and the origin of life. *Sci. Rep.* **6**, 1–11.

124 de Duve C (1995) The Beginnings of Life on Earth. *Am. Sci.* **83**, 428–437.

125 Liu XL, Shi Y, Kang JS, Oelschlaeger P & Yang KW (2015) Amino Acid Thioester Derivatives: A Highly Promising Scaffold for the Development of Metallo-β-lactamase L1 Inhibitors. *ACS Med. Chem. Lett.* **6**, 660–664.

126 Fukuyama T, Lin SC & Li L (1990) Facile reduction of ethyl thiol esters to aldehydes: application to a total synthesis of (+)-neothramycin A methyl ether. *J. Am. Chem. Soc.* **112**, 7050–7051.

127 Masamune S, Yamamoto H, Kamata S & Fukuzawa A (1975) Syntheses of macrolide antibiotics. II. Methymycin. *J. Am. Chem. Soc.* **97**, 3513–3515.

128 Corey EJ & Nicolaou KC (1974) Efficient and mild lactonization method for the synthesis of macrolides. *J. Am. Chem. Soc.* **96**, 5614–5616.

129 Trott O & Olson AJ (2010) AutoDock Vina: improving the speed and accuracy of docking with a new scoring function, efficient optimization, and multithreading. *J. Comput. Chem.* **31**, 455–61.

130 Pettersen EF, Goddard TD, Huang CC, Couch GS, Greenblatt DM, Meng EC & Ferrin TE (2004) UCSF Chimera--A visualization system for exploratory research and analysis. *J. Comput. Chem.* **25**, 1605–1612.

131 Voss NR & Gerstein M (2010) 3V: Cavity, channel and cleft volume calculator and extractor. *Nucleic Acids Res.* **38**, 555–562.

132 Parthasarathy A, Pierik AJ, Kahnt J, Zelder O & Buckel W (2011) Substrate Specificity of 2-Hydroxyglutaryl-CoA Dehydratase from Clostridium symbiosum : Toward a Bio-Based Production of Adipic Acid. *Biochemistry* **50**, 3540–3550.

133 Henikoff S & Henikoff JG (1992) Amino acid substitution matrices from protein blocks. *Proc. Natl. Acad. Sci. U. S. A.* **89**, 10915–9.

134 Yep A, Kenyon GL & McLeish MJ (2008) Saturation mutagenesis of putative catalytic residues of benzoylformate decarboxylase provides a challenge to the accepted mechanism. *Proc. Natl. Acad. Sci.* **105**, 5733–5738.

135 Hutchison CA, Chuang RY, Noskov VN, Assad-Garcia N, Deerinck TJ, Ellisman MH, Gill J, Kannan K, Karas BJ, Ma L, Pelletier JF, Qi ZQ, Richter RA, Strychalski EA, Sun L, Suzuki Y, Tsvetanova B, Wise KS, Smith HO, Glass JI, Merryman C, Gibson DG & Venter JC (2016) Design and synthesis of a minimal bacterial genome. *Science* **351**, 1–11.

136 Müller M, Sprenger GA & Pohl M (2013) CC bond formation using ThDP-dependent lyases. *Curr. Opin. Chem. Biol.* **17**, 261–270.

137 Müller M, Gocke D & Pohl M (2009) Thiamin diphosphate in biological chemistry: exploitation of diverse thiamin diphosphate-dependent enzymes for asymmetric chemoenzymatic synthesis. *FEBS J.* **276**, 2894–2904.

138 Lindqvist Y, Schneider G, Ermler U & Sundström M (1992) Three-dimensional structure of transketolase, a thiamine diphosphate dependent enzyme, at 2.5 A resolution. *EMBO J.* **11**, 2373–9.

139 Kaplun A, Binshtein E, Vyazmensky M, Steinmetz A, Barak Z, Chipman DM, Tittmann K & Shaanan B (2008) Glyoxylate carboligase lacks the canonical active site glutamate of thiamine-dependent enzymes. *Nat. Chem. Biol.* **4**, 113–118.

140 Brammer LA & Meyers CF (2009) Revealing Substrate Promiscuity of 1-Deoxy- d -xylulose 5-Phosphate Synthase. *Org. Lett.* **11**, 4748–4751.

141 Mosbacher TG, Mueller M & Schulz GE (2005) Structure and mechanism of the ThDP-dependent benzaldehyde lyase from Pseudomonas fluorescens. *FEBS J.* **272**, 6067–6076.

142 Baykal A, Chakraborty S, Dodoo A & Jordan F (2006) Synthesis with good enantiomeric excess of both enantiomers of alpha-ketols and acetolactates by two thiamin diphosphate-dependent decarboxylases. *Bioorg. Chem.* **34**, 380–93.

143 Sergienko EA & Jordan F (2001) Catalytic acid-base groups in yeast pyruvate decarboxylase. 3. A steady-state kinetic model consistent with the behavior of both wild-type and variant enzymes at all relevant pH values. *Biochemistry* **40**, 7382–403.

144 Nemeria N, Tittmann K, Joseph E, Zhou L, Vazquez-Coll MB, Arjunan P, Hübner G, Furey W & Jordan F (2005) Glutamate 636 of the *Escherichia coli* Pyruvate Dehydrogenase-E1 Participates in Active Center Communication and Behaves as an Engineered Acetolactate Synthase with Unusual Stereoselectivity. *J. Biol. Chem.* **280**, 21473–21482.

145 Beigi M, Waltzer S, Fries A, Eggeling L, Sprenger GA & Müller M (2013) TCA cycle involved enzymes SucA and Kgd, as well as MenD: Efficient biocatalysts for asymmetric C-C bond formation. *Org. Lett.* **15**, 452–455.

146 Ward OP & Singh A (2000) Enzymatic asymmetric synthesis by decarboxylases. *Curr. Opin. Biotechnol.* **11**, 520–6.

147 Patel H, Shim DJ, Farinas ET & Jordan F (2013) Investigation of the donor and acceptor range for chiral carboligation catalyzed by the E1 component of the 2-oxoglutarate dehydrogenase complex. *J. Mol. Catal. B Enzym.* **98**, 42–45.

148 Meyer D, Walter L, Kolter G, Pohl M, Müller M & Tittmann K (2011) Conversion of Pyruvate Decarboxylase into an Enantioselective Carboligase with Biosynthetic Potential. *J. Am. Chem. Soc.* **133**, 3609–3616.

149 Hult K & Berglund P (2007) Enzyme promiscuity: mechanism and applications. *Trends Biotechnol.* **25**, 231–238.

150 Chen R (2001) Enzyme engineering: rational redesign versus directed evolution. *Trends Biotechnol.* **19**, 13–4.

151 Dresen C, Richter M, Pohl M, Lüideke S & Müller M (2010) The enzymatic asymmetric conjugate umpolung reaction. *Angew. Chemie - Int. Ed.* **49**, 6600–6603.

152 Pohl M, Sprenger GA & Müller M (2004) A new perspective on thiamine catalysis. *Curr. Opin. Biotechnol.* **15**, 335–342.

153 Kasparyan E, Richter M, Dresen C, Walter LS, Fuchs G, Leeper FJ, Wacker T, Andrade SLA, Kolter G, Pohl M & Müller M (2014) Asymmetric Stetter reactions catalyzed by thiamine diphosphate-dependent enzymes. *Appl. Microbiol. Biotechnol.* **98**, 9681–9690.

154 Fang QK, Han Z, Grover P, Kessler D, Senanayake* CH & Wald SA (2000) Rapid access to enantiopure bupropion and its major metabolite by stereospecific nucleophilic substitution on an α-ketotriflate. *Tetrahedron: Asymmetry* **11**, 3659–3663.

155 Hideaki Kakeya, Masayuki Morishita, Hiroyuki Koshino, Tetsu-ichiro Morita, Kimiko Kobayashi A & Osada* H (1999) Cytoxazone: A Novel Cytokine Modulator Containing a 2-Oxazolidinone Ring Produced by Streptomyces sp. *J. Org. Chem.* **64**, 1052–1053.

156 Stermitz FR, Tawara-Matsuda J, Lorenz P, Mueller P, Zenewicz L & Lewis K (2000) 5'-Methoxyhydnocarpin-D and pheophorbide A: Berberis species components that potentiate berberine growth inhibition of resistant Staphylococcus aureus. *J. Nat. Prod.* **63**, 1146–9.

157 Westphal R, Vogel C, Schmitz C, Pleiss J, Müller M, Pohl M & Rother D (2014) A tailor-made chimeric thiamine diphosphate dependent enzyme for the direct asymmetric synthesis of (S)-benzoins. *Angew. Chemie - Int. Ed.* **53**, 9376–9379.

158 Fang M, MacOva A, Hanson KL, Kos J & Palmer DRJ (2011) Using substrate analogues to probe the kinetic mechanism and active site of Escherichia coli MenD. *Biochemistry* **50**, 8712–8721.

159 Schapfl M, Baier S, Fries A, Ferlaino S, Waltzer S, Müller M & Sprenger GA (2018) Extended substrate range of thiamine diphosphate-dependent MenD enzyme by coupling of two C–C-bonding reactions. *Appl. Microbiol. Biotechnol.* **102**, 8359–8372.

160 Palaniappan C, Sharma V, Hudspeth MES & Meganathan R (1992) Menaquinone (Vitamin K2) Biosynthesis: Evidence that the Escherichia coli menD Gene Encodes Both 2-Succinyl-6-Hydroxy-2,4-Cyclohexadiene-1-Carboxylic Acid Synthase and ot-Ketoglutarate Decarboxylase Activities. *J. Bacteriol.* **174**, 8111–8118.

161 Dawson A, Fyfe PK & Hunter WN (2008) Specificity and Reactivity in Menaquinone Biosynthesis: The Structure of Escherichia coli MenD (2-Succinyl-5-Enolpyruvyl-6-Hydroxy-3-Cyclohexadiene-1-Carboxylate Synthase). *J. Mol. Biol.* **384**, 1353–1368.

162 Sergienko EA & Jordan F (2001) Catalytic acid-base groups in yeast pyruvate decarboxylase. 2. Insights into the specific roles of D28 and E477 from the rates and stereospecificity of formation of carboligase side products. *Biochemistry* **40**, 7369–81.